Government of **Western Australia**
Department of **Mines, Industry Regulation and Safety**

**RECORD 2019/8**

# METAMORPHIC AND ISOTOPIC CHARACTERISATION OF PROTEROZOIC BELTS AT THE MARGINS OF THE NORTH AND WEST AUSTRALIAN CRATONS

**by**
**J Anderson**
**Department of Earth Sciences, The University of Adelaide**

**Geological Survey of Western Australia**

THE UNIVERSITY of ADELAIDE

Government of **Western Australia**
Department of **Mines, Industry Regulation and Safety**

**RECORD 2019/8**

# METAMORPHIC AND ISOTOPIC CHARACTERISATION OF PROTEROZOIC BELTS AT THE MARGINS OF THE NORTH AND WEST AUSTRALIAN CRATONS

**by**
**J Anderson**
**Department of Earth Sciences, The University of Adelaide**

**PERTH 2019**

**Geological Survey of Western Australia**

**REFERENCE**
**The recommended reference for this publication is:**
Anderson, J 2019, Metamorphic and isotopic characterisation of Proterozoic belts at the margins of the North and West Australian Cratons: Geological Survey of Western Australia, Record 2019/8, 43p.

**ISBN** 978-1-74168-855-9
**ISSN** 2204-4345

Grid references in this publication refer to the Geocentric Datum of Australia 1994 (GDA94). Locations mentioned in the text are referenced using Map Grid Australia (MGA) coordinates, Zone 50. All locations are quoted to at least the nearest 100 m.



**About this publication**
This Record is a chapter from a PhD thesis of The University of Adelaide. The chapter was researched, written and compiled as part of an informal agreement between the Geological Survey of Western Australia (GSWA) and The University of Adelaide. Although GSWA provided access to the samples necessary for this chapter's research, the scientific content of the Record, and the drafting of figures, was the responsibility of the author. No editing has been undertaken by GSWA.


**Published 2019 by the Geological Survey of Western Australia**
This Record is published in digital format (PDF) and is available online at <www.dmp.wa.gov.au/GSWApublications>.




**Further details of geoscience products and maps are available from:**
Information Centre
Department of Mines, Industry Regulation and Safety
100 Plain Street
EAST PERTH WESTERN AUSTRALIA 6004
Telephone: +61 8 9222 3459 Facsimile: +61 8 9222 3444
**www.dmp.wa.gov.au/GSWApublications**

**Cover image:** Sunset over the Yalgoo Mineral Field. Photograph by T Ivanic, DMIRS


THE UNIVERSITY of ADELAIDE

# Metamorphic and isotopic characterisation of Proterozoic belts at the margins of the North and West Australian Cratons

JADE ANDERSON

Department of Earth Sciences
University of Adelaide

This thesis is submitted in fulfillment of the
requirements for the degree of Doctor of Philosophy

November 2015

# Mesoproterozoic metamorphism in the Rudall Province: revising the timeline of the Yapungku Orogeny and implications for cratonic Australia assembly


## ABSTRACT

LA−ICP−MS U−Pb zircon and monazite geochronology from metasedimentary rocks from the Connaughton and Talbot Terranes in the western Rudall Province, North Australia provides evidence for two metamorphic events at *c.* 1665 Ma and between *c.* 1380−1275 Ma. *P*−*T* (*pressure*−*temperature*) pseudosection modelling of a staurolite–biotite bearing assemblage from the Talbot Terrane suggests peak *P*−*T* conditions of ~5.5−8.5 kbar, ~600−650 °C were attained at *c.* 1285 Ma. *P*−*T* modelling on garnet−clinopyroxene-bearing mafic amphibolite from the Rudall Province shows that peak metamorphic conditions of ~8–11 kbar, and minimum ~620–650 °C were attained at *c.* 1380 Ma and followed a clockwise retrograde evolution. The geochronology and *P*−*T* modelling suggest that the age of regional metamorphism ($M_2$, Yapungku Orogeny) is Mesoproterozoic rather than *c.* 1800−1765 Ma. If regional metamorphism in the Rudall Province does reflect the collision of the North and West Australian Cratons, it occurred during the Mesoproterozoic and not the Paleoproterozoic as has previously long been assumed. Metamorphic age data and physical conditions of metamorphism from the Rudall Province may reflect a stage-wise tectonic evolution, involving the accretion of ribbons, and outboard migration of subduction and the back-arc over time, producing both medium-*P*, and high-thermal gradient conditions. In this proposed scenario, the system was closed during the final amalgamation of the North Australian Craton to the accreted ribbons (West Australian Craton) during the Mesoproterozoic.


## 1. Introduction

The Rudall Province occurs at the north-eastern margin of the West Australian Craton (WAC) and has long been recognised as occupying a critical location for understanding the Australian continent assembly (e.g. Clarke, 1991; Smithies and Bagas, 1997; Bagas, 2004; Betts et al., 2006; Cawood and Korsch, 2008; Payne et al., 2009). The Rudall Province is one of the few localities in Australia where Proterozoic-aged medium to high pressure metamorphic assemblages are preserved (minimum apparent thermal gradients of ~60–80 °C.kbar$^{-1}$). Evidence for regional, moderate-thermal gradient conditions (corresponding to eclogite-high pressure granulite thermal gradients of Brown, 2007), combined with evidence for thrust stacking and magmatism has led to the proposal that the Rudall Province records crustal thickening associated with the collision of the WAC and North Australian Craton (NAC) at *c.* 1830−1765 Ma (e.g. Bagas, 2004; Cawood and Korsch, 2008).

Despite its apparent importance in the assembly of Proterozoic Australia, the Rudall Province is an understudied region, and as a consequence, the tectonic evolution of the Rudall Province and its implications for the assembly of Proterozoic Australia is still notional rather than demonstrated (e.g. Maidment, 2007, 2014). The Rudall Province is considered to have a protracted tectonic history spanning at least *c.* 1300 M. y. from the Paleoproterozoic to the late Neoproterozoic–Cambrian (e.g. Bagas et al., 2000; Bagas, 2004; Kirkland et al., 2013). U–Pb zircon geochronology from voluminous felsic magmatic rocks of the Kalkan Supersuite comprises the largest dataset for constraining the absolute timing of tectonism in the Rudall Province (Nelson, 1995, 1996; Kirkland et al., 2013). However, the Kalkan Supersuite, and consequently the majority of the geochronological dataset, is restricted to the time interval *c*. 1800–1765 Ma, which comprises only the oldest part of the history (Nelson, 1995, 1996; Kirkland et al., 2013). At present, absolute time-related interpretations for metasedimentary rocks of the Rudall Province are largely based on extrapolation of

magmatic rock geochronology to fit structural and metamorphic constraints. Metasediments comprise approximately 10−60 % of the terranes within the outcropping Rudall Province (Bagas et al., 2000) and therefore present an effectively untapped opportunity to understand the fuller tectonic—including metamorphic and temporal—history.

In this contribution we present an integrated metamorphic and U−Pb monazite and zircon geochronology study on metamorphic rocks of the Talbot and Connaughton Terranes of the Rudall Province. The aim of this study is to more completely understand the metamorphic evolution of the Yapungku Orogeny ($M_2$) and its implications for the timing of assembly of the WAC and NAC.

## 2. Geological Background

The Paleo- to Mesoproterozoic Rudall Province is located within the approximately 2000 km long, north-west trending, late Neoproterozoic to Cambrian-aged Paterson Orogen, which is exposed along the eastern margin of the Pilbara Craton in north-western Australia. The Paterson Orogen continues into the Musgrave Province in central Australia (Fig. 1) where it is known as the Petermann Orogen (e.g. Bagas and Smithies, 1998; Camacho and McDougall, 2000; Wade et al., 2005; Raimondo et al., 2009, 2010; Walsh et al., 2013).

The Rudall Province contains Paleoproterozoic–Mesoproterozoic metaigneous rocks and metasedimentary rocks with Paleoproterozoic protolith depositional ages (Nelson, 1995, 1996; Smithies and Bagas, 1997; Bagas and Smithies, 1998; Bagas, 2004; Kirkland et al., 2013). The Rudall Province has experienced a number of phases of tectonism, which have been assigned to the following events: a) the Yapungku Orogeny ($D_1$−$D_2$) spanning *c.* 1800−1765 Ma and corresponding to the emplacement of voluminous felsic magmatic rocks of the Kalkan Supersuite; b) the Miles Orogeny ($D_3$−$D_4$) at *c.* 650 Ma; c) the Blake Movement ($D_5$), a poorly constrained Neoproterozoic

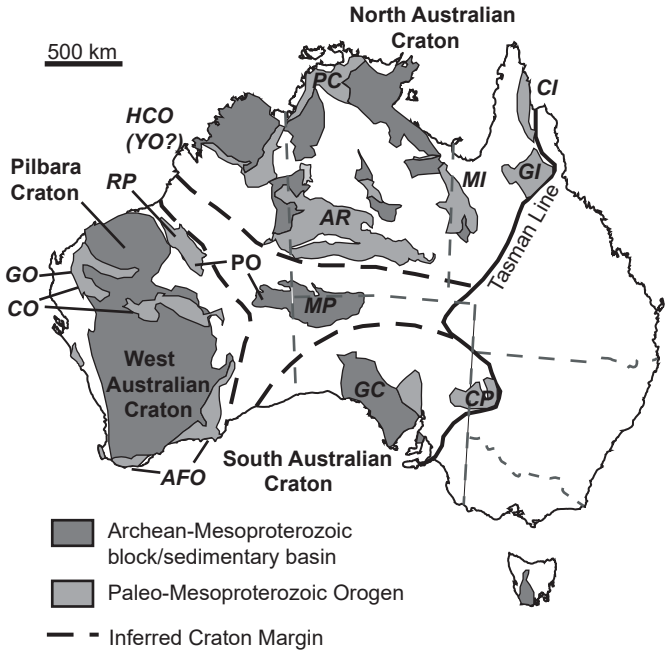


Fig. 1. Simplified map of Australia showing Archean-Mesoproterozoic geological components. AFO = Albany Fraser Orogen, AR = Arunta Region, CI = Coen Inlier, CO = Capricorn Orogen, CP = Curnamona Province, GC = Gawler Craton, GO = Gascoyne Orogen, HCO = Halls Creek Orogen, MI = Mount Isa Inlier, MP = Musgrave Province, PC = Pine Creek Orogen, PO = Paterson Orogen, RP = Rudall Province, YO = Yampi Orogen. Modified after Cawood and Korsch (2008) and Walsh et al. (2013).

deformation; and d) the Paterson Orogeny (D6; c. ≥550 Ma; Smithies and Bagas, 1997; Bagas and Smithies, 1998; Bagas et al., 2000; Bagas, 2004; Czarnota et al., 2009; Kirkland et al., 2013). Earlier work ascribed $D_2$ and $M_2$ to a *c.* 1300 Ma event based on Rb–Sr ages obtained from felsic magmatic rocks (Chin and de Laeter, 1981; Clarke, 1991). This timeline is broadly contemporaneous with the crystallisation of interpreted post- $D_2$ intrusive rocks and minor evidence for metamorphic zircon growth between *c.* 1310 and 1220 Ma (Nelson, 1995, 1996; Bagas, 2004; Kirkland et al., 2013). However, subsequent studies have favoured a Paleoproterozoic *c.* 1800−1760 Ma age for $D_2$ and $M_2$ based on zircon U−Pb data for magmatic crystallisation ages from the Kalkan Supersuite that were interpreted to be syn-deformational with regional medium to high-*P* metamorphism (Nelson, 1995, 1996; Smithies and Bagas, 1997; Bagas, 2004). This event has been interpreted to record the amalgamation of the NAC with the WAC (e.g. Li, 2000; Bagas, 2004) and has been adopted by virtually all recent paleo-tectonic reconstructions of Proterozoic Australia (e.g. Betts et al., 2002; Betts and Giles, 2006; Cawood and Korsch, 2008; Payne et al., 2009; Huston et al., 2012; Johnson, 2013). As a result, the regional significance of *c*. 1300 Ma ages has diminished somewhat.

Unconformably overlying the Rudall Province are deformed but poorly age-constrained late Mesoproterozoic to early Neoproterozoic sedimentary rocks of the Yeneena Supergroup, which are overlain by Phanerozoic cover sequences (Bagas and Smithies, 1998; Williams and Bagas, 1999; Bagas, 2004). Rocks of the Rudall Province have variably undergone retrogression to greenschist facies (Bagas and Smithies, 1998), which may be related to the Miles ($D_4$) and/or *c*. 550 Ma Paterson ($D_6$) orogenies.

Three terranes have been distinguished in the Rudall Province. To the southwest, the Talbot and Connaughton Terranes record similar poly-deformation histories but are distinguished on lithological differences, with the exception of the voluminous orthogneisses that occur in both terranes (Fig. 2). The Talbot and Connaughton Terranes are separated by an east-dipping thrust, interpreted to have formed during or before the Yapungku Orogeny and are commonly interpreted to have undergone similar tectonic histories thereafter ($D_1$ or $D_2$; Smithies and Bagas, 1997; Bagas, 2004). A kyanite−sillimanite isograd in the Connaughton and Talbot Terranes is interpreted to have formed during $M_2$ (Smithies and Bagas, 1997). To the north-east, the poorly outcropping Tabletop Terrane contains early Mesoproterozoic granitoids and is separated from the Talbot and Connaughton Terranes by the Camel–Tabletop Fault Zone (Smithies and Bagas, 1997). The relationship between the Tabletop Terrane and the Talbot and Connaughton Terranes is uncertain. The geology of the Connaughton, Talbot and Tabletop Terranes are described below, and existing constraints on the tectonic evolution of the Rudall Province are summarised in Table 1.

### *2.1 Talbot Terrane*

The Talbot Terrane is composed of sedimentary derived and granitoid rocks that have been multiply deformed and metamorphosed to amphibolite facies (Smithies and Bagas, 1997; Bagas and Smithies, 1998; Bagas, 2004). Clarke (1991) divided the metasedimentary rocks of the Talbot Terrane into: 1) an older Yandagooge Formation, which appears to record a poorly preserved, high-thermal gradient $M_1$–$D_1$ event; and 2) the younger Tjingkulatjatjarra Formation, inferred to post-date $D_1$–$M_1$ and the majority of the emplacement of orthogneisses. Both formations and many of the orthogneisses of the Kalkan Supersuite are considered to record the $M_2$–$D_2$ Yapungku Orogeny, associated with crustal thickening (Watarra Orogeny of Clarke, 1991). There are no direct age data on the timing of $D_1$–$M_1$; however, two orthogneiss samples reported to contain $S_1$ and $S_2$ fabrics yield zircon U–Pb magmatic crystallisation ages of *c.* 2015 Ma (Sample 104932; Nelson, 1995; Hickman and Bagas, 1998) and *c.* 1801 Ma (Sample 112310; Nelson, 1995; Kirkland et al., 2013). A major phase of felsic magmatism occurred at *c.* 1800–1765 Ma, based on U–Pb zircon age data from orthogneisses assigned to the Kalkan Supersuite. These granitoids are

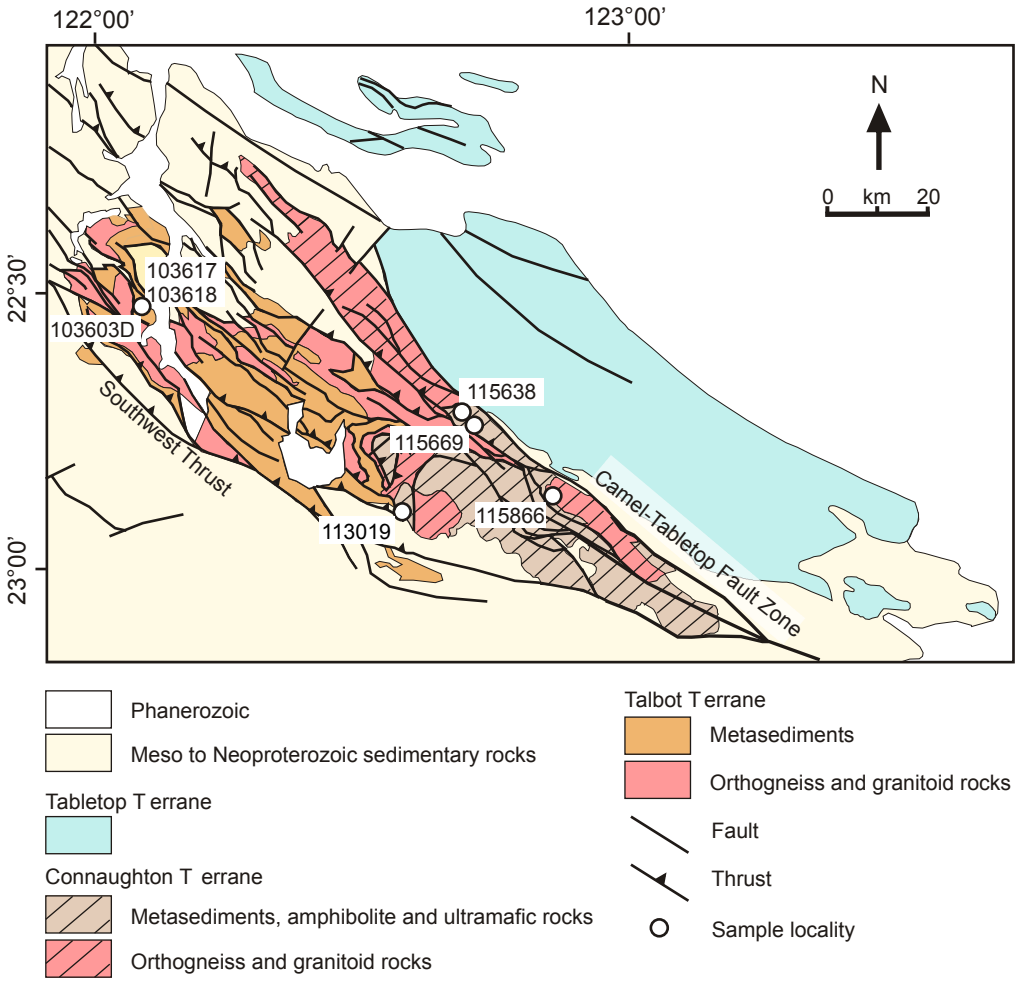


Fig. 2. Map of the Rudall Province, showing lithological associations, major structures and sample locations. Modified from Geological Survey of Western Australia (1999).

interpreted to be coeval with $M_2$–$D_2$ and have been variably deformed during $D_2$ (cf. Nelson, 1995; Bagas, 2004; Kirkland et al., 2013). The younger age limit on the timing of $D_2$–$M_2$ is interpreted to be *c.* 1765 Ma, based on U–Pb zircon age data from an aplite dyke considered to cross-cut the $S_2$ foliation (Nelson, 1995; Bagas, 2004). Evidence for a major phase of Mesoproterozoic tectonism in the Talbot Terrane is limited, though a monzogranite that cuts $D_2$ fabrics yields a U−Pb zircon age of *c.* 1476 Ma (Nelson, 1996; Bagas, 2004). Qualitative *P*−*T* conditions for the $M_2$ event were previously estimated to have reached approximately ≥5 kbar and 600 °C, based on the presence of kyanite–staurolite and garnet–staurolite bearing assemblages (Clarke, 1991). However, these metamorphic mineral assemblages, and therefore *P*–*T* conditions, have not been temporally quantified to have grown during $D_2$−$M_2$.

### *2.2 Connaughton Terrane*

The Connaughton Terrane contains multiply deformed banded iron-formation, metasediments, metachert, orthogneiss and metagranitoids and voluminous deformed mafic rocks that have been metamorphosed at amphibolite to granulite facies conditions (Bagas and Smithies, 1998; Bagas et al., 2000). Available zircon U−Pb geochronology of two samples of the voluminous orthogneisses and metagranitoids of the Kalkan Supersuite yield U−Pb zircon magmatic crystallisation ages of *c.* 1780−1770 Ma and are interpreted to be coeval with $D_2$, similar to the Talbot Terrane (Nelson, 1995, 1996; Bagas, 2004). A garnet-bearing microgneiss and pegmatite, both interpreted to post-date $D_2$ yield U−Pb zircon magmatic crystallisation ages of *c.* 1222 and *c.* 1291 Ma respectively (Nelson, 1995, 1996). Recently, Kirkland et al (2013) reinterpreted a *c.* 1200 Ma U–Pb zircon analysis from the

**Table 1. Geological history of the Rudall Province**

| Events | Talbot Terrane | Connaughton Terrane | Tabletop Terrane | Constraining data | Reference |
|---|---|---|---|---|---|
| <*c.* 2800 Ma | | | Sedimentation: Maximum depositional age for quartzite | U-Pb zircon geochronology | Maidment, (2007) |
| >1800 Ma | Sedimentation of older turbiditic succession | Sedimentation | | Minimum age defined by pre D1 intrusives | Hickman and Bagas, (1998); Bagas, (2004) |
| c. 2015* Ma, 1800 Ma | Pre D1 granitoids | ? | | Crystallisation ages of banded orthogneiss interpreted to contain early foliations. | Nelson, (1995); Hickman and Bagas, (1998); Kirkland et al. (2013) |
| ***c.* 1800 Ma Yapungku Orogeny (D1-M1)** | D1: Layer parallel shear, layer parallel schistosity | D1: Poorly preserved but inferred S1 inclusion trails in some garnet grains in amphibolite | ? | Age inferred based on pre and post D1 intrusives of *c.* 1800 Ma, no direct age constraints | Nelson, (1995); Bagas, (2004); see Kirkland et al. (2013) for reinterpretation of U-Pb data |
| | M1: Amphibolite facies metamorphism, andalusite bearing assemblages (high apparent thermal gradients) | M1: Poorly preserved but inferred assemblage of garnet, epidote, hornblende, apatite in mafic amphibolite | | | |
| *c.* 1790 Ma | Sedimentation (deposition of Fingoon Quartzite) | | | Maximum depositional age of protolith to Fingoon Quartzite | Nelson, (1995) |
| ***c.* 1800-1760 Ma Yapungku Orogeny (D2-M2)^** | D2: N-NW trending isoclinal folds, E to NE dipping thrusts with younger thrusts to the E-NE, W to SW movement, S2 commonly defined by alignment of micas and quartz | D2: N-NW trending isoclinal folds, E to NE dipping thrusts with younger thrusts to the E- NE, W to SW movement | ? | Age constrained by crystallisation ages of interpreted pre, syn and post granitoids | Bagas (2004); Bagas et al, (2000) |
| | M2: amphibolite facies metamorphism, ~ > 5 kbar, 600 ° C | M2: amphibolite-granulite facies, peak conditions ~12 kbar, up to ~800 °C, followed by steep decompression | | thermobarometry on amphibolite and biotite-garnet gneiss samples | Clarke (1991); Smithies and Bagas (1997) |
| *c.* 1800-1765 Ma | Emplacement of the Kalkan Supersuite | Emplacement of the Kalkan Supersuite | | | Kirkland et al. (2013); Nelson, (1995; 1996) |
| post- D2 | | Inferred metamorphism of orthopyroxene-garnet gneiss ('charnockite'), ~2.4−3.7 kbar, 770−860 °C | | thermobarometry | Smithies and Bagas (1997) |
| *c.* 1590-1550 Ma | | | Calc-alkaline magmatism of the Krackatinny Supersuite | U-Pb zircon geochronology | Maidment (2007), Maidment (2014) |
| *c.* 1475-1450 Ma | Crystallisation of monzogranite (post-D2 pre D4) | | Crystallisation of granodiorite (post D2- pre D4) | U-Pb zircon geochronology | Nelson (1996); Bagas (2004) |
| *c* . 1330 Ma | Isochron age from orthogneiss (interpreted as metamorphic) | | | Rb-Sr | Chin and de Laeter (1981) |
| *c.* 1310-1222 Ma | | Crystallisation of post D2 garnet microgneiss, reinterpreted as metamorphic age (one analysis) | Crystallisation of interpreted post D2 intrusives, pegmatite | U-Pb zircon | Bagas (2004); Nelson (1995; 1996); Kirkland et al (2013) |
| ***c.* 650 Ma Miles Orogney (D3-4, M3-4)** | D3: local recumbent folding, D4: upright, tight folding, SW directed compression, S4 axial surface cleavage | D4: upright, tight folding, SW directed compression, S4 axial surface cleavage | D4: upright, tight folding, SW directed compression, S4 axial surface cleavage, formation of the Camel-Tabletop Shear Zone | Minimum age constrained by post-D4 intrusive crystallisation age | Czarnota et al (2009) and references therin |
| | M3-4: greenschist facies metamorphism | M3-4: greenschist facies metamorphism | | | |
| ***c.* 800-610 Ma Blake Movement (D5)** | Local deformation, NW- directed compression, open folds | Local deformation | Local deformation | | Bagas, (2004); Bagas et al. (2000) |
| ***c.* 550 Ma Paterson Orogeny (D6)** | D6: Brittle deformation, NNE- directed compression, WNW-NW striking strike slip and thrust faults | D6: Brittle deformation, NNE- directed compression, WNW-NW striking strike slip and thrust faults | D6: Brittle deformation, NNE-directed compression, WNW-NW striking strike slip and thrust faults | Maximum age constrained by deposition of the *c.* 610 Ma glaciogenic Boondawari Formation, correlated with the Petermann Orogeny | Bagas (2004) and references therein; Bagas et al. (2000) |

* May be inherited ^ Disputed in this study ? Unknown

garnet-bearing microgneiss as metamorphic based on Cathodoluminescence zircon imagery.

Quantitative *P*−*T* estimates for metamorphic mineral assemblages in the Connaughton Terrane are based on conventional thermobarometry for garnet–clinopyroxene, orthopyroxene–clinopyoxene, garnet–biotite and orthopyroxene–garnet bearing assemblages (Smithies and Bagas, 1997). The *P*–*T* conditions have been attributed to $M_2$ (i.e. *c*. 1800–1765 Ma). Estimated peak *P*−*T* conditions of up to ~12 kbar and ~770 °C were obtained from mafic amphibolite from the 'kyanite zone', and ~800 °C at 7 kbar were obtained from orthopyroxene-clinopyroxene bearing amphibolite from the 'sillimanite zone' (Smithies and Bagas, 1997). The *P*−*T* evolution of the Connaughton as well as Talbot Terrane was inferred by Smithies and Bagas (1997) to have followed a steeply decompressive clockwise path, based on the presence of symplectic plagioclase-hornblende coronas on garnet in some mafic amphibolites. *P*−*T* estimates corresponding to very high thermal gradient conditions (~2.4−3.7 kbar, ~770−860 °C; thermal gradient of approximately 210–360 °C kbar $^{-1}$) were obtained from an orthopyroxene–garnet gneiss that is interpreted to record post $M_2$−$D_2$ conditions driven by magmatism (Smithies and Bagas, 1997).

### *2.3 Tabletop Terrane*

The Tabletop Terrane is separated from the Talbot and Connaughton Terranes by the southeast trending Camel–Tabletop Fault that postdates the Kalkan Supersuite. Outcropping areas of the Tabletop Terrane are comprised of volumetrically extensive felsic and mafic intrusives that have been metamorphosed to greenschist facies, dolerite dykes, ultramafic schists and low-volume supracrustal rocks (Bagas and Smithies, 1998). The Krackatinny Supersuite exhibits calc-alkaline geochemical signatures and were largely emplaced at *c.* 1590−1550 Ma (Maidment, 2007; Neumann and Fraser, 2007). Other felsic intrusives record U−Pb zircon magmatic crystallisation ages of *c.* 1476 Ma and 1310 Ma (Nelson, 1996; Bagas, 2004). No metamorphic work has been undertaken on rocks from the Tabletop Terrane.

### *2.4 Constraints on tectonic boundaries in the Rudall Province*

Earlier work on the Rudall Complex assigned rocks in the Talbot Terrane to belong to an eastern and western supracrustal suite based on distinct lithologies and magmatic ages (Bagas, 2004). Bagas (2004) suggested that the eastern and western supracrustal suites of the Rudall Province preserved early magmatic and metamorphic histories that were similar to the Paleoproterozoic Arunta Region (eastern supracrustal) and Gascoyne Complex (western supracrustal), and suggested that the boundary between these supracrustal suites may represent a terrane boundary between the NAC and WAC. Whereas there is an apparent absence of the Kalkan Supersuite in the Tabletop Terrane, the Camel-Tabletop Fault is not interpreted as a major crustal boundary given the common crustal source region of the Kalkan Supersuite and Tabletop granitic rocks (Kirkland et al., 2013). Kirkland et al. (2013) presented Hf isotopic data for interpreted magmatic and inherited zircon from previously dated (U–Pb zircon), variably deformed granitoids of the Kalkan Supersuite and intrusive rocks with younger crystallisation ages or age components between 1450 and 1200 Ma from the Connaughton, Talbot and Tabletop Terrane (Kirkland et al., 2013). The isotopic dataset of Kirkland et al. (2013) indicates the rocks of the Rudall Province were sourced from crust similar to that of the WAC. As such, the location of the suture between the WAC and NAC is likely to be to the east of the Rudall Province.

## 3. Sample descriptions

The aim of this study is to directly determine the timing of the peak regional metamorphism by dating minerals that grew during the metamorphic development, as opposed to previous studies that sought to constrain the timing of deformational/metamorphic events via dating of magmatic rocks with inferred emplacement relationships to deformation.

Samples for this study come from the Connaughton and Talbot Terranes and were obtained from the Geological Survey of Western Australia legacy collections. U–Pb zircon geochronology was conducted on an unmigmatised garnet-diopside bearing amphibolite. Additionally, zircon and garnet trace element chemistry was collected to assist in linking metamorphic silicate phases to zircon growth. U−Pb monazite geochronology was conducted on three metapelitic samples from the Talbot Terrane (within the Tjingkulatjatjarra Formation of Clarke, 1991) and three metasedimentary samples from the Connaughton Terrane. *P–T* pseudosections were calculated for one of the dated metapelitic samples from the Talbot Terrane and a garnet–diopside bearing amphibolite from the Connaughton Terrane.

### *3.1 Sample 103603D: Kyanite-bearing metapelite (Talbot Terrane)*

Bladed kyanite (up to 5 mm) forms aggregates of up to ~15 mm that have aspect ratios of 1:1 to 1:3 (the latter with long axis aligned parallel to schistosity, Figure 3a). Albite is blocky and sub to euhedral (up to 10 mm along long axis). Chlorite (up to 2 mm) and muscovite (up to 6 mm) occur as grains oriented parallel with the foliation and as unoriented grains, and commonly surround and stop at the boundaries of kyanite. Muscovite and chlorite additionally separate kyanite and plagioclase. Fine-grained rutile–ilmenite grains and apatite occur in contact with chlorite, plagioclase, muscovite and retrograde sericite (<0.5 mm). Monazite grains occur as inclusions in chlorite, muscovite and sericite. Kyanite, plagioclase, quartz and rutile–ilmenite are interpreted to comprise the peak metamorphic assemblage, which has been overprinted by retrograde chlorite–muscovite and later sericite.

### *3.2 Samples 103617 and 103618: staurolite-biotite bearing metapelites (Talbot Terrane)*

Sample 103617 exhibits a single foliation defined by subhedral biotite (up to about 10 mm) and in places by staurolite (up to 15 mm long, aspect ratio about 1:1–1:15). Staurolite occurs as poikiloblasts with inclusions of quartz, plagioclase and ilmenite (<0.5 mm), and inclusion poor grains, with some poikiloblastic staurolite occurring as rims on inclusion-poor staurolite grains (Figure 3b). Quartz (up to 6 mm), plagioclase (up to 5 mm), subhedral apatite (< 1 mm), intergrowths of rutile−magnetite (potentially previously ilmenite <1 mm) and fine grained magnetite (<< 1 mm) comprise the matrix. Fine-grained ilmenite additionally occurs within staurolite fractures. Subhedral to anhedral chlorite (up to 10 mm, aspect ratio 1:1−1:3) typically occurs as oriented and unoriented grains, in contact with biotite and staurolite, and commonly infills embayed staurolite grain boundaries. Chlorite is interpreted to have grown at the expense of staurolite, and there is late sericite development. Monazite occurs as inclusions in staurolite and within the matrix. The peak assemblage for sample 103617 is interpreted to be staurolite–plagioclase–quartz–ilmenite–magnetite. Chlorite is interpreted to post-date peak metamorphism. All minerals except chlorite and sericite have previously been interpreted as being stable during $S_2$ (Clarke, pers. comm).

Sample 103618 contains an S–C style fabric in which biotite, staurolite and chlorite define the S and C planes. Staurolite grains are curvilinear in 2D sections, up to 8 mm long and typically have aspect ratios from 1:1 to 1:10 (Figure 3c). Staurolite commonly occurs in aggregates intergrown with quartz and plagioclase that are interpreted to be poikiloblasts. In places these poikiloblasts are wrapped by biotite and chlorite foliae. Subhedral biotite and chlorite (up to 6 mm long) are intergrown with each other, define the fabric and are in direct contact with matrix quartz (< 2mm), plagioclase (< 5 mm) and magnetite (<1 mm). Both chlorite and biotite are in direct contact with staurolite. Ilmenite grains (and ilmenite-rutile intergrowths) are fine grained (<0.5 mm) occur as inclusions in staurolite, in contact with biotite and in the matrix and are commonly aligned parallel to the foliation. Magnetite grains are typically anhedral, unoriented, up to 1 mm in size and occur in the matrix. Monazite grains occur as staurolite inclusions and in the matrix. The peak assemblage for sample 103618 is interpreted to be staurolite–plagioclase–

quartz–chlorite–biotite–magnetite–ilmenite.

### *3.3 Sample 115638: Quartz-garnet-sillimanite gneiss (Connaughton Terrane)*

Sample 115638 was described by Smithies and Bagas (1997) but not used for thermobarometry. The sample contains equant subhedral garnet grains (< 2 mm) that are typically poikiloblastic, containing fine-grained lobate quartz and K-feldspar, and subhedral rutile inclusions (typically <0.5 mm, Figure 3d). Prismatic sillimanite is <1 mm in length and occurs as oriented and unoriented grains, in areas deflecting around garnet. Sillimanite, quartz and K-feldspar (<0.5–2 mm, aspect ratios of 1:1 to 1:3 aligned with the foliation), rutile and ilmenite grains (< 0.5 mm) comprise the matrix and are in contact with garnet. The foliation is defined in places defined by K-feldspar, quartz and sillimanite. Monazite grains occur the matrix and as inclusions in garnet. The interpreted peak mineral assemblage is garnet–sillimanite–plagioclase–K-feldspar–quartz–rutile–ilmenite. Garnet and sillimanite were interpreted by Smithies and Bagas (1997) as late- to post-$D_2$ based on the observation that sillimanite grains define as well as cross cut the foliation, and some garnet grains that show minimal or no deflection of the $S_2$ foliation.

### *3.4 Sample 115669: Kyanite-sillimanite quartzite (Connaughton Terrane)*

Sample 115669 was described by Smithies and Bagas (1997). The sample is quartz -rich and contains kyanite and sillimanite. At the scale of the thin section, localised strain varies from medium to high on the basis of the aspect ratios of quartz in different layers of the fabric (~1:1−1:5, Figure 3e). Prismatic to bladed kyanite (<1 mm long) is interpreted to have been variably recrystallised parallel to foliation, and is partly replaced by acicular to fibrolitic sillimanite (<<1 mm). Sillimanite defines the fabric and also cross cuts the fabric, overprinting quartz and kyanite. Ilmenite–magnetite porphyroblasts (up to about 5 mm long) also occur in the sample and are partially surrounded by chloritoid, which is interpreted to be replacing the porphyroblasts. Quartz (<2 mm) comprises the bulk of the matrix, with minor fine-grained muscovite also present. Monazite grains occur in the matrix. Smithies and Bagas (1997) inferred sample 115669 to be located close to the sillimanite–kyanite isograd. In addition, they inferred and that sillimanite growth was late with respect to $D_2$, and the change from kyanite to sillimanite stability occurred on the prograde path of a single tectonic cycle.

### *3.5 Sample 115866: Garnet-orthopyroxene gneiss (Connaughton Terrane)*

This sample is located close to the Camel–Tabletop Fault zone in the Connaughton Terrane, and was termed a charnockite by Bagas and Smithies (1998). Bagas et al. (2000) reinterpreted the rock to potentially represent quartzofeldspathic/psammitic metasediment. Smithies and Bagas (1997) used this sample for conventional thermobarometry and retrieved very high thermal gradient conditions (~2–4 kbar, 800 °C). The lithology was interpreted to have a foliation unrelated to $S_2$ and therefore could relate to a thermal/metamorphic event post-dating $D_2$ (Smithies and Bagas, 1997). The gneissic fabric is defined by discontinuous layers of orthopyroxene, garnet, ilmenite and magnetite alternating with layers of abundant plagioclase, quartz, K-feldspar and perthite/mesoperthite. Garnet is fine grained (< 1mm) and occurs in a number of morphologies: 1) as equant grains in the matrix; 2) as coronae on fine-grained (<1 mm) magnetite or ilmenite; 3) as quartz–garnet symplectites surrounding, or in contact with, magnetite or ilmenite (e.g. Figure 3f); and 4) in contact and partly surrounded by fine-grained quartz–biotite symplectites. Orthopyroxene occurs as aggregates up to 2 mm in size. Magnetite and ilmenite grains that are mantled by garnet or garnet–quartz symplectites commonly occur next to orthopyroxene. Other grains of magnetite(-spinel) and ilmenite (both <1 mm) are not mantled by garnet, but may be mantled by fine-grained biotite. Anhedral quartz, plagioclase and perthite/mesoperthite (approximately 0.5–2 mm) occur in the matrix, with subhedral to anhedral biotite (<3 mm). Monazite grains occur in the matrix, in contact with quartz/feldspar or magnetite(-spinel), or biotite. The peak assemblage is interpreted to

have been orthopyroxene–garnet–magnetite–ilmenite–plagioclase–K-feldspar–quartz and melt.

### *3.6 Sample 113019: Garnet−diopside amphibolite (Connaughton Terrane)*

Sample 113019 is from the western Connaughton Terrane within the kyanite zone from the same lithology for which medium to high−*P* estimates for the Yapungku Orogeny were obtained by Smithies and Bagas (1997). It is a foliated unmigmatised garnet−diopside-bearing amphibolite. Garnet grains

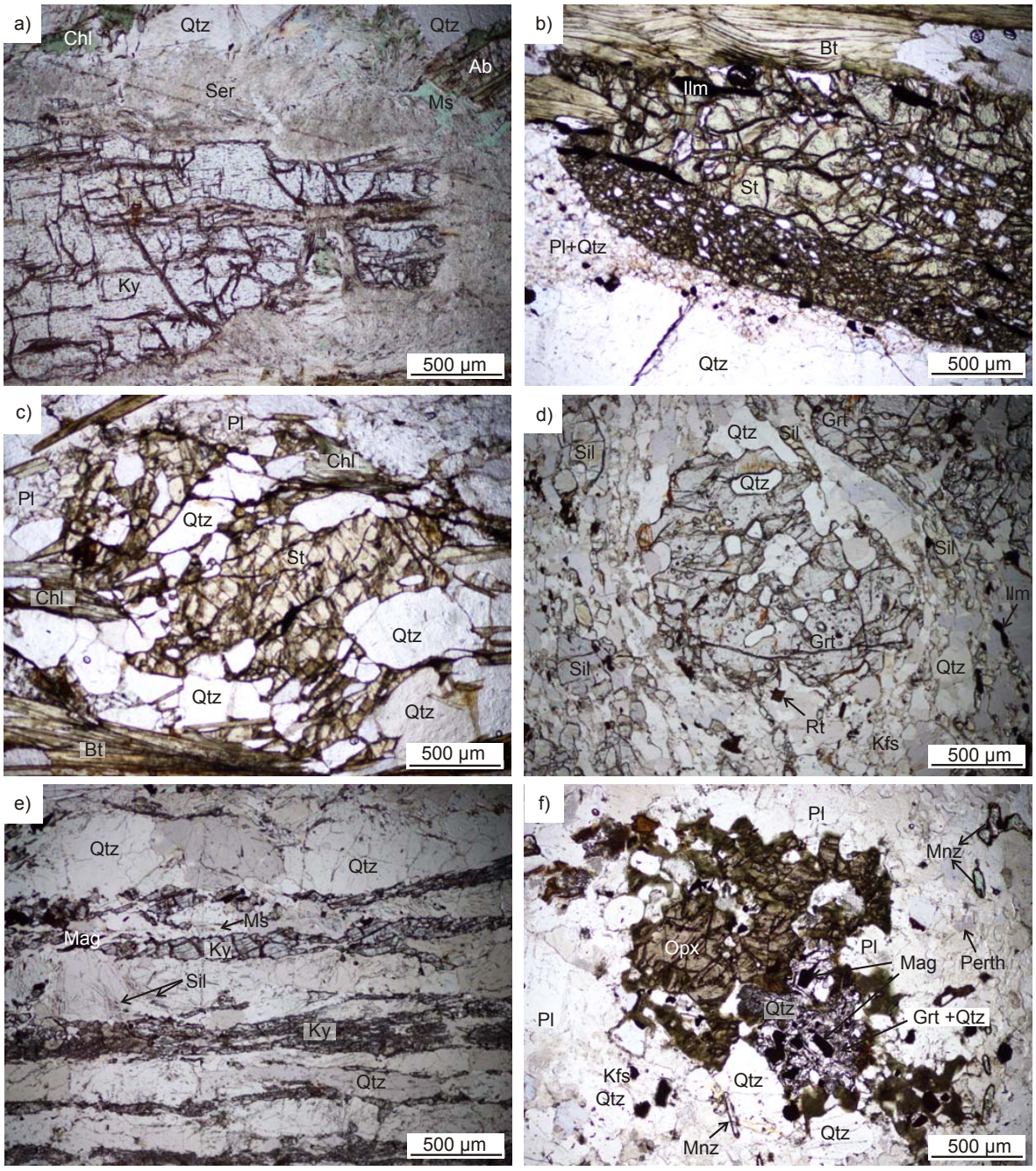


Fig. 3. Thin section photos of samples used in this study: a) Sample 103603D, kyanite surrounded by fine grained sericite, and chlorite, quartz, albite and muscovite, b) sample 103617, staurolite with inclusion rich domains, in contact with plagioclase, quartz, ilmenite and biotite, c) sample 103618, staurolite, plagioclase and quartz wrapped by biotite, d) sample 115638, poikiloblastic garnet in a quartz, K-feldspar, sillimanite, rutile and ilmenite matrix. Sillimanite is both in contact with and in areas wraps around garnet, defining the fabric of the rock, e) sample 115669, kyanite−sillimanite−quartz−magnetite sample, kyanite is in areas recrystallised parallel to the fabric, and fine-grained acicular sillimanite occurs as oriented grains parallel to the fabric and unoriented grains, and f) sample 115866, orthopyroxene adjacent to magnetite mantled by garnet−quartz symplectites in a K-feldspar, (meso)perthite, plagioclase, quartz matrix. Monazite is locally abundant.

(~0.5−1.5 mm in diameter) are typically equant and contain very-fine-grained (<< 0.5 mm) titanite, quartz, plagioclase, hornblende and rare zircon inclusions that are unoriented or occur either as inclusion trails that transect the garnet grain or in the core of the garnet (Fig. 4). Diopside is fine-grained (< 1 mm) and occurs with matrix minerals plagioclase (< 2 mm, anhedral), quartz (< 1mm, anhedral), hornblende (< 2mm, subhedral to anhedral) and minor apatite and pyrite (< 0.5 mm). Hornblende is foliated and also partially surrounds garnet and diopside as fine−medium sized grains (< 2mm). Hornblende also occurs as part of a fine-grained and locally developed symplectic intergrowth with plagioclase ± quartz ± titanite, partially separating garnet from matrix hornblende or diopside grains. The peak mineral assemblage is interpreted to be garnet−diopside−hornblende−plagioclase−quartz−titanite−apatite.

## 4. Analytical Techniques

### *4.1 Electron Microprobe Analysis (EPMA) spot and elemental maps*

Mineral chemical composition analyses were obtained using a Cameca SXFive electron microprobe at the University of Adelaide using a beam current of 20 nA and accelerating voltage of 15 kV. Monazite elemental maps were obtained using a beam current of 200 nA and accelerating voltage of 15–20 kV. Y, Th, Ce, U and Pb were mapped using WDS and P was mapped using EDS.

### *4.2 Zircon and Monazite U–Pb Geochronology*

Zircon from sample 113019 and monazite from the remaining six samples from the Rudall Province were analysed for U–Pb geochronology using the Laser Ablation–Inductively Coupled Plasma–Mass Spectrometer (LA−ICP−MS) at Adelaide Microscopy, University of Adelaide. Zircon from sample 113019 (garnet−diopside amphibolite) was prepared using panning, Franz and heavy liquid techniques at Geotrack International, and mounted in epoxy resin. Prior to laser ablation, zircon grains were imaged using a Gatan Cathodoluminescence (CL) detector attached to a Phillips XL40 SEM. Monazite grains were imaged using a Phillips XL30 SEM.

U–Pb analyses of zircon and monazite were obtained using an Agilent 7500cs ICP–MS with a New Wave 213 nm Nd–YAG laser in a helium ablation atmosphere. For zircon, a laser spot size of 20–30 µm, repetition rate of 5 Hz and laser intensity of 80–100 % was used. A 30 second gas blank was initially measured followed by 80 seconds of zircon sample ablation. The laser was fired for 10 seconds with the shutter closed prior to ablation in order to allow for beam and crystal stabilization. Analyses measured isotopes $^{204}$Pb, $^{206}$Pb, $^{207}$Pb, $^{208}$Pb, $^{232}$Th and $^{238}$U for 10, 15, 30, 10, 10, 15 ms respectively for zircon. Common lead was not corrected due to an unresolvable interference of $^{204}$Hg and $^{204}$Pb peaks. However, $^{204}$Pb was monitored to assess the common lead of each analysis.

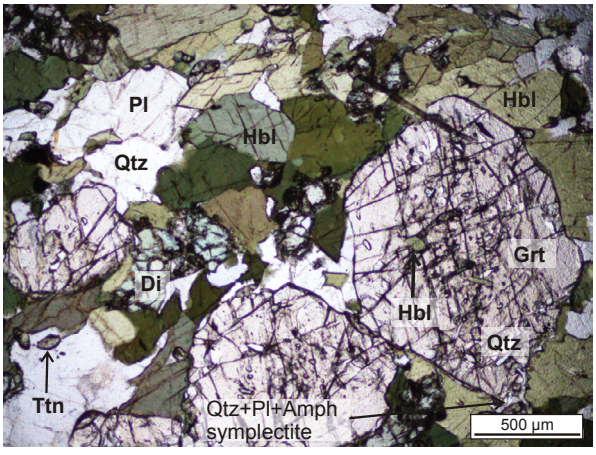


Figure 4. Photomicrograph of sample 113019 showing peak assemblage garnet, diopside, hornblende, quartz, plagioclase and titanite. Quartz, plagioclase, amphibole symplectite separating garnet and matrix hornblende is also shown.

For monazite, a 15–16 μm spot size, repetition rate of 5 Hz and laser intensity of 80–100 % was used. A 30 second gas blank was initially measured followed by 40 to 50 seconds of monazite sample ablation. The laser was fired for 10 seconds with the shutter closed prior to ablation in order to allow for beam and crystal stabilisation. Analyses measured isotopes $^{204}$Pb, $^{206}$Pb, $^{207}$ Pb and $^{238}$U for 10, 15, 30 and 15 ms respectively for monazite. Common lead was not corrected for zircon or monazite analyses due to an unresolvable interference of $^{204}$Hg and $^{204}$Pb peaks. However, $^{204}$Pb was monitored to assess the common lead of each analysis.

Zircon and monazite data was corrected for mass-bias and fractionation using the real-time correction program Glitter v. 4.23 (Griffin et al., 2008). Gemoc zircon standard GJ-1 was used to correct for mass bias and fractionation (TIMS normalisation data: $^{207}$Pb/$^{206}$Pb = 608.3 Ma, $^{206}$Pb/$^{238}$U = 600.7 Ma and $^{207}$Pb/$^{235}$U = 602.2 Ma; Jackson *et al.* 2004). An uncertainty of 1% was assigned to the age of the GJ-1 zircon standard. Accuracy of zircon analyses were monitored by analysing internal standards Plesovice (ID TIMS $^{206}$Pb/$^{238}$U age = 337.13 ± 0.37 Ma; Sláma *et al.* 2008) and OG-1 (ID TIMS $^{207}$Pb/$^{206}$Pb age = 3465.4 ± 0.6 Ma; Stern et al., 2009) prior to and throughout unknown analysis runs. Average Plesovice ages obtained during this study were $^{207}$Pb/$^{235}$U = 339 ± 4 Ma (95 % confidence, *n* = 16, MSWD = 1.9), $^{207}$Pb/$^{206}$Pb = 339 ± 17 Ma (MSWD = 0.38) and $^{206}$Pb/$^{238}$U = 340 ± 2.9 Ma (MSWD = 2.9). Average OG-1 ages obtained during this study were $^{207}$Pb/$^{206}$Pb = 3464 ± 15 Ma (95 % confidence, *n* = 6, MSWD = 0.6), $^{207}$Pb/$^{235}$U = 3461 ± 37 Ma (MSWD = 6.3), and $^{206}$Pb/$^{238}$U = 3458 ± 110 Ma (MSWD = 9.4).

Monazite standard Madel was used to correct for mass bias and fractionation for monazite analyses (TIMS Madel age: $^{207}$Pb/$^{206}$Pb = 490.0 Ma, $^{206}$Pb/$^{238}$U = 518.37 Ma and $^{207}$Pb/$^{235}$U = 513.13 Ma; Payne et al., 2008, updated with additional TIMS data). 1% uncertainty was given to the age of the Madel standard for sample age error calculations. Accuracy was monitored by analysing the 222 (*c.* 450 Ma; Maidment, 2005) monazite standard prior to and throughout unknown analysis runs. Average 222 ages obtained throughout this study were $^{207}$Pb/$^{235}$U = 454 ± 2 Ma (95 % confidence, *n* = 59, MSWD = 1.2), $^{207}$Pb/$^{206}$Pb = 461 ± 7 Ma (MSWD = 0.46) and $^{206}$Pb/$^{238}$U = 452 ± 2 Ma (MSWD = 1.5). Conventional concordia, weighted averages, and linear probability plots were generated using Isoplot version 4.11 (Ludwig, 2008).

### *4.3 Zircon and garnet REE: Sample 113019*

REE and trace elements of zircon and garnet grains were analysed using the LA−ICP−MS at Adelaide Microscopy). Zircon grains were analysed in grain mounts, whereas garnet grains were analysed in situ. Moderately luminescent zircon with homogenous, fir-tree zoned and irregular/patchy zones with pre-collected U–Th–Pb data were analysed. LA–ICP–MS REE chemistry of garnet grains were obtained via transects across garnet grains over pre-collected EPMA spot analysis transects. Analyses for zircon and garnet were conducted using 30 μm laser spot size at 100 % intensity and 5 Hz repetition rate. Total acquisition time was 100 seconds for zircon and 150 seconds for garnet, and incorporated 30 seconds of background acquisition and 10 seconds of laser firing with the shutter closed at the start of each zircon and garnet analysis. External standard Nist 610 was used to correct for fractionation and mass bias (Pearce *et al.* 1997), and standards Nist 612 and BHVO were used as internal standards to monitor the accuracy of analyses. Data was corrected using GLITTER software (Van Achterbergh *et al.* 2001). Analyses were calibrated internally using Hf oxide weight percent measurements on zircon domains and Ca oxide weight percent measurements on garnet corresponding to spot locations of LA–ICP–MS REE and trace element analyses using Cameca SX51 microprobe at Adelaide Microscopy. An accelerating voltage of 15 kV and beam current of 20 nA was used.

### *4.4 Mineral equilibria modelling*

Bulk chemical compositions of samples 103618 and 113019 were determined using whole-rock geochemical analyses. Major element concentrations were determined by X-ray fluorescence (XRF), using a Panalytical

2404 XRF unit at Franklin and Marshall College, United States. Samples were prepared for analysis by fusion of the milled sample with lithium tetraborate. Estimates on the proportion of $Fe_2O_3$ to FeO in the rocks were made by estimating the modal abundance of minerals in a sample and combining that information with oxide wt% compositions of $Fe^{3+}$ bearing minerals recast for $Fe_2O_3$ using the stoichiometric method of Droop (1987). For staurolite–magnetite–ilmenite bearing sample 103618, 85% of the analysed $Fe_2O_3$ was converted to FeO.

*P*–*T* pseudosections were calculated using THERMOCALC v3.33 (October 2009 update of Powell and Holland, 1988), with the internally consistent dataset of Holland and Powell (1998; tc-ds55, Nov. 2003 update). The model chemical system NCKFMASHTO ($Na_2O$–$CaO$–$K_2O$–$FeO$–$MgO$–$Al_2O_3$–$SiO_2$–$H_2O$–$TiO_2$–$Fe_2O_3$) was used for *P*–*T* pseudosection calculations for sample 103618 using *a*–*x* relationships of White et al. (2007) for biotite, garnet and silicate melt, White et al. (2000) for ilmenite and hematite, Holland and Powell (2003) for K-feldspar and plagioclase, Holland and Powell (1998) for cordierite, staurolite and epidote, Coggon and Holland (2002) for muscovite and paragonite, Holland et al. (1998) for chlorite and White et al. (2000) for magnetite.

For sample 113019, the model chemical system NCFMASHTO ($Na_2O$–$CaO$–$FeO$–$MgO$–$Al_2O_3$–$SiO_2$–$H_2O$–$TiO_2$–$Fe_2O_3$) was used for sample 113019 using *a*–*x* relationships of Green et al. (2007) for clinopyroxene, Diener et al. (2007) for hornblende, White et al. (2007) for garnet, Holland and Powell (1998) for epidote, Holland et al. (1998) for chlorite, Holland and Powell (2003) for plagioclase and White et al. (2000) for ilmenite. Estimates on the proportion of $Fe_2O_3$ to FeO were made by estimating the modal abundance of minerals in the sample and combining that information with oxide wt.% compositions of $Fe^{3+}$ bearing minerals recast for $Fe_2O_3$ using the stoichiometric method of Droop (1987). 90% of the analysed $Fe_2O_3$ was converted to FeO for sample 113019. Water was set to excess (water saturated) for samples 103618 and 113019 as peak *P*–*T* conditions of both samples are interpreted to be subsolidus.

## 5. Results

Representative EPMA spot analyses are provided in Table 2 and mineral chemistry is detailed in Appendix 1.

### *5.1 In situ monazite U–Pb Geochronology*

Representative EPMA maps and BSE images of monazite for sample 115638 and 115866 are shown in Figure 5. BSE images of monazite grains from samples 103603D, 103617, 103618 and 115669 are shown in Figure 6a–d. Cathodoluminescence images of zircon from sample 113019 are show in Figure 6e. U–Pb geochronology data are provided in Appendix 2.

#### *5.1.1. Sample 103603D (kyanite–bearing pelite, Talbot Terrane)*

Monazite grains occur as inclusions in chlorite, muscovite and sericite, do not show zoning in BSE imagery and range in size from ~50 to 200 μm. Twenty analyses were obtained (Fig. 7a, b). Seventeen analyses are within 5 % concordance, lie on a linear array in the plotted linear probability diagram, and are interpreted to comprise one age population. The above concordant analyses yield a $Pb^{207}/Pb^{206}$ age weighted average of 1275 ± 11 Ma (*n* = 17, MSWD = 0.3, 95 % confidence).

#### *5.1.2. Sample 103617 (staurolite–bearing pelite, Talbot Terrane)*

Monazite grains range from ~20 to 100 μm and show variable internal morphologies in BSE imagery varying from no zoning, irregular/patchy zoning to monazite grains with lighter cores. Thirty-five analyses were obtained from monazite grains located within the matrix and as inclusions in staurolite grains (Fig. 7c). 100 ± 5 % concordant analyses were included in the linearised probability plot (Fig. 7d). 25 analyses form a linear array on Figure 7d and are interpreted as one age population. These analyses yield a $Pb^{207}/Pb^{206}$ age weighted average of 1666 ± 8 Ma (*n* = 25, MSWD = 0.73, 95 % confidence).

Table 2. Representative mineral compositions for samples 103617 and 103618

| **Sample** | 103617 | 103617 | 103617 | 103617 | 103617 | 103617 | 103618 | 103618 | 103618 | 103618 | 103618 | 103618 | 103618 |
|---|---|---|---|---|---|---|---|---|---|---|---|---|---|
| **Mineral** | Chl | Bt | St | Qtz | Pl | Mag | Chl | Bt | St | Qtz | Pl | Mag | Ilm |
| **ID number** | 1 | 51 | 18 | 30 | 34 | 40 | 72 | 42 | 4 | | 44 | 67 | 36 |
| $SiO_2$ | 26.29 | 34.93 | 26.36 | 98.66 | 65.80 | 0.35 | 24.65 | 33.96 | 25.90 | 99.11 | 67.42 | 0.31 | 0.04 |
| $TiO_2$ | 0.42 | 1.13 | 0.55 | 0.00 | 0.01 | 0.06 | 0.08 | 1.42 | 0.55 | 0.01 | 0.00 | 0.03 | 52.12 |
| $Al2O_3$ | 22.56 | 17.96 | 52.88 | 0.01 | 19.79 | 0.14 | 22.46 | 19.30 | 52.02 | 0.02 | 18.57 | 0.46 | 0.01 |
| $Cr2O_3$ | 0.02 | 0.00 | 0.00 | 0.01 | 0.00 | 0.00 | 0.01 | 0.03 | 0.00 | 0.01 | 0.00 | 0.00 | 0.01 |
| FeO | 19.63 | 17.41 | 13.23 | 0.02 | 0.00 | 90.49 | 21.38 | 18.19 | 14.67 | 0.00 | 0.00 | 87.10 | 44.52 |
| MnO | 0.07 | 0.08 | 0.26 | 0.01 | 0.00 | 0.04 | 0.10 | 0.05 | 0.22 | 0.00 | 0.01 | 0.01 | 1.28 |
| MgO | 18.83 | 14.51 | 2.07 | 0.00 | 0.00 | 0.05 | 18.48 | 13.33 | 1.83 | 0.00 | 0.00 | 0.01 | 0.31 |
| ZnO | 0.00 | 0.00 | 0.14 | 0.00 | 0.03 | 0.05 | 0.02 | 0.03 | 0.00 | 0.00 | 0.03 | 0.03 | 0.06 |
| CaO | 0.00 | 0.00 | 0.01 | 0.01 | 0.49 | 0.04 | 0.02 | 0.07 | 0.01 | 0.00 | 0.78 | 0.03 | 0.00 |
| $Na_2O$ | 0.01 | 0.16 | 0.00 | 0.02 | 11.75 | 0.02 | 0.00 | 0.20 | 0.00 | 0.00 | 11.72 | 0.04 | 0.01 |
| $K_2O$ | 0.56 | 8.13 | 0.00 | 0.00 | 0.05 | 0.04 | 0.06 | 7.37 | 0.01 | 0.01 | 0.04 | 0.00 | 0.01 |
| **Total** | 88.39 | 94.31 | 95.51 | 98.73 | 97.92 | 91.29 | 87.25 | 93.95 | 95.22 | 99.17 | 98.56 | 88.02 | 98.37 |
| **No. Oxygens** | 14 | 11 | 46 | 2 | 8 | 4 | 14 | 11 | 46 | 2 | 8 | 4 | 3 |
| Si | 2.67 | 2.65 | 7.51 | 1.00 | 2.95 | 0.01 | 2.56 | 2.59 | 7.46 | 1.00 | 3.00 | 0.01 | 0.00 |
| Ti | 0.03 | 0.06 | 0.12 | 0.00 | 0.00 | 0.00 | 0.01 | 0.08 | 0.12 | 0.00 | 0.00 | 0.00 | 1.00 |
| Al | 2.70 | 1.61 | 17.75 | 0.00 | 1.04 | 0.01 | 2.75 | 1.73 | 17.65 | 0.00 | 0.97 | 0.02 | 0.00 |
| Cr | 0.00 | 0.00 | 0.00 | 0.00 | 0.00 | 0.00 | 0.00 | 0.00 | 0.00 | 0.00 | 0.00 | 0.00 | 0.00 |
| $Fe^{3+}$ | | | | | | 1.97 | | | | | | 1.95 | 0.00 |
| $Fe^{2+}$ | 1.66 | 1.10 | 3.15 | 0.00 | 0.00 | 1.00 | 1.86 | 1.16 | 3.53 | 0.00 | 0.00 | 1.00 | 0.95 |
| $Mn^{2+}$ | 0.01 | 0.01 | 0.06 | 0.00 | 0.00 | 0.00 | 0.01 | 0.00 | 0.05 | 0.00 | 0.00 | 0.00 | 0.03 |
| Mg | 2.85 | 1.64 | 0.88 | 0.00 | 0.00 | 0.00 | 2.86 | 1.51 | 0.78 | 0.00 | 0.00 | 0.00 | 0.01 |
| Zn | 0.00 | 0.00 | 0.03 | 0.00 | 0.00 | 0.00 | 0.00 | 0.00 | 0.00 | 0.00 | | 0.00 | 0.00 |
| Ca | 0.00 | 0.00 | 0.00 | 0.00 | 0.02 | 0.00 | 0.00 | 0.01 | 0.00 | 0.00 | 0.04 | 0.00 | 0.00 |
| Na | 0.00 | 0.02 | 0.00 | 0.00 | 1.02 | 0.00 | 0.00 | 0.03 | 0.00 | 0.00 | 1.01 | 0.00 | 0.00 |
| K | 0.07 | 0.79 | 0.00 | 0.00 | 0.00 | 0.00 | 0.01 | 0.72 | 0.00 | 0.00 | 0.00 | 0.00 | 0.00 |
| **Total Cations (S)** | 10 | 8 | 29.5 | 1 | 5 | 3 | 10 | 8 | 30 | 1 | 5 | 3 | 2 |
| *X*(Mg) = (Mg/(Fe+Mg)) | 0.63 | 0.60 | 0.22 | | | | 0.61 | 0.57 | 0.18 | | | | 0.01 |
| *X*(Na) = (Na/(Na+Ca) | | | | | 0.98 | | | | | | 0.96 | | |
| *X*(Mg) = (Mg/(Mg+Zn+$Fe^{2+}$+Mn) | | | | | | | | | | | | | 0.01 |

### *5.1.3. Sample 103618 (staurolite−bearing pelite, Talbot Terrane)*

Monazite grains are ~40–200 μm in size, occur both in the matrix and as inclusions within staurolite, and display internal morphologies in BSE imagery that vary from no zoning to patchy zoning. 25 analyses were obtained, with 23 analyses are within 100 ± 5 % concordance and are shown in linearised probability plot (Fig. 7e, f). A $Pb^{207}/Pb^{206}$ age weighted average of 1283 ± 9 Ma ($n$ = 22, MSWD = 0.58, 95 % confidence) was calculated from analyses which lie along a linear array. One older analysis from a monazite grain located in the matrix was excluded from the weighted average.

### *5.1.4. Sample 115638 (garnet−sillimanite gneiss, Connaughton Terrane)*

Monazite grains are ~20–150 μm in size and show internal morphologies in BSE imagery that range from no visible zoning, zoning with either darker or lighter cores, and concentric zoning. Th and Y elemental maps of representative monazite grains show monazite grains commonly contain a Th enriched core and do not show appreciable Y zoning. Th-poor rims were too narrow to be analysed using LA–ICP–MS. Eighteen analyses were obtained from monazite grains located within the matrix and as inclusions in garnet grains. Sixteen analyses yield results within 100 ± 5 % concordance. These concordant analyses were included in the linearised probability diagram and lie on a linear array (Fig. 8a, b). The above concordant analyses are interpreted to comprise one age population and yield $Pb^{207}/Pb^{206}$ age weighted average of 1307 ± 12 Ma ($n$ = 16, MSWD = 0.87, 95 % confidence).

### *5.1.5. Sample 115669 (kyanite−sillimanite quartzite, Connaughton Terrane)*

Monazite grains vary in size from 20 to 200 μm and exhibit internal morphologies that vary from no visible zoning, patchy/irregular zoning to darker or lighter cores under BSE. Nineteen analyses were obtained on monazite

Table 2. Representative mineral compositions for samples 115866 and 113019

| **Sample** | 115866 | 115866 | 115866 | 115866 | 115866 | 115866 | 115866 | 115866 | 115866 | 113019 | 113019 | 113019 | 113019 | 113019 | 113019 | 113019 |
|---|---|---|---|---|---|---|---|---|---|---|---|---|---|---|---|---|
| **Mineral** | Grt- matrix | Grt-Corona | Opx | Pl | Kfs | Qtz | Mag | Ilm | Bt | Grt-rim | Grt-core | Di | Hbl | Pl | Ttn | Qtz |
| **ID number** | 54 | 91 | 86 | 27 | 30 | 22 | 83 | 97 | 13 | 3 | 19 | 99 | 34 | 103 | 37 | 36 |
| $SiO_2$ | 38.31 | 37.59 | 45.13 | 60.00 | 65.35 | 97.45 | 0.04 | 0.05 | 39.44 | 38.47 | 38.08 | 51.85 | 41.38 | 62.67 | 30.42 | 96.53 |
| $TiO_2$ | 0.04 | 0.03 | 0.24 | 0.04 | 0.03 | 0.07 | 0.04 | 49.07 | 2.03 | 0.03 | 0.14 | 0.19 | 1.16 | 0.00 | 37.02 | 0.00 |
| $Al2O_3$ | 21.37 | 20.98 | 9.89 | 24.50 | 19.77 | 0.16 | 0.27 | 0.02 | 15.15 | 20.85 | 20.62 | 4.11 | 11.95 | 23.43 | 1.17 | 0.02 |
| $Cr2O_3$ | 0.03 | 0.01 | 0.02 | 0.00 | 0.01 | 0.02 | 0.10 | 0.01 | 0.00 | 0.04 | 0.01 | 0.05 | 0.03 | 0.06 | 0.01 | 0.00 |
| FeO | 25.85 | 26.96 | 23.07 | 0.06 | 0.04 | 0.05 | 87.96 | 45.92 | 9.69 | 25.05 | 24.61 | 10.42 | 17.55 | 0.08 | 0.57 | 0.52 |
| MnO | 2.31 | 2.49 | 0.64 | 0.01 | 0.00 | 0.00 | 0.08 | 0.76 | 0.08 | 1.04 | 0.82 | 0.10 | 0.11 | 0.01 | 0.01 | 0.00 |
| MgO | 10.02 | 9.30 | 19.04 | 0.00 | 0.00 | 0.01 | 0.00 | 0.70 | 19.76 | 3.18 | 3.45 | 11.14 | 10.35 | 0.00 | 0.00 | 0.00 |
| ZnO | 0.00 | 0.05 | 0.00 | 0.04 | 0.00 | 0.00 | 0.04 | 0.09 | 0.00 | 0.00 | 0.00 | 0.01 | 0.05 | 0.00 | 0.00 | 0.00 |
| CaO | 0.85 | 0.81 | 0.05 | 6.36 | 0.89 | 0.00 | 0.02 | 0.02 | 0.01 | 11.68 | 12.35 | 19.85 | 10.63 | 4.77 | 29.05 | 0.05 |
| $Na_2O$ | 0.01 | 0.00 | 0.02 | 8.06 | 2.62 | 0.00 | 0.02 | 0.01 | 0.04 | 0.00 | 0.00 | 2.02 | 2.19 | 8.86 | 0.01 | 0.00 |
| $K_2O$ | 0.00 | 0.01 | 0.00 | 0.14 | 11.66 | 0.04 | 0.00 | 0.01 | 9.37 | 0.00 | 0.01 | 0.00 | 0.22 | 0.05 | 0.00 | 0.00 |
| **Total** | 98.78 | 98.24 | 98.11 | 99.21 | 100.37 | 97.80 | 88.57 | 96.65 | 95.57 | 100.34 | 100.10 | 99.74 | 95.62 | 99.91 | 98.26 | 97.12 |
| **No. Oxygens** | 12 | 12 | 6 | 8 | 8 | 2 | 4 | 3 | 11 | 12 | 12 | 6 | 23 | 8 | 5 | 2 |
| Si | 2.99 | 2.97 | 1.70 | 2.69 | 2.96 | 1.00 | 0.00 | 0.00 | 2.85 | 3.02 | 3.00 | 1.94 | 6.36 | 2.78 | 1.01 | 1.00 |
| Ti | 0.00 | 0.00 | 0.01 | 0.00 | 0.00 | 0.00 | 0.00 | 0.96 | 0.11 | 0.00 | 0.01 | 0.01 | 0.13 | 0.00 | 0.93 | 0.00 |
| Al | 1.96 | 1.95 | 0.45 | 1.30 | 1.05 | 0.00 | 0.01 | 0.00 | 1.29 | 1.93 | 1.91 | 0.18 | 2.17 | 1.22 | 0.05 | 0.00 |
| Cr | 0.00 | 0.00 | 0.00 | 0.00 | 0.00 | 0.00 | 0.00 | 0.00 | 0.00 | 0.00 | 0.00 | 0.00 | 0.00 | 0.00 | 0.00 | 0.00 |
| $Fe^{3+}$ | | | 0.13 | | | | 1.98 | 0.08 | | | | 0.09 | | | | |
| $Fe^{2+}$ | 1.69 | 1.78 | 0.60 | 0.00 | 0.00 | 0.00 | 1.00 | 0.91 | 0.58 | 1.64 | 1.62 | 0.33 | 2.26 | 0.00 | 0.02 | 0.00 |
| $Mn^{2+}$ | 0.15 | 0.17 | 0.02 | 0.00 | 0.00 | 0.00 | 0.00 | 0.02 | 0.00 | 0.07 | 0.05 | 0.00 | 0.01 | 0.00 | 0.00 | 0.00 |
| Mg | 1.16 | 1.10 | 1.08 | 0.00 | 0.00 | 0.00 | 0.00 | 0.03 | 2.13 | 0.37 | 0.40 | 0.62 | 2.37 | 0.00 | 0.00 | 0.00 |
| Zn | 0.00 | 0.00 | 0.00 | 0.00 | 0.00 | 0.00 | 0.00 | 0.00 | 0.00 | 0.00 | 0.00 | 0.00 | 0.01 | 0.00 | 0.00 | 0.00 |
| Ca | 0.07 | 0.07 | 0.00 | 0.31 | 0.04 | 0.00 | 0.00 | 0.00 | 0.00 | 0.98 | 1.04 | 0.80 | 1.75 | 0.23 | 1.04 | 0.00 |
| Na | 0.00 | 0.00 | 0.00 | 0.70 | 0.23 | 0.00 | 0.00 | 0.00 | 0.01 | 0.00 | 0.00 | 0.15 | 0.65 | 0.76 | 0.00 | 0.00 |
| K | 0.00 | 0.00 | 0.00 | 0.01 | 0.67 | 0.00 | 0.00 | 0.00 | 0.86 | 0.00 | 0.00 | 0.00 | 0.04 | 0.00 | 0.00 | 0.00 |
| **Total Cations (S)** | 8 | 8 | 4 | 5 | 5 | 1 | 3 | 2 | 8 | 8 | 8 | 4 | 16 | 5 | 3 | 1 |
| *X*Mg = (Mg/(Fe+Mg)) | 0.41 | 0.38 | 0.64 | | | | | 0.03 | 0.78 | 0.18 | 0.20 | 0.66 | 0.51 | | | |
| *X*Mg = (Mg/(Mg+Zn+$Fe^{2+}$+Mn) | | | | | | | | 0.03 | | | | | | | | |
| *X*(Alm) | 0.55 | 0.57 | | | | | | | | 0.54 | 0.52 | | | | | |
| *X*(Py) | 0.38 | 0.35 | | | | | | | | 0.12 | 0.13 | | | | | |
| *X*(Grs) | 0.02 | 0.02 | | | | | | | | 0.32 | 0.33 | | | | | |
| *X*(Spss) | 0.05 | 0.05 | | | | | | | | 0.02 | 0.02 | | | | | |
| *X*( An) = (Ca/(Ca+Na+K) | | | | 0.30 | 0.05 | | | | | | | | | 0.23 | | |
| *X*(Or) = (K/(Na+Ca+K) | | | | 0.01 | 0.71 | | | | | | | | | 0.00 | | |

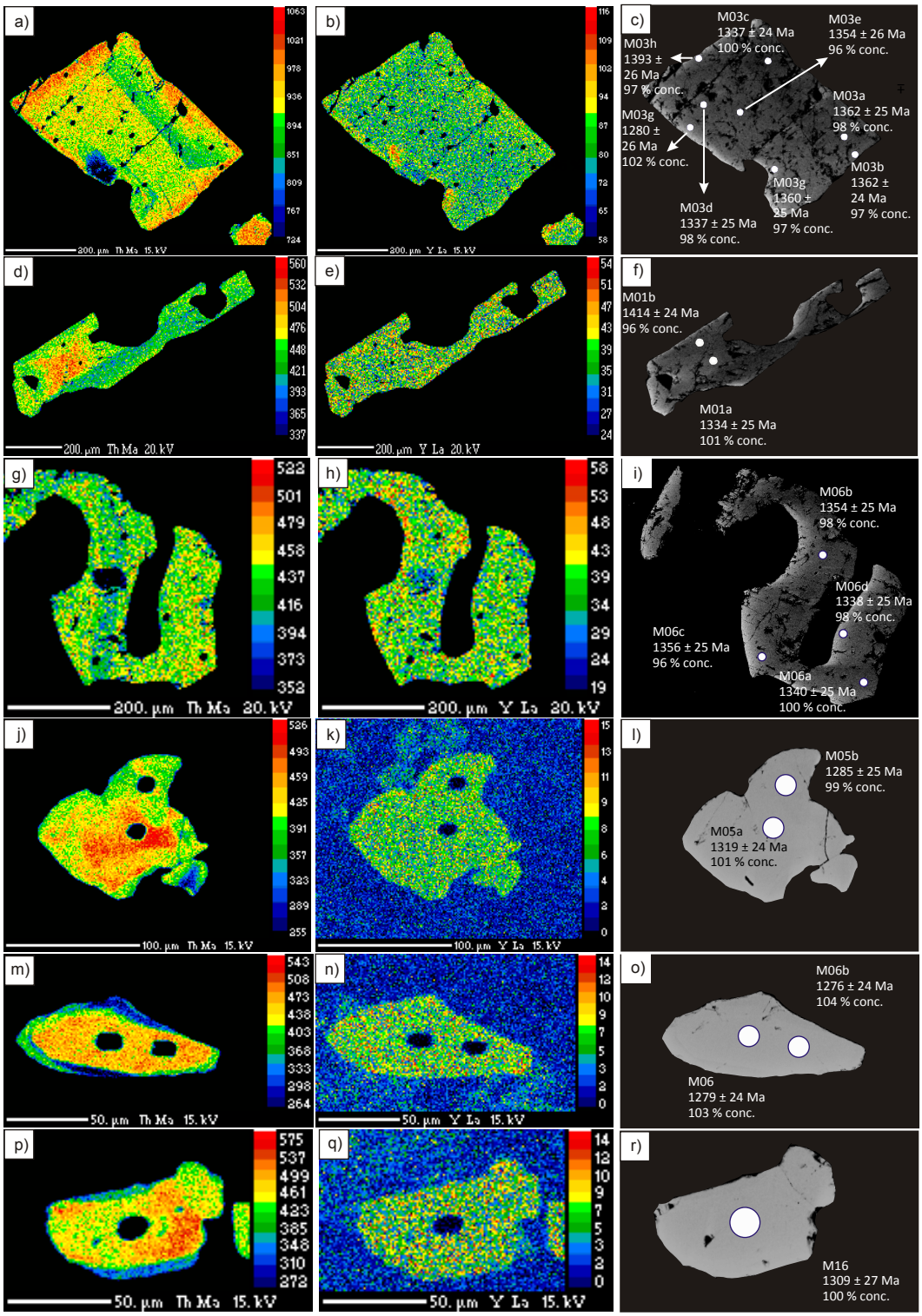


Fig. 5. Th and Y EPMA maps, and BSE images of monazite grains from samples 115866 (a–i) and 115638 (j–r) with location of LA-ICP-MS spot and $^{207}Pb/^{206}Pb$ ages shown.

grains from the matrix. Seventeen analyses yield results within 100 ± 5 % concordancy and plot on a linear array (Fig. 8c, d). These analyses are considered to be one population and yield a $Pb^{207}/Pb^{206}$ age weighted average of 1295 ± 11 Ma ($n$ = 17, MSWD = 0.63, 95 % confidence).

### *5.1.6. Sample 115866 (garnet–orthopyroxene gneiss, Connaughton Terrane)*

Monazite grains are ~50 to 1000 µm in size and show internal morphologies in BSE imagery that vary from no visible zoning, lighter cores to irregular zoning. Th and Y

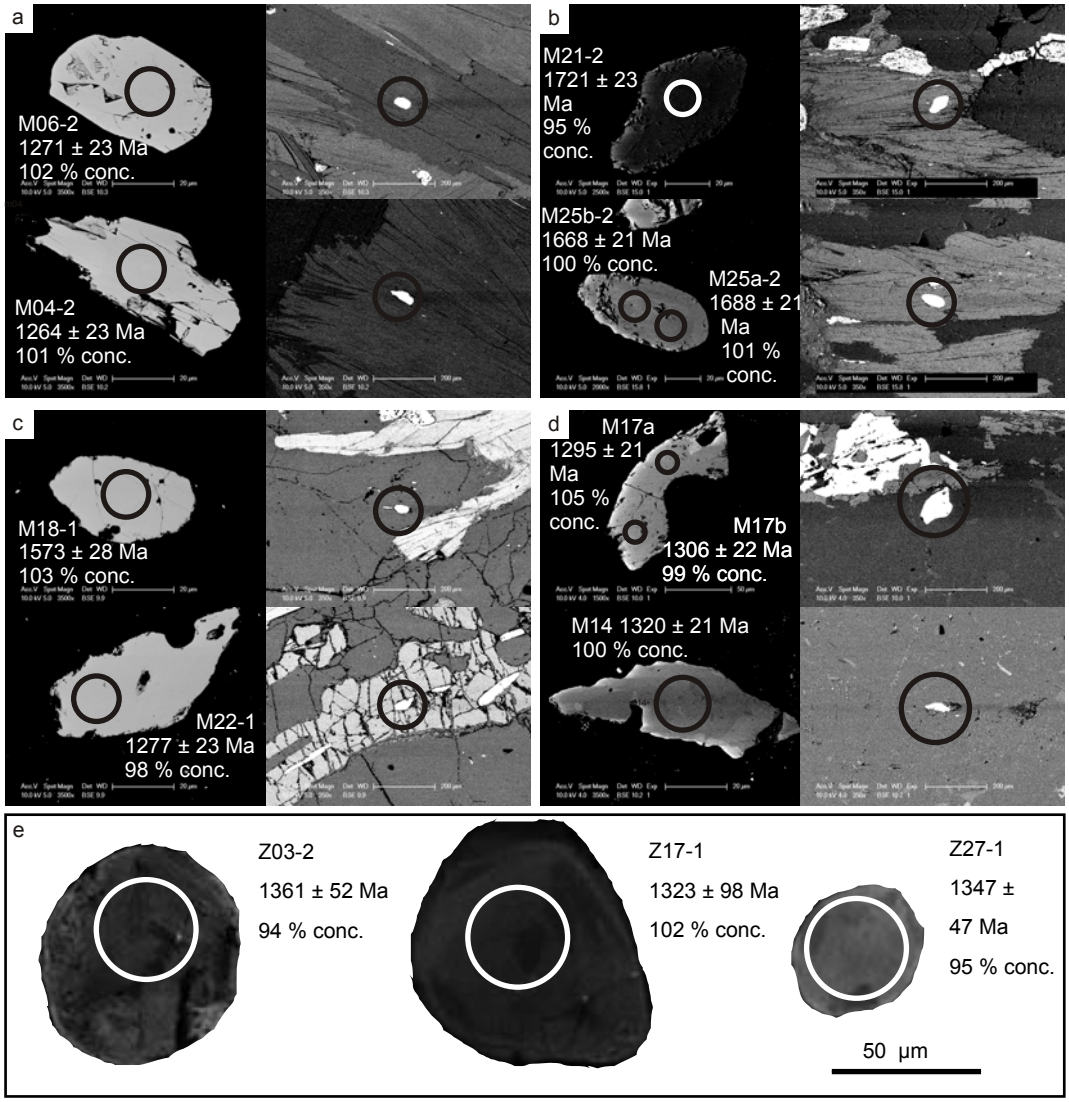


Fig. 6. BSE images of monazite grains from a) sample 103603D, b) sample 103617, c) sample 103618, and d) 115669. Cathodoluminescence images of zircon from sample 113019 (e).

elemental maps for representative monazite grains show zoning in Th, with higher Th in cores for some grains, and at grain boundaries for other grains (Fig. 5a–i). Y zoning in monazite grains are limited to patchy domains of higher or lower Y or some increase in Y at the edges of grains. There is no consistent correspondence between Th or Y and age. Thirty-three analyses were obtained from grains located in the matrix; in contact with quartz and feldspar with some grains also in contact with magnetite and/or spinel or fine grained biotite. Thirty-one analyses are within 100 ± 5 % concordance and of these analyses all but one are considered to be one population using a linearised probability plot (Fig. 8e, f). The age population yields a calculated $Pb^{207}/Pb^{206}$ age weighted average of 1341 ± 10 Ma ($n$ = 30, MSWD = 1.13, 95 % confidence). No correspondence between age and internal morphology or textural location was observed.

### *5.2 Zircon U–Pb Geochronology*

In cathodoluminescence imagery, zircon grains typically show moderately luminescent irregular/patchy zoning that in some grains overprint faint linear or concentric zoning or surround a small (<20 µm), strongly luminescent core. Fir-tree zoning in some grains is similar to those of zircons that have grown or recrystallized during high-grade metamorphism (Fig. 5e; Corfu et al., 2003). Sixty-six analyses were obtained from homogeneous, patchy/irregular and fir-tree zoned domains. Rims and highly luminescent cores were too narrow or small to be analysed via LA–ICP–MS. Zircon analyses commonly

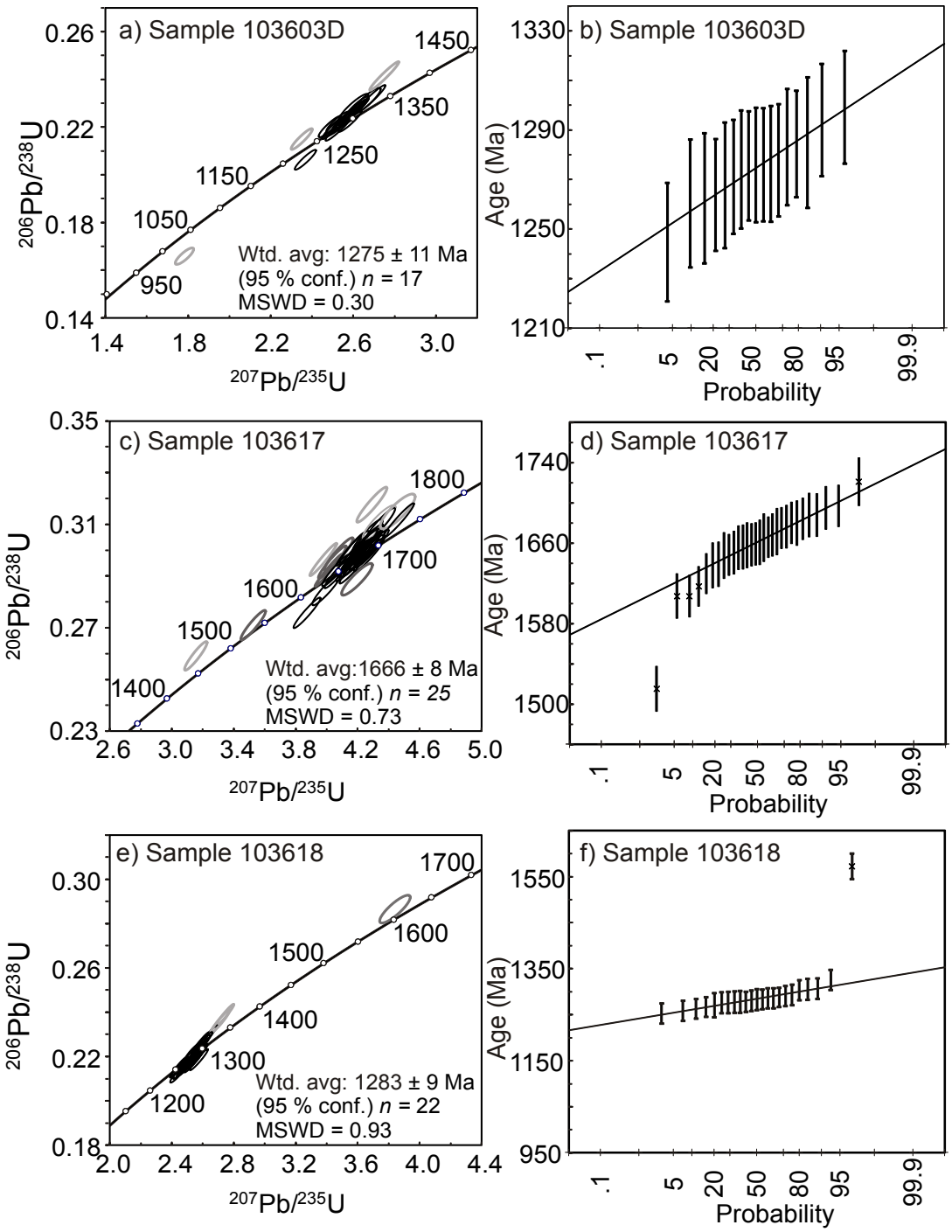


Fig. 7. Monazite age data for the Talbot Terrane showing $^{207}Pb/^{206}Pb$ age weighted averages, concordia and linearised probability diagrams for samples. Black ellipses indicate 100 ± 5 % concordant analyses that form along a straight line in linearised probability density diagrams, and are used to calculate age weighted averages. Light grey ellipses indicate >5 % discordant analyses that are not included in either weighted average calculations or the linearised probability diagrams. Medium grey ellipses indicate analyses indicate analyses that are within 100 ± 5 % concordancy but do not lie on a straight line in the linearised probability plots (shown as analyses with crosses), and are not included in weighted average calculations.

yielded low $^{206}Pb$, $^{207}Pb$, $^{208}Pb$ and $^{238}U$ cps, and analyses with noisy isotopic signals were not included in calculations (full dataset is provided in Appendix 2). Thirty analyses are displayed in Figure 8g−h. Nineteen analyses are within 100 ± 10 % concordance and yield a $^{207}Pb/^{206}Pb$ age range between 1433 and 1323 Ma. A $^{207}Pb/^{206}Pb$ weighted average age for the above < 10 % discordant analyses of 1377 ± 26 Ma was calculated ($n$ = 19, MSWD = 0.35, 95 % confidence).

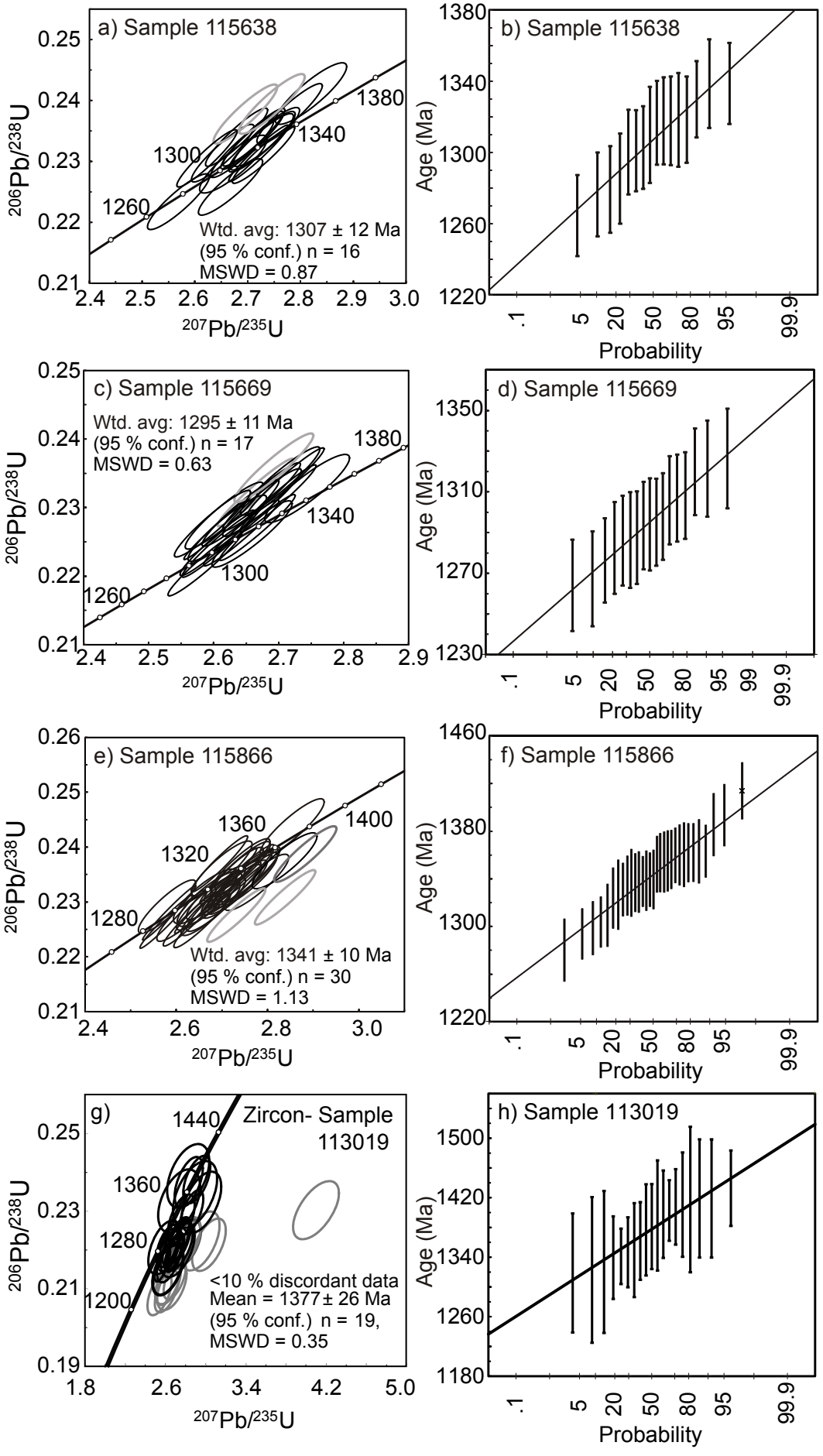
a) Sample 115638
Wtd. avg: 1307 ± 12 Ma
(95 % conf.) n = 16
MSWD = 0.87
b) Sample 115638
c) Sample 115669
Wtd. avg: 1295 ± 11 Ma
(95 % conf.) n = 17
MSWD = 0.63
d) Sample 115669
e) Sample 115866
Wtd. avg: 1341 ± 10 Ma
(95 % conf.) n = 30
MSWD = 1.13
f) Sample 115866
g) Zircon- Sample 113019
<10 % discordant data
Mean = 1377± 26 Ma
(95 % conf.) n = 19,
MSWD = 0.35
h) Sample 113019
206Pb/238U
207Pb/235U
Age (Ma)
Probability

Fig. 8 (previous page), a–f) monazite age data for the Connaughton Terrane showing $^{207}Pb/^{206}Pb$ age weighted averages, concordia and linearised probability diagrams. See Figure 7 caption for monazite concordia ellipse shading explanation, g–h) zircon age data for sample 113019 showing $^{207}Pb/^{206}Pb$ age weighted average, concordia and linearised probability diagrams. Black ellipses are 100 ± 10% concordant analyses used in calculation of $^{207}Pb/^{206}Pb$ age weighted average. Light grey ellipses are analyses are >10% discordant.

### *5.3 Zircon and garnet trace element characteristics*

Representative trace-element chemistry for garnet and zircon grains from sample 113019 is provided in Appendix 2 and chondrite normalised REE patterns are shown in Fig. 9. Trace element abundances in garnet were measured by LA–ICP–MS spot analyses across two garnet grains ~1500 μm in diameter. Both garnet grains contain inclusion-rich cores and inclusion-poor rims. Chondrite-normalized REE patterns for garnet show variable but more enriched and steeper HREE within the cores of garnet ($Lu_N/Gd_N$ = 12.64–72.96; $Lu_N$ = 60–373) relative to garnet rims ($Lu_N/Gd_N$ = 1.71–5.07; $Lu_N$ = 13–34). 100 ± 10% concordant zircon grains have HREE patterns are enriched relative to chondrite and show patterns that vary from shallow to steep ($Lu_N$ = 24–557; $Lu_N/Gd_N$ = 1.66–11.35). Core analysis 06 contains two orders of magnitude higher concentration of Zr, and is considered likely to be contaminated by very fine (~5 μm) inclusion(s) of zircon present in garnet grains (Appendix 2, not plotted in Figure 9). Eu anomalies were not able to be calculated for some garnet analyses due to Sm concentrations below detection limit. However, for analyses where the Eu anomaly was able to be calculated, the garnet 1 core lacks a pronounced Eu anomaly (Eu/Eu* = 1.04), whereas the garnet 1 rim has a negative Eu anomaly (Eu/Eu* = 0.63). For zircon analyses where the Eu anomaly was able to be calculated, zircon has a positive Eu anomaly (Eu/Eu* = 1.18–1.55).

### *5.4 P–T phase diagram modelling*

#### *5.4.1. Sample 103618 (staurolite–biotite-bearing pelite, Talbot Terrane)*

The calculated *P–T* pseudosection for sample 103618 based on the geochemical whole rock analysis is presented in Figure 10a. The peak assemblage for sample 103618 is interpreted as staurolite–biotite–chlorite–plagioclase–quartz–ilmenite–magnetite and is interpreted to have formed under subsolidus conditions. $H_2O$ was set to excess and for simplicity is assumed to have been part of the peak assemblage. The stability field corresponding to the peak *P–T* assemblage occurs at ~5.5–8.5 kbar, 600–650 °C (70–120 °C $kbar^{-1}$), which is taken as the best estimate for peak *P–T* conditions.

#### *5.4.2. Sample 113019 (garnet–diopside bearing amphibolite, Connaughton Terrane)*

A *P–T* pseudosection calculated for sample 113019 is presented in Fig. 10b. The stability field corresponding to the interpreted peak assemblage garnet–diopside–plagioclase–hornblende–quartz–titanite(sphene)–$H_2O$ (outlined in bold), occurs at ~8–11 kbar, ~620–650 °C, and corresponds to apparent thermal gradients of ~60–80 °C.$kbar^{-1}$. The post-peak evolution is interpreted to involve a relative decrease in garnet and diopside abundance, and relative increase in plagioclase and hornblende abundance. Using relative modal proportion trends for garnet, diopside, hornblende and plagioclase, the post-peak evolution is inferred to have involved a decrease in *P* and *T*. This *P–T* evolution is similar to that inferred by Smithies and Bagas (1997).

## 6. Discussion

### *6.1 Garnet and zircon chemistry*

Trace element analyses from garnet-bearing amphibolite (sample 113019) in the Rudall Province show enriched, positive sloping normalized HREE trends for garnet cores, and typically show enriched, shallowly positive sloping to negatively sloping normalized HREE trends for garnet rims (Fig. 9), suggesting that during the growth of garnet rims, garnet may have been competing with another phase for HREE (cf. Rubatto, 2002). Zircon REE analyses show positive sloping HREE trends, suggesting that zircon grains may have grown at a time where chemical communication with a HREE reservoir

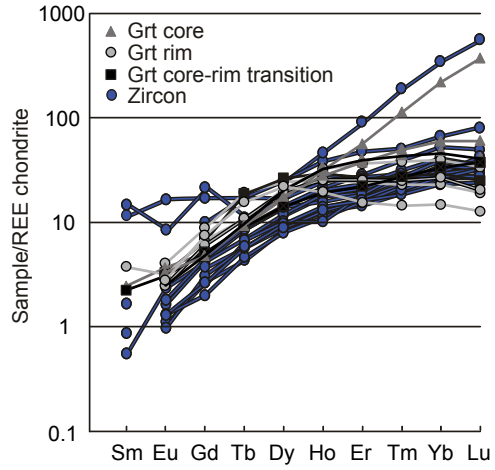


Fig. 9. Chondrite normalised garnet and zircon REE data for sample 113019.

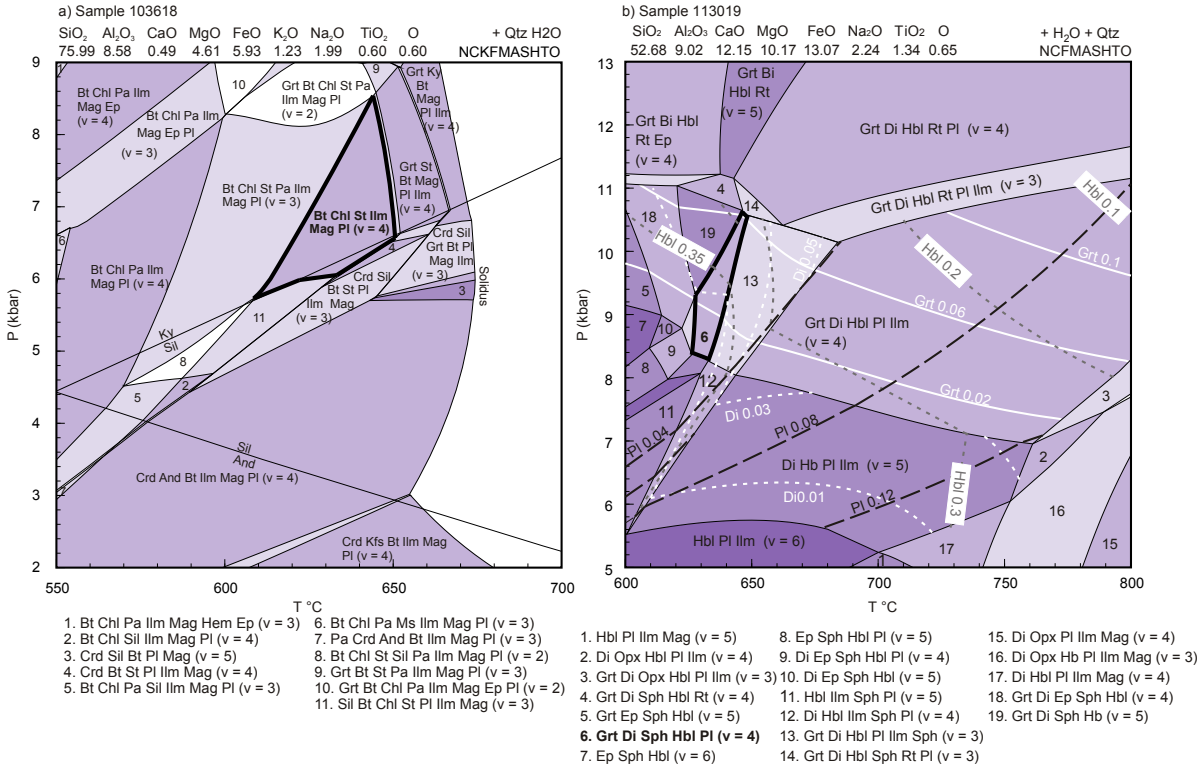


Fig. 10. *P–T* pseudosections for a) sample 103618, peak stability field biotite–chlorite–staurolite–plagioclase–ilmenite–magnetite–quartz–$H_2O$ (v = 4) is shown in bold, and b) P–T pseudosection for sample 113019. Peak stability field garnet–diopside–plagioclase–sphene–hornblende–quartz–$H_2O$ (v = 4) is shown in bold. Modal abundance contours are shown for hornblende (Hbl), plagioclase (Pl) and diopside (Di).

occurred (Fig. 9; cf. Rubatto et al., 2013). Titanite can also incorporate Zr and REEs (e.g. Storkey et al., 2005; Hayden et al., 2008), and it is therefore possible that the positive HREE slope in zircon reflects zircon growth while either titanite or garnet was decreasing in abundance. Mid to heavy REE distribution coefficients of zircon/garnet ($^{REE}D_{zir/gt}$) are close to 1 (Fig. 9), which is similar to empirical $^{REE}D_{zir/gt}$ values obtained where zircon and garnet are interpreted to have co-existed together (e.g. Whitehouse and Platt, 2003; Taylor et al., 2014). The zircon U–Pb age data from diopside–garnet bearing amphibolite sample 113019 is therefore considered to record the timing of moderate-thermal gradient, medium to high-*P* metamorphism (weighted average of 1377 ± 26 Ma).

### *6.2 Timing of regional metamorphism in the Rudall Province*

The Rudall Province is interpreted to have undergone multiple phases of deformation during the Paleoproterozoic to late Neoproterozoic (e.g. Smithies and Bagas, 1997; Bagas et al., 2000; Bagas, 2004). The earliest identified metamorphic event, the $M_1$–$D_1$ phase of the Yapungku Orogeny, produced layer parallel schistosity and is interpreted to have developed poorly preserved andalusite bearing assemblages (Hickman and Bagas, 1999). These rare $M_1$ assemblages have not been dated directly, but have been inferred to be *c.* 1800 Ma, based on a recently reinterpreted intrusive age of the protolith to a banded orthogneiss (*c.* 1801 Ma; Kirkland et al., 2013) that is interpreted to have intruded pre or early $D_1$, and the *c.* 1800–1760 Ma ages of post-$D_1$ intrusives of the Kalkan Supersuite (Nelson, 1995; Hickman and Bagas, 1998). Andalusite bearing assemblages could reflect contact metamorphism associated with the intrusion of the Kalkan Supersuite.

The timing of the $D_2$–$M_2$ phase of the Yapungku Orogeny was previously interpreted to be *c.* 1800–1765 Ma based on intrusive protolith ages of the variably deformed Kalkan Supersuite, which is considered to have intruded throughout the Yapungku Orogeny (e.g. Nelson, 1995, 1996; Hickman and Bagas, 1998; Bagas et al., 2000; Bagas, 2004). The minimum age for the Yapunkgu Orogeny was constrained at 1778 ± 16 Ma using zircon U−Pb age data from an aplite dyke that is inferred to have intruded a syn-$D_2$ serpentinised ultramafic rock (Nelson, 1995; Bagas, 2004). However, Maidment (2014) recognised that aplite dykes in the Rudall Province are variably overprinted by $S_2$ and therefore may only provide a maximum age constraint for the $D_2$ Yapungku Orogeny. In this study, zircon and in situ monazite U–Pb age data were collected from samples from the Talbot and Connaughton Terranes in order to provide further direct age constraints on metasedimentary-derived rocks. The samples have previously been inferred to contain: 1) $S_1$ inclusion trails in garnet (sample 113019), 2) an $S_2$ fabric (samples 103603D, 103617, 103618, 113019, 115638, 115669); and 3) inferred to be late to post $S_2$ (sample 115866; garnet in sample 115638; sillimanite in sample 115669; results summarised in Table 3; structural characteristics from Smithies and Bagas, 1997; Bagas and Smithies, 1998; Clarke pers. comm). Metamorphic zircon age data combined with zircon and garnet trace element chemistry from sample 113019 is suggestive of moderate thermal gradient, high grade metamorphism occurring at *c.* 1377 Ma. The zircon U–Pb age data from sample 113019, although imprecise does not show more than one age population. This may indicate that if the inclusion trails in garnet do indeed represent an earlier fabric than the main $S_2$ fabric of the rock (e.g. Bagas and Smithies, 1998), both fabrics developed in a shorter time span than the resolution of the LA–ICP–MS data, or the analysed zircon does not record or preserve the development of both fabrics.

A number of workers have argued that monazite growth or recrystallisation can occur under a variety of conditions during subsolidus metamorphism (e.g. Pyle and Spear, 2003; Kohn and Malloy, 2004; Rubatto et al., 2006; Corrie and Kohn, 2008; Spear and Pyle, 2010; Gasser et al., 2012), high-grade metamorphism and/or along the retrograde path during high-grade metamorphism in rocks that have melted (e.g. Rubatto, 2002; Rubatto et al., 2006; Kelsey et al., 2007; Kelsey et al., 2008; Gasser et al., 2012; Korhonen et al., 2013; Rubatto et al., 2013; Clark et al., 2014; Yakymchuk and Brown, 2014), and diagenesis, hydrothermal mineralisation or fluid alteration/flow (e.g. Williams et al., 2011; Muhling et al., 2012; Halpin et al., 2014). Monazite U–Pb analyses from samples from the Connaughton Terrane together yield age populations between *c.* 1340−1295 Ma. This age range is somewhat younger than an imprecise U−Pb age weighted average of *c.* 1377 ± 26 Ma from metamorphic zircons obtained from a garnet-bearing amphibolite (sample 113019). Whereas as an absence of leucosomes in sample 115669 (quartz-rich, kyanite−sillimanite−quartz metasediment) may suggest that partial melting was limited or did not occur, samples 115638 and 115866 contain leucosomes that are interpreted as a record of partial melting. For rocks that have melted for a typical metapelitic or greywacke composition, it has

been suggested based on thermobarometric modelling that monazite is likely to record an age along the retrograde metamorphic *P–T* path (Kelsey et al., 2008; Yakymchuk and Brown, 2014). The monazite grains in these samples are interpreted to have grown on the high-*T* retrograde part of the *P–T* path and may record the crossing of the elevated solidus at *c.* 1341–1307 Ma (e.g. Korhonen et al., 2013). Sample 115669 (kyanite−sillimanite bearing quartzite) is younger outside of uncertainty of sample 115866. As some of the kyanite grains appear to be partially recrystallised parallel to the foliation, it is possible that the high strain foliation development in sample 115669 occurred locally (e.g. close to shear zones) and/or that tectonism during the Mesoproterozoic may be diachronous or involve multiple phases (discussed below).

In the Talbot Terrane, two monazite U–Pb age brackets are obvious in the dataset from this study, at *c.* 1665 Ma and *c.* 1285–1275 Ma. The *c.* 1665 Ma age population was obtained from a single sample (sample 130617; staurolite-bearing schist), whereas the *c.* 1285–1275 Ma age populations were obtained from a staurolite-bearing schist (sample 103618), which is interpreted to contain a S−C fabric defined by chlorite, biotite and staurolite, and a retrogressed kyanite-bearing metapelite (sample 103603D). Some monazite grains in all three samples occur at silicate mineral grain boundaries, in contact with retrograde chlorite or sericite or contain very fine grained inclusions. It is therefore possible that some grains may have grown or recrystallised after peak metamorphism (e.g. during retrogression in sample kyanite bearing sample 103603D). However, the U–Pb ages obtained from the above monazite grains (i.e. silicate grain boundaries) are instinguishable from the remainder of monazite ages from each sample and from the Talbot Terrane are therefore considered to comprise single population in each sample.

The results do not support the contention that the regional peak metamorphism in the Rudall Province was synchronous with the emplacement of the *c.* 1800−1760 Ma Kalkan Supersuite. Instead, the age data suggests that the Rudall Province underwent its main episodes of metamorphism and associated deformation well after the emplacement of the Kalkan Supersuite in the Mesoproterozoic. We consider that the *c.* 1665 Ma monazite age population obtained from a single metapelite in the Talbot Terrane possibly records a poorly preserved tectonothermal event that reached amphibolite facies in the Talbot Terrane. However, it however remains unclear whether the rocks in the Connaughton Terrane also experienced this event.

### *6.3 Characterising physical and thermal conditions of metamorphism in the Rudall Province*

*P–T* pseudosections were calculated for staurolite-bearing sample 103618 from the Talbot Terrane, and garnet–diopside bearing amphibolite sample 113019 from the Connaughton Terrane to investigate the physical conditions of metamorphism. Existing metamorphic work from the Rudall Province has focused on the elucidation of the Yapungku Orogeny ($D_2$–$M_2$) in both the Talbot and Connaughton Terranes assuming the age is *c.* 1800−1760 Ma (Clarke, 1991; Smithies and Bagas, 1997). Rocks in the Talbot and Connaughton Terrane have been interpreted to have experienced moderate-thermal gradient conditions, followed by a steeply decompressive post-peak *P–T* evolution during the Yapungku Orogeny (Smithies and Bagas, 1997).

In this study, amphibolite sample 113019 of the Connaughton Terrane is interpreted to have reached peak *P−T* conditions of ~8–11 kbar, 620–650 °C (apparent thermal gradients of ~60−80 °C $kbar^{-1}$), followed by a clockwise post-peak evolution. The inferred clockwise post-peak evolution for amphibolite sample is similar to the steeply decompressive post peak *P–T* evolution inferred by Smithies and Bagas (1997), yet the peak temperature obtained in this study is somewhat lower than those obtained by Smithies and Bagas (1997) for the same garnet-bearing amphibolite lithology (up to ~12 kbar, ~770 °C in Smithies and Bagas, 1997). This may be a result of a difference in methodology (conventional thermobarometry compared to *P–T* pseudosection, see Powell

and Holland, 2008). It is possible that the discrepancy in temperature estimates may be partly related to the modelled stability of ilmenite and titanite in the pseudosection for sample 113019. In Fig. 10b, the stability field for the peak assemblage is bounded at the high-*T* side by the introduction of ilmenite stability, which is not present in the sample. In the adjacent higher-*T* stability field containing ilmenite (field 13), modelled ilmenite is present in small modal proportions (<0.02). It is possible that the modelled stability of titanite and ilmenite in *P–T* space may be sensitive to small differences in the modelled bulk rock composition compared to the true bulk composition (e.g. small differences in $Fe^{3+}$ or Ti). As a result, we consider Smithies and Bagas (1997) temperature estimates of ~770 °C as the upper limit for the estimated temperature experienced by the garnet-bearing amphibolite during the $D_2$ Yapungku Orogeny. *P−T* constraints from staurolite-bearing sample 103618 from the Talbot Terrane in this study implies a moderate to high thermal-gradient regime during Mesoproterozoic metamorphism (~75−110 °C $kbar^{-1}$), and is comparable to qualitative *P–T* estimates obtained by Clarke (1991). Due to a lack of reaction microstructures in sample 103618 (Talbot Terrane), the post-peak evolution could not be constrained.

Smithies and Bagas (1997) describe a ~400 $m^2$ garnet−orthopyroxene bearing outcrop ('charnockite' unit in Bagas and Smithies, 1998), from which they obtained very high-thermal gradient *P–T* conditions (~2–4 kbar, ~800 ºC), and interpreted the unit to have been metamorphosed after $D_2$–$M_2$, resulting from possible higher crustal level, post- $D_2$ granitoids. Garnet–orthopyroxene sample 115866 comes from the same locality and is petrographically identical to the garnet-orthopyroxene sample of Smithies and Bagas (1997). The inferred *P−T* evolution of the garnet–orthopyroxene bearing rock (Smithies and Bagas, 1997) contrasts with: a) the constrained lower-thermal gradient regime calculated for the mafic-amphibolites from the Connaughton Terrane, and b) the decompressional post-peak *P−T* evolution inferred for $M_2$−$D_2$ (Smithies and Bagas, 1997; this study). Within the Connaughton Terrane, a post-$D_2$ garnet microgneiss and pegmatite yield U−Pb zircon crystallisation ages of *c.* 1222 and *c.* 1291 Ma respectively (Nelson, 1995, 1996), with a zircon analysis of *c.* 1200 Ma from the garnet microgneiss recently reinterpreted as metamorphic (Kirkland et al., 2013). These constraints suggest that late partial melts probably accompanied Mesoproterozoic metamorphism in the Rudall Province. It is possible that the orthopyroxene-garnet gneiss underwent metamorphism proximal and related to as yet unidentified *c.* 1340 Ma magmatism.

### *6.4 Implications for the assembly of the NAC and WAC*

The Yapungku Orogeny has been interpreted to reflect the collision of the NAC and WAC, which has been used as a basic element of most models that describe the assembly and development of Proterozoic Australia (e.g. Betts and Giles, 2006; Cawood and Korsch, 2008; Payne et al., 2009). The metamorphic record of the Yapungku Orogeny has been interpreted to record thrust stacking and crustal thickening, leading to amphibolite and granulite facies metamorphism (e.g. Smithies and Bagas, 1997; Bagas, 2004).

Mesoproterozoic monazite U–Pb age populations obtained in this study range from *c.* 1340–1275 Ma, and zircon U–Pb age data from amphibolite sample 113019 yielded an age population of *c.*1377 Ma. We consider that both the moderate- to high thermal gradient Yapungku Orogeny ($M_2$–$D_2$) and localised high-thermal gradient metamorphism in the Rudall Province are most likely to be Mesoproterozoic-aged, based on the Mesoproterozoic-aged monazite and zircon obtained in this study. Together the zircon and monazite ages span ~100 M.y. (Fig. 11; Table 3). It is possible that this age range reflects: a) monazite and zircon from moderate thermal gradient rocks growing along different stages of the *P–T* evolution (e.g. possibly zircon growth on the prograde path, monazite recrystallisation in sample 103603D and 103618 post-dating peak metamorphism), b) diachroneity in metamorphism/deformation between terranes and some magmatically-driven metamorphism at least on a local scale,

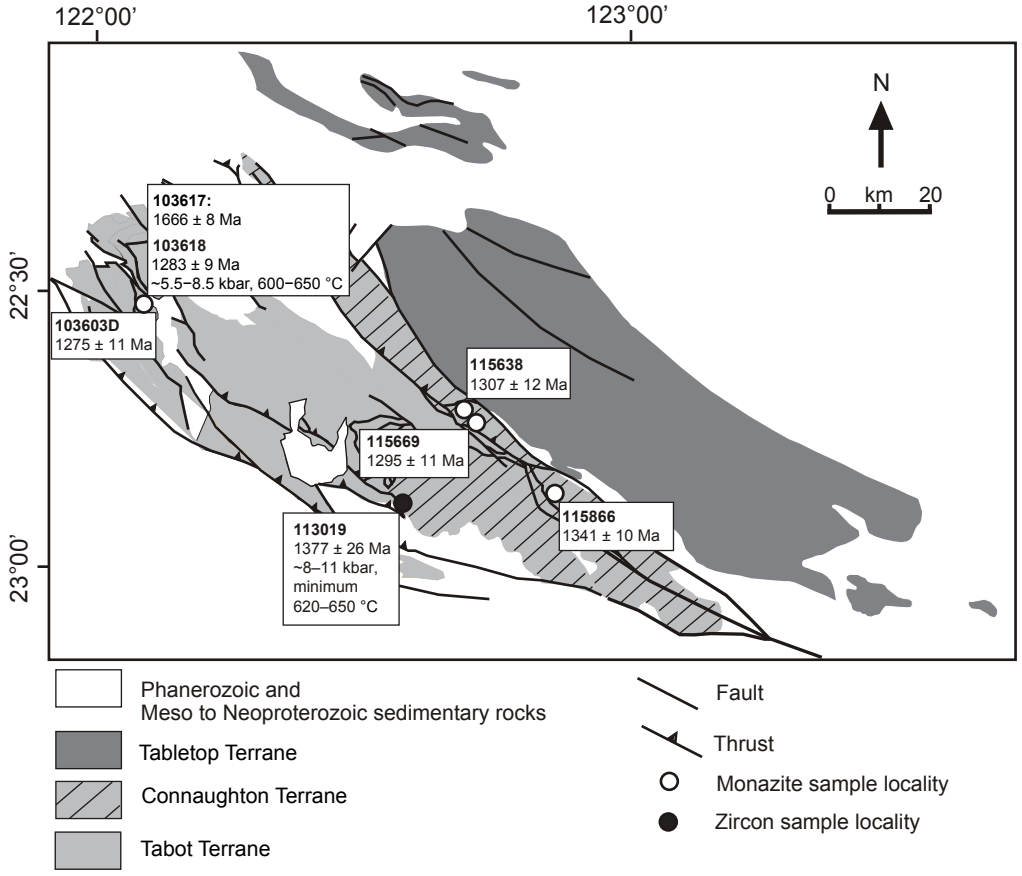


Fig. 11. Simplified map of the Rudall Province showing spatial distribution of zircon and monazite age data and *P–T* constraints from this study.

Table 3. Summary of U–Pb monazite and zircon age data, and *P–T* estimates obtained in this study

| Terrane | Sample | Easting (m E) | Northing (m N) | Mineralogy | Fabric^ | Monazite Age (Ma, 95 % conf.) | *P–T* estimates (kbar, °C) |
|---|---|---|---|---|---|---|---|
| Talbot | 103603D | 404733 | 7511111 | Ky-Pl-Rt-Ilm (+Chl-Ms-Ser) bearing metapelite | S2 | 1275 ± 11 | |
| Talbot | 103617 | 405958 | 7511738 | St-Bt-Pl-Ilm-Mag-Qtz, (+Chl) metapelite | S2 | 1666 ± 8 | |
| Talbot | 103618 | 405958 | 7511738 | St-Bt-Pl-Ilm-Qtz-Chl-Mag metapelite | S2 | 1283 ± 9 | ~5.5–8.5, 600–650 |
| Connaughton | 115638 | 466506 | 7489683 | Grt-Sil-Pl-Kfs-Qtz-Rt-Ilm metasediment | S2, late-post S2? | 1307 ± 12 | |
| Connaughton | 115669 | 469624 | 7485385 | Ky-Sil-Qtz-Ilm-Mag (+Ms, Ctd) metasediment | S2, sillimanite late-post S2? | 1295 ± 11 | |
| Connaughton | 115866 | 485181 | 7472585 | Opx-Grt-Mag-Ilm-Pl-Kfs-Qtz (+ Bt-Chl) gneiss | post-S2 | 1341 ± 10 | |
| Connaughton | 113019 | 457200 | 7467600 | Di-Grt-Pl-Qtz-Hb-Ttn mafic amphibolite | S1(?)/S2 | 1377 ± 26 | ~8–11, 620–650, decreasing *P–T* post-peak evolution |

^ From Smithies and Bagas (1997); Bagas and Smithies (1998) or Clarke (pers. comm)

Co-ordinates in UTM, GDA 94, Zone 51K, approximate from aerial photography

c) a long-lived metamorphic/tectonic event, or d) different metamorphic events. Of these alternatives, we tentatively suggest that the range of metamorphic ages is best explained through a stage-wise development of the Rudall Province that involved the accretion of 'ribbons' that were previously derived from the margin of the WAC (cf. Kirkland et al., 2013). In the above proposed tectonic scenario, both moderate thermal gradient and high thermal gradient metamorphic conditions could be attained via accretion (or reattachment) and subsequent outboard migration of subduction, placing accreted the ribbon(s) in a back-arc/arc setting. In this proposed scenario, the final closure of the system probably occurred at *c.* 1300−1280 Ma, or later, marked by the collision of the NAC with ribbons that accreted with the WAC. In this model, the suture between the NAC and accretionary edge to the WAC would lie to the northeast of the Rudall Province, consistent with Kirkland et al. (2013) who showed that the rocks of the Rudall Province have affinities to the WAC.

In the step-wise Mesoproterozoic accretion hypothesis outlined previously, the Yapungku Orogeny is not a single event. Instead, we envisage it to be an accretionary system marked by episodes of thermally contrasting metamorphism that record either the accretion of ribbons or inter-accretionary extension during the Mesoproterozoic. It is not clear to what extent the Rudall Province records the complete amalgamation of the WAC and NAC. The arrangement of rock units and Mesoproterozoic age domains within the Rudall Province have been complicated by later reworking, most notably during the Miles Orogeny and the late Neoproterozoic to Cambrian Paterson Orogeny, the latter involving a substantial amount of strike-slip movement (e.g. Hickman and Bagas, 1999; Bagas, 2004).

The Mesoproterozoic-aged medium-*P* metamorphism in the Rudall Province broadly coincides with the timing of major phases of tectonism in the Musgrave and Albany Fraser Orogens (e.g. Myers et al., 1996; Giles et al., 2004; Betts and Giles, 2006; Cawood and Korsch, 2008; Wade et al., 2008; Aitken and Betts, 2009; Spaggiari et al., 2009; Smithies et al., 2011). Stage I of the Albany Fraser Orogeny (*c.* 1340–1260 Ma) has been interpreted to be a response to the collision of the WAC with the SAC/Mawson Continent (e.g. Clark et al., 2000) and/or alternatively reflect the closure of a marginal ocean basin and accretion of the Loongana Magmatic Arc to the WAC, prior to the final convergence of the WAC and SAC/Mawson Continent (Spaggiari et al., 2014). In the western Musgrave Province, the tectonic setting of the *c.* 1345–1292 Ma Mount West Orogeny remains uncertain. However, the Mount West Orogeny involved the emplacement of metaluminous, calc to calc-alkaline granitoids of the Wankanki Supersuite, which are geochemically similar to those that occur in modern day continental-arc settings (Smithies et al., 2010; Smithies et al., 2011).

The temporal similarities of Mesoproterozoic tectonism in the Albany-Fraser Orogen, Musgrave and Rudall Provinces and the spatial occurrence of these three provinces/orogens either on the margin of, or between, older Archean–Paleoproterozoic cratonic elements suggests that Mesoproterozoic tectonism may reflect the protracted amalgamation of the WAC, NAC and SAC between *c.* 1375 and 1150 Ma (e.g. Myers et al., 1996; Smits et al., 2014).

### *6.5 Implications for supercontinent Nuna reconstructions*

Globally, the *c.* 1400−1300 Ma timeline corresponds to the interpreted initiation of the breakup of supercontinent Nuna (Pisarevsky et al., 2014a; Pisarevsky et al., 2014b). An implication for the proposed Mesoproterozoic assembly of Proterozoic Australia is that the need for the components of Australia to be connected during supercontinent Nuna is no longer required. Recent paleomagnetic constraints from the WAC indicate Australia and Laurentia were widely separated by *c.* 1210 Ma (Pisarevsky et al., 2014b). We suggest that following the accretion of the NAC to Laurentia at *c.* 1550−1500 Ma in either a modified SWEAT (South West U.S.-East Antarctic; Moores, 1991) or AUSWUS (Australia-Western U.S.; Karlstrom et al., 1999) style

configuration (Fig. 12a), the NAC migrated as a ribbon away from Laurentia at *c.* 1450 Ma (e.g. Medig et al., 2014) and collided with the WAC at *c.* 1300 Ma (Fig. 12b). In Laurentia, removal of the NAC ribbon coincided with the formation of the rift Belt Superbasin system. The Mawson Continent (SAC and east Antarctica) collided with the NAC−WAC between *c.* 1250−1150 Ma (e.g. Smits et al., 2014). If correct, Laurentia and Australia have been disconnected since the late Mesoproterozoic and a Neoproterozoic SWEAT connection is not likely. In our preferred model, a Mesoproterozoic AUSWUS-style connection by *c.* 1250 Ma (Fig. 12c) allows the transcontinental Musgrave-Albany Fraser orogen (Smits et al., 2014) to directly connect with the Grenvillian super-orogen (cf. Van Kranendonk and Kirkland, 2013).

## 7. Conclusions

The age of the Yapungku Orogeny in the Rudall Province has long been interpreted to be Paleoproterozoic. However, monazite age data from metasedimentary rocks of the Connaughton and Talbot Terrane indicate the Yapungku Orogeny ($D_2$−$M_2$) is Mesoproterozoic-aged. We propose that medium-*P* metamorphism with moderate to high-thermal gradients reflects the amalgamation of the WAC and NAC during the Mesoproterozoic rather than Paleoproterozoic via a stage-wise evolution. If this is correct, a Mesoproterozoic timeline for the amalgamation of the major cratonic elements of Proterozoic Australia is supported, which feasibly occurred during the breakup stages of supercontinent Nuna.

## References


Aitken, A.R.A., Betts, P.G., 2009. Constraints on the Proterozoic supercontinent cycle from the structural evolution of the south-central Musgrave Province, central Australia. Precambrian Research 168, 284-300.

Bagas, L., 2004. Proterozoic evolution and tectonic setting of the northwest Paterson Orogen, Western Australia. Precam brian Research 128, 475-496.

Bagas, L., Smithies, R.H., 1998. Geology of the Connaughton 1:100 000 Sheet, 1:100 000 Geological Series Explanatory Notes. Geological Survey of Western Australia, Perth, p. 38.

Bagas, L., Williams, I.R., Hickman, A.H., 2000. Rudall, 1:250 000 Geological Series Explanatory Notes, 2 ed. Western Australia Geological Survey, Perth, p. 50.

Betts, P.G., Giles, D., 2006. The 1800-1100 Ma tectonic evolution of Australia. Precambrian Research 144, 92-125.

Betts, P.G., Giles, D., Lister, G.S., Frick, L.R., 2002. Evolution of the Australian Lithosphere. Australian Journal of Earth Sciences 49, 661-695.

Betts, P.G., Giles, D., Mark, G., Lister, G.S., Goleby, B.R., Ailleres, L., 2006. Synthesis of the proterozoic evolution of the Mt Isa Inlier. Australian Journal of Earth Sciences 53, 187-211.

Brown, M., 2007. Metamorphic conditions in orogenic belts: a re cord of secular change. International Geology Review 49, 193-234.

Camacho, A., McDougall, I., 2000. Intracratonic, strike-slip parti tioned transpression and the formation and exhumation of eclogite facies rocks: An example from the Musgrave Block, central Australia. Tectonics 19, 978-996.

Cawood, P.A., Korsch, R.J., 2008. Assembling Australia: Proterozo


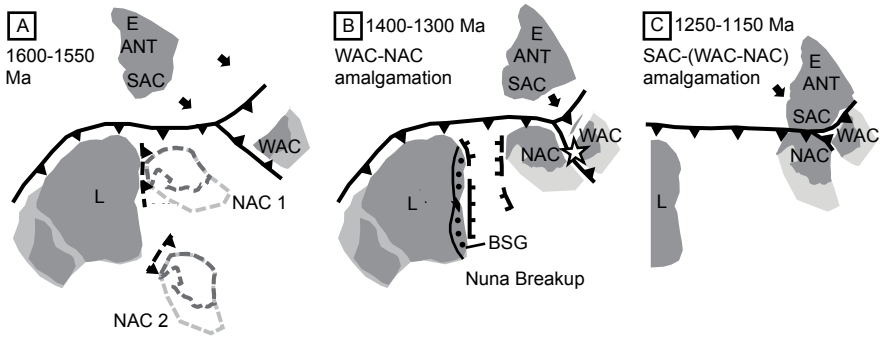


Fig. 12. Simplified schematic tectonic model of Proterozoic Australia and Laurentia at *c.* 1600−1550 Ma− arc extending from Laurentia to the WAC. Also shown are possible modified AUSWUS (NAC1; after Karlstrom et al., 1999) and SWEAT-like configurations (NAC2; after Moores, 1991). B: 1400−1300 Ma− NAC extracted from western Laurentia at around 1450 Ma, associated with development of Belt Supergroup rift system, docking of the WAC to NAC reflected by the Yapungku Orogeny in the Rudall Province (star), and commencement of Stage I of the Albany Fraser Orogeny (AFO) at *c.* 1330 Ma in modified AUSWUS style configuration. C: 1250−1150 Ma− final convergence of major cratonic elements of Proterozoic Australia (reconstruction following Li and Evans, 2011). BSG = Belt Supergroup and equivalents (Medig et al., 2014), L = Laurentia, E ANT = E Antarctica, SAC = South Australian Craton, NAC = North Australian Craton, WAC = West Australian Craton.

ic building of a continent. Precambrian Research 166, 1-38.
Chin, R.J., de Laeter, J.R., 1981. The relationship of new Rb-Sr iso topic dates from the Rudall Complex to the geology of the Paterson Province, Geological Survey of Western Australia Annual Report 1980, Perth, pp. 132-139.
Clark, C., Kirkland, C.L., Spaggiari, C.V., Oorschot, C., Wingate, M.T.D., Taylor, R.J., 2014. Proterozoic granulite forma tion driven by mafic magmatism: An example from the Fraser Range Metamorphics, Western Australia. Precambrian Research 240, 1-21.
Clark, D.J., Hensen, B.J., Kinny, P.D., 2000. Geochronological constraints for a two-stage history of the Albany-Fraser Orogen, Western Australia. Precambrian Research 102, 155-183.
Clarke, G.L., 1991. Proterozoic Tectonic Reworking In the Rudall Complex, Western Australia. Australian Journal of Earth Sciences 38, 31-44.
Coggon, R., Holland, T.J.B., 2002. Mixing properties of phengitic micas and revised garnet-phengite thermobarometers. Journal of Metamorphic Geology 20, 683-696.
Corfu, F., Hanchar, J.M., Hoskin, P.W.O., Kinny, P.D., 2003. Atlas of zircon textures, in: Hanchar, J.M., Hoskin, P.W.O. (Eds.), Zircon. Mineralogical Society of America, Reviews in Mineralogy and Geochemistry, Washington, D.C., pp. 468-500.
Corrie, S.L., Kohn, M.J., 2008. Trace-element distributions in silicates during prograde metamorphic reactions: impli cations for monazite formation. Journal of Metamorphic Geology 26, 451-464.
Czarnota, K., Gerner, E., Maidment, D., Meixner, A., Bagas, L., 2009. Paterson Area 1:250 000 Scale Solid Geology Interpretation and Depth to Basement Model. Geoscience Australia, Canberra.
Diener, J.F.A., Powell, R., White, R.W., Holland, T.J.B., 2007. A new thermodynamic model for clino- and orthoamphi boles in the system $Na_2O$-CaO-FeO-MgO-$Al_2O_3$-$SiO_2$-$H_2O$-O. Journal of Metamorphic Geology 25, 631-656.
Droop, G.T.R., 1987. A General equation for estimating Fe3+ con centrations in ferromagnesian silicates and oxides from Microprobe analyses, using stoichiometric criteria. Min eralogical Magazine 51, 431-435.
Gasser, D., Bruand, E., Rubatto, D., Stüwe, K., 2012. The behaviour of monazite from greenschist facies phyllites to anatectic gneisses: An example from the Chugach Metamorphic Complex, southern Alaska. Lithos 134–135, 108-122.
Giles, D., Betts, P.G., Lister, G.S., 2004. 1.8-1.5 Ga links between the North and South Australian Cratons and the Ear ly-Middle Proterozoic configuration of Australia. Tec tonophysics 380, 27-41.
Green, E., Holland, T., Powell, R., 2007. An order-disorder model for omphacitic pyroxenes in the system jadeite-diop side-hedenbergite-acmite, with applications to eclogitic rocks. American Mineralogist 92, 1181-1189.
Griffin, W.L., Powell, W.J., Pearson, N.J., O'Reilly, S.Y., 2008. GLITTER: data reduction software for laser ablation ICP-MS, in: Sylvester, P. (Ed.), Laser Ablation ICP-MS in the Earth Sciences: Current Practices and Outstanding Issues. Mineralogical Association of Canada. Shourt Course Series 40, pp. 308-311.
GSWA, 1999. Rudall Sheet SF 51-10, 1:250,000 map sheet, 2 ed. Geological Survey of Western Australia, Perth.
Halpin, J.A., Jensen, T., McGoldrick, P., Meffre, S., Berry, R.F., Everard, J.L., Calver, C.R., Thompson, J., Goemann, K., Whittaker, J.M., 2014. Authigenic monazite and detrital zircon dating from the Proterozoic Rocky Cape Group, Tasma nia: Links to the Belt-Purcell Supergroup, North Ameri ca. Precambrian Research 250, 50-67.
Hayden, L., Watson, E.B., Wark, D., 2008. A thermobarometer for sphene (titanite). Contributions to Mineralogy and Petrol ogy 155, 529-540.
Hickman, A.H., Bagas, L., 1998. Geology of the Rudall 1:100 000 sheet, Western Australia, Western Australia Geological Survey 1:100 000 Geological Explanatory Notes. West ern Australia Geological Survey, Perth, p. 30.
Hickman, A.H., Bagas, L., 1999. Geological evolution of the Palaeo proterozoic Talbot Terrane and adjacent Meso- and Neo-proterozoic successions, Paterson Orogen, Western Australia. Report of the Geological Survey of Western Australia, p. 91.
Holland, T., Baker, J., Powell, R., 1998. Mixing properties and activ ity-composition relationships of chlorites in the system MgO-FeO-$Al_2O_3$-$SiO_2$-H2O. European Journal of Miner alogy 10, 395-406.
Holland, T., Powell, R., 2003. Activity–composition relations for phases in petrological calculations: an asymmetric multi component formulation. Contributions to Mineralogy and Petrology 145, 492-501.
Holland, T.J.B., Powell, R., 1998. An internally consistent ther modynamic data set for phases of petrological interest. Journal of Metamorphic Geology 16, 309-343.
Huston, D., Blewett, R.S., Champion, C., 2012. Australia through time: a summary of its tectonic and metallogenic evolu tion. Elements 35, 23-43.
Johnson, S.P., 2013. WA Unearthed: The birth of supercontinents and the Proterozoic Assembly of Western Australia. Geological Survey of Western Australia, Perth.
Karlstrom, K.E., Harlan, S.S., Williams, M.L., McLelland, J., Geiss man, J.W., Ahall, K., 1999. Refining Rodinia: Geologic Evidence for the Australia-Western U.S. connection in the Proterozoic. GSA Today 9, 1-7.
Kelsey, D.E., Clark, C., Hand, M., 2008. Thermobarometric modeling of zircon and monazite growth in melt-bearing systems: examples using model metapelitic and metapsammitic granulites. Journal of Metamophic Geol ogy 26, 199-212.
Kelsey, D.E., Hand, M., Clark, C., Wilson, C.J.L., 2007. On the ap plication of in situ monazite chemical geochronology to constraining P-T-t histories in high-temperature (>850 degrees C) polymetamorphic granulites from Prydz Bay, East Antarctica. Journal of the Geological Society, Lon don 164, 667-683.
Kirkland, C.L., Johnson, S.P., Smithies, R.H., Hollis, J.A., Wingate, M.T.D., Tyler, I.M., Hickman, A.H., Cliff, J.B., Tessalina, S., Belousova, E.A., Murphy, R.C., 2013. Not-so-suspect terrane: Constraints on the crustal evolution of the Rudall Province. Precambrian Research 235, 131-149.
Kohn, M.J., Malloy, M.A., 2004. Formation of monazite via pro grade metamorphic reactions among common silicates: Implications for age determinations. Geochimica Et Cosmochimica Acta 68, 101-113.
Korhonen, F.J., Clark, C., Brown, M., Bhattacharya, S., Taylor, R., 2013. How long-lived is ultrahigh temperature (UHT) metamorphism? Constraints from zircon and monazite geochronology in the Eastern Ghats orogenic belt, India. Precambrian Research 20, 764-781.
Li, Z.X., 2000. Palaeomagnetic evidence for unification of the North and West Australian cratons by ca.1.7 Ga: new results from the Kimberley Basin of northwestern Australia. Geophysical Journal International 142, 173-180.
Li, Z.X., Evans, D.A.D., 2011. Late Neoproterozoic 40 degrees intraplate rotation within Australia allows for a tighter-fit ting and longer-lasting Rodinia. Geology 39, 39-42.
Ludwig, K.R., 2008. Isoplot: A Geochronological Toolkit for Micro soft Excel, 3.7 ed. Berkeley Geochronology Centre, Berkeley.
Maidment, D., 2005. Paleozoic high-grade metamorphism within the Centralian Superbasin, Harts Range region, central Aus tralia (PhD thesis). Australian National University, Can berra, p. 422.
Maidment, D., 2007. New timing constraints on the evolution of the Rudall Complex, Western Australia- Implications for Proterozoic Reconstructions, in: Collins, A.S. (Ed.), SGTSG 2007 Deformation in the Desert, Geological Society of Australia, Alice Springs.
Maidment, D., 2014. When did the WAC whack the NAC? Docking

of the West and North Australian Cratons, Australian Earth Science Convention. Geological Society of Austra lia Abstracts, Newcastle.

Medig, K.P.R., Thorkelson, D.J., Davis, W.J., Rainbird, R.H., Gib son, H.D., Turner, E.C., Marshall, D.D., 2014. Pinning northeastern Australia to northwestern Laurentia in the Mesoproterozoic. Precambrian Research 249, 88-99.

Moores, E.M., 1991. Southwest U.S.-East Antarctica (SWEAT) connection: A hypothesis. Geology 19, 425-428.

Muhling, J.R., Fletcher, I.R., Rasmussen, B., 2012. Dating fluid flow and Mississippi Valley type base-metal mineraliza tion in the Paleoproterozoic Earaheedy Basin, Western Australia. Precambrian Research 212–213, 75-90.

Myers, J.S., Shaw, R.D., Tyler, I.M., 1996. Tectonic evolution of Proterozoic Australia. Tectonics 15, 1431-1446.

Nelson, D.R., 1995. Compilation of SHRIMP U-Pb zircon geo chronology data, 1994. West Australian Geological Survey Record 1995/3, 244.

Nelson, D.R., 1996. Compilation of SHRIMP U-Pb zircon geo chronology data, 1995, Record 1996/5. West Australian Geological Survey, Record 1996/5, Perth, p. 168.

Neumann, N.L., Fraser, G.L., 2007. Geochronological synthesis and timespace plots for Proterozoic Australia. Geosci ence Australia, Canberra, p. 216.

Payne, J.L., Hand, M., Barovich, K.M., Reid, A., Evans, D.A.D., 2009. Correlations and reconstruction models for the 2500-1500 Ma evolution of the Mawson Continent, in:

Reddy, S.M., Mazumder, R., Evans, D.A.D., and Collins, A.S. (Ed.), Palaeoproterozoic Supercontinents and Global Evolution, pp. 319-355.

Payne, J.L., Hand, M., Barovich, K.M., Wade, B.P., 2008. Temporal constraints on the timing of high-grade metamorphism in the northern Gawler Craton; implications for assembly of the Australian Proterozoic. Australian Journal of Earth Sciences 55, 623-640.

Pisarevsky, S.A., Elming, S.-Å., Pesonen, L.J., Li, Z.-X., 2014a. Mesoproterozoic paleogeography: Supercontinent and beyond. Precambrian Research 244, 207-225.

Pisarevsky, S.A., Wingate, M.T., Li, Z.-X., Wang, X.-C., Tohver, E., Kirkland, C.L., 2014b. Age and paleomagnetism of the 1210Ma Gnowangerup–Fraser dyke swarm, Western Australia, and implications for late Mesoproterozoic paleogeography. Precambrian Research 246, 1-15.

Powell, R., Holland, T.J.B., 1988. An internally consistent thermo dynamic dataset with uncertainties and correlations: 3. Applications to geobarometry, worked examples and a computer program. J. Metamorphic Geol. 6, 173-204.

Powell, R., Holland, T.J.B., 2008. On thermobarometry. Journal of Metamorphic Geology 26, 155-179.

Pyle, J.M., Spear, F.S., 2003. Four generations of accessory-phase growth in low-pressure migmatites from SW New Hamp shire. American Mineralogist 88, 338-351.

Raimondo, T., Collins, A.S., Hand, M., Walker-Hallam, A., Smithies, R.H., Evins, P.M., Howard, H.M., 2009. Ediacaran intra continental channel flow. Geology 37, 291-294.

Raimondo, T., Collins, A.S., Hand, M., Walker-Hallam, A., Smith ies, R.H., Evins, P.M., Howard, H.M., 2010. The anato my of a deep intracontinental orogen. Tectonics 29, 1-31.

Rubatto, D., 2002. Zircon trace element geochemistry: partitioning with garnet and the link between U-Pb ages and meta morphism. Chemical Geology 184, 123-138.

Rubatto, D., Chakraborty, S., Dasgupta, S., 2013. Timescales of crustal melting in the Higher Himalayan Crystallines (Sikkim, Eastern Himalaya) inferred from trace ele ment-constrained monazite and zircon chronology. Con tributions to Mineralogy and Petrology 165, 349-372.

Rubatto, D., Hermann, J., Buick, I.S., 2006. Temperature and bulk composition control on the growth of monazite and zircon during low-pressure anatexis (Mount Stafford, central Australia). Journal of Petrology 47, 1973-1996.

Smithies, R.H., Bagas, L., 1997. High pressure amphibolite-granu lite facies metamorphism in the Paleoproterozoic Rudall Complex, central Western Australia. Precambrian Re search 83, 243-265.

Smithies, R.H., Howard, H.M., Evins, P., Kirkland, C.L., Kelsey, D.E., Hand, M., Wingate, M.T.D., Collins, A.S., 2010. Geochemistry, geochronology, and pretrogenesis of Mesoproterozoic felsic rocks in the West Musgrave Province, central Australia, and implications for the Mesoproterozoic tectonic evolution of the region. Geo logical Survey of Western Australia, Perth.

Smithies, R.H., Howard, H.M., Evins, P.M., Kirkland, C.L., Kelsey, D.E., Hand, M., Wingate, M.T.D., Collins, A.S., Belouso va, E., 2011. High-Temperature Granite Magmatism, Crust-Mantle Interaction and the Mesoproterozoic Intra continental Evolution of the Musgrave Province, Central Australia. Journal of Petrology 52, 931-958.

Smits, R.G., Collins, W.J., Hand, M., Dutch, R., Payne, J., 2014. A Proterozoic Wilson cycle identified by Hf isotopes in central Australia: Implications for the assembly of Proterozoic Australia and Rodinia. Geology 42, 231-234.

Spaggiari, C.V., Bodorkos, S., Barquero-Molina, Tyler, I.M., Wingate, M.T.D., 2009. Interpreted Bedrock Geology of the South Yilgarn and central Albany-Fraser Orogen, Western Australia. Geological Survey of Western Austra lia, Perth.

Spaggiari, C.V., Kirkland, C.L., Smithies, R.H., Wingate, M.T.D., 2014. Tectonic links between Proterozoic sedimenta ry cycles, basin formation and magmatism in the Alba ny-Fraser Orogen, Western Austraia. Geological Survey of Western Australia, Perth.

Spear, F.S., Pyle, J.M., 2010. Theoretical modeling of monazite growth in a low-Ca metapelite. Chemical Geology 273, 111-119.

Stern, R.A., Bodorkos, S., Kamo, S.L., Hickman, A.H., Corfu, F., 2009. Measurement of SIMS Instrumental Mass Frac tionation of Pb Isotopes During Zircon Dating. Geostan dards and Geoanalytical Research 33, 145-168.

Storkey, A.C., Hermann, J., Hand, M., Buick, I.S., 2005. Using in situ trace-element determinations to monitor partial-melt ing processes in metabasites. Journal of Petrology 46, 1283-1308.

Taylor, R.J.M., Clark, C., Fitzsimons, I.C.W., Santosh, M., Hand, M., Evans, N., McDonald, B., 2014. Post-peak, fluid-me diated modification of granulite facies zircon and monazite in the Trivandrum Block, southern India. Con tributions to Mineralogy and Petrology 168, 1-17.

Van Kranendonk, M.J., Kirkland, C.L., 2013. Orogenic climax of Earth: The 1.2-1.1 Ga Grenvillian superevent. Geology 41, 735-738.

Wade, B.P., Hand, M., Barovich, K.M., 2005. Nd isotopic and geochemical constraints on provenance of sedimentary rocks in the eastern Officer Basin, Australia; implications for the duration of the intracratonic Petermann Orogeny. Journal of the Geological Society, London 162, 513-530.

Wade, B.P., Kelsey, D.E., Hand, M., Barovich, K.M., 2008. The Musgrave Province: Stitching north, west and south Australia. Precambrian Research 166, 370-386.

Walsh, A.K., Raimondo, T., Kelsey, D.E., Hand, M., Pfitzner, H.L., Clark, C., 2013. Duration of high-pressure metamor phism and cooling during the intraplate Petermann Orog eny. Gondwana Research 24, 969-983.

White, Powell, Holland, Worley, 2000. The effect of TiO2 and $F_{e2}O_3$ on metapelitic assemblages at greenschist and amphibo lite facies conditions: mineral equilibria calculations in the system $K_2O$–FeO–MgO–$Al_2O_3$–$SiO_2$–$H_2O$–$TiO_2$–$Fe_2O_3$. Journal of Metamorphic Geology 18, 497-511.

White, R.W., Powell, R., Holland, T.J.B., 2007. Progress relating to calculation of partial melting equilibria for metapelites. Journal of Metamorphic Geology 25, 511-527.

Whitehouse, M.J., Platt, J.P., 2003. Dating high-grade metamor phism - constraints from rare-earth elements in zircon and garnet. Contributions to Mineralogy and Petrology 145, 61-74.

Williams, I.R., Bagas, L., 1999. Geology of the Throssell 1:100,000 sheet, 1:100,000 Geological Series Explanatory Notes.

Geological Survey of Western Australia, Perth, p. 24.
Williams, M.L., Jercinovic, M.J., Harlov, D.E., Budzyn, B., Heth erington, C.J., 2011. Resetting monazite ages during fluid-related alteration. Chemical Geology 283, 218-225.
Yakymchuk, C., Brown, M., 2014. Behaviour of zircon and monazite during crustal melting. Journal of the Geologi cal Society, London 171, 465-479.

# Supporting Information

## Appendix 1: Mineral chemistry

### *Garnet*

In sample 115866, fine-grained garnet grains located in the matrix typically have $X_{Alm}$ values that increase from core to rim (~0.54–0.62), $X_{Py}$ values that decrease from core to rim (~0.38–0.32), $X_{Grs}$ values of ~0.02 and $X_{Spss}$ values of ~0.05. Garnet occurring as coronas on magnetite or ilmenite, or within quartz-garnet intergrowths have $X_{Alm}$ values of 0.57–0.64, $X_{Py}$ values of ~0.27–0.35, $X_{Grs}$ values of ~0.02 and $X_{Spss}$ values of 0.05–0.06.

### *Pyroxene*

Orthopyroxene is present in sample 115866 and has $X_{Mg}$ values of ~0.59−0.60, with $Al_2O_3$ content of ~9.70−10.1 wt. %. Orthopyroxene has 4.05–4.35 wt. % $Fe_2O_3$ using the stoichiometric calculation method of Droop (1987). Calculated $y$(opx)1 values are 0.18−0.18 without $Fe_2O_3$ recalculation and 0.15−0.16 recalculated with $Fe_2O_3$, ($y$(opx)1 = $C_{\text{Si, total}}$ (opx) + $C_{\text{Al,total}}$ (opx – 2), where $C_i$ is cations of i). Orthopyroxene has 4.05–4.35 wt.% $Fe_2O_3$.

### *Feldspar*

Alkali feldspar in sample 115866 has $X_{Or}$ values of ~0.66–0.84 and $X_{An}$ values of ~0.01–0.07. In sample 103617 and 103618, plagioclase is albite, with $X_{Na}$ (= Na/(Na+Ca)) values of 0.98−0.99 and 0.96−0.97 respectively. Plagioclase in sample 115866 has $X_{An}$ (=Ca/(Na+Ca+K)) values of ~0.43–0.44 and $X_{Or}$ values of ~0.01 (=K/(Na+Ca+K)).

### *Staurolite*

In sample 103617, staurolite has $X_{Mg}$ values of 0.19−0.22 and ZnO wt. % values of 0.02−0.13. In sample 103618, staurolite has $X_{Mg}$ values of 0.18−0.20 and ZnO wt. % values of 0.03−0.12.

### *Biotite*

In sample 115866, biotite has $X_{Mg}$ values of 0.66−0.78 and 2.0−4.5 wt. % $TiO_2$. Biotite in sample 103617 has $X_{Mg}$ values of 0.59−0.60 and wt. % $TiO_2$ content of 1.12−1.33. Biotite in sample 103618 has $X_{Mg}$ values of ~0.56 and wt. % $TiO_2$ content of 1.16−1.42.

### *Chlorite*

Chlorite has $X_{Mg}$ values of 0.63−0.64 in sample 103617 and $X_{Mg}$ values of 0.59−0.61 in 103618.

### *Ilmenite*

Ilmenite in sample 115866 has 1.87–4.47 wt. % $Fe_2O_3$ calculated using the method of Droop (1987)x, 0.12−0.70 wt. % MgO and 1.74−2.91 wt. % MnO.

### *Magnetite-Spinel*

In sample 115866, magnetite usually occurs with spinel and/or corundum and has $Al_2O_3$ wt. % content of 0.19−0.26. Spinel occurs with magnetite and/or corundum and has ZnO content of ~9.2 wt. %, MgO content of ~3.7 wt. % and $Cr_2O_3$ values of 0.10 wt. %. In sample 103617, magnetite has $Al_2O_3$ wt. % content of 0.08−0.15, and in sample 103618, magnetite has $Al_2O_3$ wt. % content of 0.46−0.47.

Appendix 2. U-Pb isotopic age data for monazite analyses

Sample 103603D

| Spot | $^{207}Pb/^{206}Pb$ | 1 σ | $^{206}Pb/^{238}U$ | 1 σ | $^{207}Pb/^{235}U$ | 1 σ | rho | Conc. (%) | $^{207}Pb/^{206}Pb$ age | 1 σ | $^{206}Pb/^{238}U$ age | 1 σ | $^{207}Pb/^{235}U$ age | 1 σ | $^{204}Pb$ | $^{206}Pb$ | $^{207}Pb$ | $^{238}Pb$ |
|---|---|---|---|---|---|---|---|---|---|---|---|---|---|---|---|---|---|---|
| M01-2 | 0.08429 | 0.00099 | 0.22249 | 0.00297 | 2.58431 | 0.0369 | 0.93489792 | 99.68 | 1299.1 | 22.73 | 1295 | 15.64 | 1296.2 | 10.45 | 0 | 103253 | 8869 | 609471 |
| M02-2 | 0.08329 | 0.00098 | 0.22249 | 0.00297 | 2.55388 | 0.03644 | 0.9355523 | 101.50 | 1275.9 | 22.82 | 1295 | 15.65 | 1287.5 | 10.41 | 11 | 123748 | 10500 | 731353 |
| M03 | 0.08366 | 0.00093 | 0.2263 | 0.00368 | 2.60882 | 0.04331 | 0.97953328 | 102.39 | 1284.4 | 21.51 | 1315.1 | 19.36 | 1303.1 | 12.19 | 1 | 117367 | 9997 | 838540 |
| M04 | 0.08328 | 0.00094 | 0.22296 | 0.00361 | 2.55837 | 0.04246 | 0.97558162 | 101.72 | 1275.5 | 22.02 | 1297.5 | 19 | 1288.8 | 12.12 | 0 | 132627 | 11274 | 954624 |
| M04-2 | 0.08277 | 0.00097 | 0.2194 | 0.00293 | 2.50268 | 0.03572 | 0.93567466 | 101.18 | 1263.8 | 22.57 | 1278.7 | 15.49 | 1272.8 | 10.36 | 0 | 108611 | 9156 | 652075 |
| M05† | 0.08337 | 0.00097 | 0.22606 | 0.00373 | 2.59748 | 0.04432 | 0.9670247 | 102.82 | 1277.8 | 22.61 | 1313.8 | 19.59 | 1299.9 | 12.51 | 3 | 90540 | 7701 | 654079 |
| M05A-2 | 0.07933 | 0.00095 | 0.21498 | 0.00288 | 2.35029 | 0.03395 | 0.92741924 | 106.35 | 1180.4 | 23.42 | 1255.3 | 15.28 | 1227.6 | 10.29 | 0 | 77066 | 6228 | 472453 |
| M05B-2 | 0.08329 | 0.00099 | 0.2063 | 0.00276 | 2.36809 | 0.0341 | 0.92908121 | 94.77 | 1275.8 | 23.1 | 1209.1 | 14.74 | 1233 | 10.28 | 0 | 120449 | 10212 | 768824 |
| M06 | 0.0836 | 0.00101 | 0.21975 | 0.00362 | 2.53141 | 0.04376 | 0.95293848 | 99.80 | 1283.1 | 23.41 | 1280.5 | 19.14 | 1281.1 | 12.58 | 2 | 110357 | 9429 | 818324 |
| M06-2 | 0.08308 | 0.00099 | 0.22303 | 0.00298 | 2.55355 | 0.03683 | 0.92639377 | 102.11 | 1271.1 | 23.01 | 1297.9 | 15.73 | 1287.5 | 10.52 | 12 | 92784 | 7861 | 547838 |
| M07 | 0.08265 | 0.00094 | 0.24141 | 0.00396 | 2.74994 | 0.04659 | 0.96821195 | 110.54 | 1261.1 | 22.02 | 1394 | 20.58 | 1342.1 | 12.61 | 4 | 120101 | 10095 | 810566 |
| M08 | 0.08331 | 0.001 | 0.22529 | 0.00371 | 2.5864 | 0.04463 | 0.95433488 | 102.62 | 1276.3 | 23.34 | 1309.8 | 19.51 | 1296.8 | 12.63 | 12 | 108670 | 9237 | 785487 |
| M08-2 | 0.08196 | 0.00101 | 0.2202 | 0.00295 | 2.48707 | 0.03653 | 0.91210122 | 103.07 | 1244.7 | 23.94 | 1282.9 | 15.58 | 1268.3 | 10.64 | 6 | 90781 | 7582 | 541604 |
| M08B-2 | 0.08262 | 0.00111 | 0.22203 | 0.00299 | 2.52815 | 0.03914 | 0.86984435 | 102.56 | 1260.3 | 25.86 | 1292.6 | 15.75 | 1280.2 | 11.26 | 2 | 106122 | 8926 | 624915 |
| M09 | 0.08406 | 0.00098 | 0.23186 | 0.00381 | 2.68617 | 0.04603 | 0.95894051 | 103.88 | 1294 | 22.62 | 1344.2 | 19.96 | 1324.7 | 12.68 | 0 | 101091 | 8632 | 710797 |
| M10-2 | 0.08321 | 0.00102 | 0.22824 | 0.00306 | 2.61752 | 0.03844 | 0.91292752 | 104.03 | 1274 | 23.85 | 1325.3 | 16.07 | 1305.6 | 10.79 | 0 | 97200 | 8234 | 560905 |
| M11 | 0.08374 | 0.00119 | 0.21548 | 0.00353 | 2.486 | 0.04582 | 0.88881992 | 97.78 | 1286.4 | 27.36 | 1257.9 | 18.73 | 1268 | 13.35 | 0 | 88984 | 7579 | 660745 |
| M11B | 0.08368 | 0.00114 | 0.23073 | 0.00378 | 2.6598 | 0.04817 | 0.90460726 | 104.16 | 1284.9 | 26.44 | 1338.3 | 19.79 | 1317.4 | 13.36 | 2 | 152493 | 13034 | 1060496 |
| M11-2 | 0.078 | 0.00112 | 0.16591 | 0.00229 | 1.78231 | 0.02937 | 0.8376107 | 86.28 | 1146.8 | 28.38 | 989.5 | 12.64 | 1039 | 10.72 | 0 | 55559 | 4396 | 445105 |
| M12 | 0.08271 | 0.00113 | 0.22818 | 0.0038 | 2.60059 | 0.04768 | 0.90832583 | 104.96 | 1262.4 | 26.32 | 1325 | 19.96 | 1300.8 | 13.45 | 0 | 97233 | 8245 | 695816 |
| M13-2 | 0.08294 | 0.00109 | 0.22068 | 0.00296 | 2.52268 | 0.03853 | 0.87819688 | 101.40 | 1267.7 | 25.35 | 1285.5 | 15.64 | 1278.6 | 11.11 | 9 | 107849 | 9095 | 639376 |

†Discarded due to noisy isotopic signal or blasted through grain

All individual isotopic abundancesare in cps

Appendix 2. U-Pb isotopic age data for monazite analyses

Sample 103617

| Spot | $^{207}Pb/^{206}Pb$ | 1 σ | $^{206}Pb/^{238}U$ | 1 σ | $^{207}Pb/^{235}U$ | 1 σ | rho | Conc. (%) | $^{207}Pb/^{206}Pb$ age | 1 σ | $^{206}Pb/^{238}U$ age | 1 σ | $^{207}Pb/^{235}U$ age | 1 σ | $^{204}Pb$ | $^{206}Pb$ | $^{207}Pb$ | $^{238}Pb$ |
|---|---|---|---|---|---|---|---|---|---|---|---|---|---|---|---|---|---|---|
| M02 | 0.08833 | 0.00107 | 0.25912 | 0.00367 | 3.15515 | 0.0481 | 0.92905209 | 106.89 | 1389.6 | 23.03 | 1485.3 | 18.79 | 1446.3 | 11.75 | 30 | 176291 | 15868 | 947486 |
| M03 | 0.0991 | 0.00119 | 0.29852 | 0.00415 | 4.0787 | 0.06078 | 0.93290137 | 104.77 | 1607.3 | 22.26 | 1684 | 20.61 | 1650.1 | 12.15 | 15 | 95639 | 9668 | 436979 |
| M05 | 0.10184 | 0.00124 | 0.28485 | 0.00407 | 3.99963 | 0.06131 | 0.93210897 | 97.45 | 1658 | 22.46 | 1615.7 | 20.41 | 1634.1 | 12.45 | 0 | 44006 | 4561 | 215751 |
| M09A | 0.10081 | 0.00121 | 0.29228 | 0.0041 | 4.06223 | 0.06067 | 0.93923717 | 100.85 | 1639 | 22.03 | 1652.9 | 20.45 | 1646.8 | 12.17 | 0 | 55744 | 5739 | 262309 |
| M09B | 0.10144 | 0.00117 | 0.29146 | 0.00408 | 4.07596 | 0.05995 | 0.9517479 | 99.89 | 1650.6 | 21.26 | 1648.8 | 20.36 | 1649.5 | 11.99 | 1 | 79107 | 8174 | 374404 |
| M09C | 0.09736 | 0.00107 | 0.2964 | 0.00415 | 3.97815 | 0.0574 | 0.97037402 | 106.31 | 1574.1 | 20.47 | 1673.4 | 20.65 | 1629.7 | 11.71 | 13 | 167945 | 16675 | 787037 |
| M10 | 0.09962 | 0.00107 | 0.29222 | 0.0041 | 4.01159 | 0.05735 | 0.98142482 | 102.20 | 1617 | 19.85 | 1652.6 | 20.47 | 1636.5 | 11.62 | 9 | 131794 | 13349 | 629009 |
| M10 | 0.1017 | 0.00121 | 0.302 | 0.0043 | 4.23392 | 0.06389 | 0.9435638 | 102.77 | 1655.4 | 21.88 | 1701.2 | 21.28 | 1680.6 | 12.39 | 14 | 36005 | 3735 | 166461 |
| M13 | 0.10278 | 0.00115 | 0.29627 | 0.00417 | 4.19771 | 0.06124 | 0.96477408 | 99.87 | 1675 | 20.52 | 1672.8 | 20.72 | 1673.6 | 11.96 | 29 | 166658 | 17457 | 783417 |
| M14 | 0.10031 | 0.00109 | 0.30032 | 0.00422 | 4.15136 | 0.05969 | 0.9772755 | 103.87 | 1629.8 | 20.02 | 1692.9 | 20.92 | 1664.5 | 11.76 | 0 | 96384 | 9805 | 447326 |
| M14 | 0.10187 | 0.00117 | 0.27578 | 0.00391 | 3.87293 | 0.0575 | 0.95496135 | 94.67 | 1658.5 | 21.05 | 1570.1 | 19.78 | 1608.1 | 11.98 | 3 | 78190 | 8123 | 397418 |
| M15 | 0.10132 | 0.00112 | 0.2976 | 0.00419 | 4.15507 | 0.06034 | 0.96951411 | 101.89 | 1648.3 | 20.39 | 1679.4 | 20.83 | 1665.2 | 11.89 | 14 | 65136 | 6696 | 305053 |
| M16 | 0.09803 | 0.00115 | 0.31761 | 0.00449 | 4.29185 | 0.06444 | 0.94154521 | 112.04 | 1587 | 21.79 | 1778.1 | 21.98 | 1691.8 | 12.36 | 13 | 130007 | 12973 | 570973 |
| M20A | 0.1035 | 0.00124 | 0.2996 | 0.00421 | 4.27554 | 0.06412 | 0.93699602 | 100.08 | 1687.9 | 21.99 | 1689.3 | 20.87 | 1688.7 | 12.34 | 3 | 74146 | 7838 | 341114 |
| M20B | 0.10287 | 0.00119 | 0.2992 | 0.00424 | 4.24359 | 0.06339 | 0.94867386 | 100.64 | 1676.5 | 21.31 | 1687.3 | 21.01 | 1682.5 | 12.27 | 12 | 63454 | 6608 | 295997 |
| M21 | 0.10539 | 0.00137 | 0.28874 | 0.00407 | 4.19573 | 0.06598 | 0.89636044 | 95.01 | 1721.1 | 23.75 | 1635.2 | 20.35 | 1673.2 | 12.89 | 16 | 102977 | 11039 | 489332 |
| M22 | 0.09911 | 0.00113 | 0.29538 | 0.00414 | 4.03632 | 0.05931 | 0.95384305 | 103.79 | 1607.4 | 21.02 | 1668.4 | 20.61 | 1641.5 | 11.96 | 9 | 221001 | 22209 | 1038721 |
| M24 | 0.09435 | 0.00113 | 0.27101 | 0.00378 | 3.52559 | 0.05282 | 0.93097902 | 102.03 | 1515.2 | 22.43 | 1545.9 | 19.17 | 1533 | 11.85 | 8 | 265715 | 25547 | 1347540 |
| M25 | 0.10306 | 0.00117 | 0.29846 | 0.00418 | 4.23873 | 0.06192 | 0.95872699 | 100.22 | 1680 | 20.75 | 1683.7 | 20.77 | 1681.6 | 12 | 11 | 89373 | 9346 | 414588 |
| M25A | 0.1035 | 0.0012 | 0.30156 | 0.00426 | 4.30347 | 0.06416 | 0.94752415 | 100.66 | 1687.9 | 21.18 | 1699.1 | 21.12 | 1694 | 12.28 | 0 | 85681 | 8982 | 396832 |
| M25B | 0.1024 | 0.00117 | 0.29424 | 0.00417 | 4.15431 | 0.06184 | 0.95205878 | 99.68 | 1668.1 | 21.04 | 1662.7 | 20.76 | 1665.1 | 12.18 | 12 | 156692 | 16266 | 746395 |
| M26 | 0.10227 | 0.00112 | 0.29848 | 0.0042 | 4.20664 | 0.06109 | 0.96894534 | 101.08 | 1665.8 | 20.21 | 1683.8 | 20.85 | 1675.3 | 11.91 | 16 | 119666 | 12375 | 559438 |
| M26 | 0.1039 | 0.00122 | 0.29821 | 0.00423 | 4.27215 | 0.0642 | 0.94390792 | 99.26 | 1695 | 21.44 | 1682.4 | 20.99 | 1688 | 12.36 | 0 | 92910 | 9793 | 435863 |
| M27 | 0.10402 | 0.00117 | 0.31149 | 0.0044 | 4.46503 | 0.06547 | 0.96336443 | 103.01 | 1697 | 20.52 | 1748 | 21.61 | 1724.5 | 12.16 | 6 | 75067 | 7899 | 336333 |
| M28† | 0.08665 | 0.00117 | 0.28249 | 0.0041 | 3.37246 | 0.05186 | 0.94383282 | 118.56 | 1352.8 | 25.83 | 1603.9 | 20.6 | 1498 | 12.04 | 0 | 186639 | 19175 | 921340 |
| M29 | 0.10265 | 0.00147 | 0.315 | 0.00446 | 4.45814 | 0.07473 | 0.84466213 | 105.54 | 1672.6 | 26.23 | 1765.3 | 21.85 | 1723.2 | 13.9 | 21 | 513981 | 53284 | 2237393 |
| M29 | 0.10329 | 0.00116 | 0.29336 | 0.00414 | 4.17584 | 0.06147 | 0.95869416 | 98.47 | 1684.1 | 20.54 | 1658.3 | 20.65 | 1669.3 | 12.06 | 1 | 188703 | 19672 | 900403 |
| M30† | 0.09957 | 0.00141 | 0.29234 | 0.0042 | 4.00931 | 0.06735 | 0.85525 | 102.30 | 1616.1 | 26.16 | 1653.2 | 20.94 | 1636.1 | 13.65 | 0 | 225107 | 22623 | 1070407 |
| M31 | 0.10306 | 0.00125 | 0.30082 | 0.00427 | 4.27462 | 0.06557 | 0.92536591 | 100.92 | 1680 | 22.31 | 1695.4 | 21.15 | 1688.5 | 12.62 | 0 | 78296 | 8158 | 363143 |
| M31† | 0.11059 | 0.0015 | 0.29124 | 0.00415 | 4.43727 | 0.072 | 0.87817371 | 91.08 | 1809.1 | 24.41 | 1647.7 | 20.71 | 1719.3 | 13.45 | 152 | 136741 | 15311 | 649041 |
| M33 | 0.10075 | 0.00122 | 0.30103 | 0.00424 | 4.17949 | 0.06308 | 0.93322783 | 103.57 | 1637.9 | 22.32 | 1696.4 | 21.01 | 1670 | 12.37 | 0 | 68391 | 7022 | 313601 |
| M34 | 0.102 | 0.00124 | 0.30359 | 0.00427 | 4.2671 | 0.06446 | 0.93107128 | 102.91 | 1660.8 | 22.28 | 1709.1 | 21.13 | 1687 | 12.43 | 0 | 61841 | 6411 | 280877 |
| M35 | 0.10191 | 0.00116 | 0.29767 | 0.0042 | 4.18074 | 0.06161 | 0.95745015 | 101.24 | 1659.3 | 20.97 | 1679.8 | 20.85 | 1670.3 | 12.07 | 8 | 59158 | 6113 | 276523 |
| M37 | 0.10259 | 0.0013 | 0.29599 | 0.00417 | 4.18449 | 0.06461 | 0.91243473 | 99.99 | 1671.5 | 23.19 | 1671.4 | 20.77 | 1671 | 12.65 | 7 | 103497 | 10850 | 481617 |
| M38A | 0.10174 | 0.00122 | 0.30973 | 0.00436 | 4.34289 | 0.06527 | 0.9366308 | 105.02 | 1656.2 | 22.04 | 1739.4 | 21.44 | 1701.5 | 12.4 | 17 | 103846 | 10776 | 463486 |
| M39A | 0.10225 | 0.00132 | 0.302 | 0.00428 | 4.25559 | 0.06669 | 0.90434864 | 102.15 | 1665.4 | 23.78 | 1701.2 | 21.17 | 1684.8 | 12.88 | 9 | 71246 | 7439 | 324946 |
| M39B | 0.10127 | 0.00126 | 0.30552 | 0.00431 | 4.26398 | 0.06539 | 0.91990175 | 104.31 | 1647.6 | 22.97 | 1718.6 | 21.27 | 1686.4 | 12.61 | 32 | 56677 | 5848 | 255532 |
| M39C | 0.10133 | 0.00139 | 0.3107 | 0.00445 | 4.33852 | 0.0705 | 0.88139634 | 105.80 | 1648.6 | 25.23 | 1744.2 | 21.89 | 1700.7 | 13.41 | 0 | 39286 | 4068 | 174482 |

Appendix 2. U-Pb isotopic age data for monazite analyses

Sample 103618

| Spot | $^{207}Pb/^{206}Pb$ | 1 σ | $^{206}Pb/^{238}U$ | 1 σ | $^{207}Pb/^{235}U$ | 1 σ | rho | Conc. (%) | $^{207}Pb/^{206}Pb$ age | 1 σ | $^{206}Pb/^{238}U$ age | 1 σ | $^{207}Pb/^{235}U$ age | 1 σ | $^{204}Pb$ | $^{206}Pb$ | $^{207}Pb$ | $^{238}Pb$ | Session |
|---|---|---|---|---|---|---|---|---|---|---|---|---|---|---|---|---|---|---|---|
| M05† | 0.08161 | 0.00112 | 0.2204 | 0.00322 | 2.47859 | 0.04087 | 0.886022 | 103.87 | 1236.2 | 26.79 | 1284 | 17 | 1265.8 | 11.93 | 0 | 98269 | 8371 | 631242 | 1 |
| M01 | 0.08345 | 0.00097 | 0.23575 | 0.00335 | 2.71139 | 0.04033 | 0.955338 | 106.64 | 1279.5 | 22.5 | 1364.5 | 17.48 | 1331.6 | 11.03 | 9 | 141522 | 12169 | 842220 | 1 |
| M06 | 0.08333 | 0.00093 | 0.23852 | 0.00336 | 2.74007 | 0.03983 | 0.969094 | 108.02 | 1276.6 | 21.66 | 1379 | 17.5 | 1339.4 | 10.81 | 0 | 189990 | 16266 | 1112818 | 1 |
| M04† | 0.08348 | 0.00118 | 0.22136 | 0.00324 | 2.54637 | 0.04271 | 0.872645 | 100.70 | 1280.2 | 27.27 | 1289.1 | 17.1 | 1285.4 | 12.23 | 14 | 96047 | 8281 | 614151 | 1 |
| M03A | 0.08274 | 0.00092 | 0.21816 | 0.00308 | 2.48843 | 0.03613 | 0.972373 | 100.73 | 1263 | 21.46 | 1272.2 | 16.29 | 1268.7 | 10.52 | 0 | 88150 | 7504 | 564351 | 1 |
| M03B | 0.0836 | 0.00092 | 0.21846 | 0.00308 | 2.51781 | 0.03643 | 0.974412 | 99.28 | 1283 | 21.41 | 1273.7 | 16.3 | 1277.2 | 10.51 | 0 | 86570 | 7432 | 553906 | 1 |
| M07 | 0.08455 | 0.001 | 0.219 | 0.0031 | 2.55253 | 0.03837 | 0.941665 | 97.82 | 1305.1 | 22.92 | 1276.6 | 16.4 | 1287.2 | 10.97 | 13 | 167333 | 14549 | 1066284 | 1 |
| M09A | 0.08254 | 0.00094 | 0.21531 | 0.00305 | 2.45019 | 0.03615 | 0.960124 | 99.90 | 1258.4 | 21.96 | 1257.1 | 16.19 | 1257.5 | 10.64 | 9 | 86028 | 7301 | 559808 | 1 |
| M09B | 0.08231 | 0.00093 | 0.21513 | 0.00305 | 2.44147 | 0.03594 | 0.963102 | 100.25 | 1253 | 21.82 | 1256.1 | 16.17 | 1254.9 | 10.6 | 0 | 101262 | 8564 | 659647 | 1 |
| M10 | 0.08459 | 0.0011 | 0.2316 | 0.00332 | 2.70075 | 0.04277 | 0.9052 | 102.82 | 1306.1 | 24.99 | 1342.9 | 17.35 | 1328.7 | 11.74 | 6 | 135627 | 11819 | 819309 | 1 |
| M12 | 0.0837 | 0.00095 | 0.21607 | 0.00302 | 2.49333 | 0.03633 | 0.959239 | 98.12 | 1285.3 | 21.94 | 1261.1 | 16.03 | 1270.1 | 10.56 | 6 | 112014 | 9587 | 718104 | 1 |
| M15 | 0.08337 | 0.00102 | 0.22501 | 0.00316 | 2.58645 | 0.03919 | 0.92686 | 102.39 | 1277.7 | 23.66 | 1308.3 | 16.63 | 1296.8 | 11.1 | 0 | 138163 | 11769 | 847777 | 1 |
| M16A | 0.08371 | 0.00096 | 0.21542 | 0.00301 | 2.48638 | 0.03649 | 0.952081 | 97.81 | 1285.7 | 22.32 | 1257.6 | 15.97 | 1268.1 | 10.63 | 8 | 110848 | 9487 | 710712 | 1 |
| M16B | 0.08393 | 0.00096 | 0.21617 | 0.00302 | 2.50146 | 0.03659 | 0.955086 | 97.75 | 1290.7 | 22.05 | 1261.6 | 16 | 1272.5 | 10.61 | 2 | 102221 | 8735 | 653264 | 1 |
| M18 | 0.09729 | 0.00145 | 0.28653 | 0.00415 | 3.84091 | 0.06537 | 0.851008 | 103.27 | 1572.8 | 27.66 | 1624.2 | 20.78 | 1601.4 | 13.71 | 10 | 64012 | 6510 | 309019 | 1 |
| M19 | 0.08305 | 0.00112 | 0.22177 | 0.00313 | 2.53986 | 0.04075 | 0.879678 | 101.63 | 1270.5 | 26.03 | 1291.2 | 16.51 | 1283.5 | 11.69 | 9 | 126780 | 10765 | 785603 | 1 |
| M21 | 0.08336 | 0.001 | 0.21271 | 0.00296 | 2.44482 | 0.03656 | 0.93056 | 97.32 | 1277.5 | 23.41 | 1243.2 | 15.76 | 1255.9 | 10.78 | 0 | 131465 | 11217 | 848123 | 1 |
| M22 | 0.08333 | 0.00101 | 0.21447 | 0.00299 | 2.46407 | 0.03674 | 0.935015 | 98.10 | 1276.8 | 23.45 | 1252.6 | 15.85 | 1261.6 | 10.77 | 2 | 127972 | 10987 | 817952 | 1 |
| M01 | 0.08379 | 0.00091 | 0.22363 | 0.00321 | 2.58316 | 0.03794 | 0.977302 | 101.06 | 1287.3 | 20.97 | 1301 | 16.93 | 1295.9 | 10.75 | 0 | 212360 | 18085 | 1355867 | 2 |
| M02A | 0.08339 | 0.00093 | 0.22918 | 0.00328 | 2.63465 | 0.03914 | 0.963384 | 104.09 | 1277.9 | 21.75 | 1330.2 | 17.22 | 1310.4 | 10.94 | 25 | 201684 | 17090 | 1249872 | 2 |
| M02B | 0.0829 | 0.00092 | 0.22607 | 0.00326 | 2.58334 | 0.03846 | 0.968606 | 103.74 | 1266.5 | 21.42 | 1313.9 | 17.11 | 1295.9 | 10.9 | 1 | 180899 | 15230 | 1142888 | 2 |
| M03 | 0.08461 | 0.00097 | 0.21755 | 0.00313 | 2.5373 | 0.03829 | 0.953392 | 97.14 | 1306.3 | 22.18 | 1268.9 | 16.58 | 1282.8 | 10.99 | 12 | 181287 | 15570 | 1186791 | 2 |
| M08 | 0.08546 | 0.00097 | 0.21857 | 0.00315 | 2.57474 | 0.0387 | 0.958832 | 96.13 | 1325.6 | 21.8 | 1274.3 | 16.67 | 1293.5 | 10.99 | 16 | 239103 | 20735 | 1562628 | 2 |
| M09 | 0.08448 | 0.00097 | 0.22089 | 0.00319 | 2.57225 | 0.03911 | 0.949817 | 98.72 | 1303.3 | 22.23 | 1286.6 | 16.86 | 1292.8 | 11.12 | 15 | 210256 | 18009 | 1361882 | 2 |
| M09B | 0.08348 | 0.00096 | 0.2261 | 0.00329 | 2.60166 | 0.03974 | 0.952616 | 102.66 | 1280 | 22.36 | 1314 | 17.28 | 1301.1 | 11.2 | 7 | 197316 | 16697 | 1255307 | 2 |
| M10† | 0.08403 | 0.00097 | 0.21896 | 0.00318 | 2.53629 | 0.03886 | 0.947891 | 98.72 | 1292.9 | 22.36 | 1276.4 | 16.82 | 1282.5 | 11.16 | 14 | 215173 | 18306 | 1412650 | 2 |
| M14 | 0.0836 | 0.00098 | 0.22077 | 0.00321 | 2.54404 | 0.03928 | 0.941711 | 100.26 | 1282.7 | 22.72 | 1286 | 16.97 | 1284.7 | 11.25 | 5 | 196916 | 16651 | 1283563 | 2 |
| M15 | 0.08332 | 0.00098 | 0.21475 | 0.00314 | 2.46636 | 0.03824 | 0.943051 | 98.27 | 1276.2 | 22.82 | 1254.1 | 16.64 | 1262.2 | 11.2 | 4 | 234961 | 19791 | 1579914 | 2 |

Appendix 2. U-Pb isotopic age data for monazite analyses

Sample 115638

| Spot | $^{207}Pb/^{206}Pb$ | 1 σ | $^{206}Pb/^{238}U$ | 1 σ | $^{207}Pb/^{235}U$ | 1 σ | rho | Conc. (%) | $^{207}Pb/^{206}Pb$ age | 1 σ | $^{206}Pb/^{238}U$ age | 1 σ | $^{207}Pb/^{235}U$ age | 1 σ | $^{204}Pb$ | $^{206}Pb$ | $^{207}Pb$ | $^{238}Pb$ |
|---|---|---|---|---|---|---|---|---|---|---|---|---|---|---|---|---|---|---|
| M01† | 0.10027 | 0.00241 | 0.22379 | 0.00367 | 3.09319 | 0.07487 | 0.67752317 | 79.90 | 1629.2 | 44.09 | 1301.8 | 19.32 | 1431 | 18.57 | 56 | 14594 | 1511 | 86888 |
| M05A | 0.08433 | 0.00104 | 0.2271 | 0.00313 | 2.63933 | 0.03931 | 0.92537519 | 101.47 | 1300.2 | 23.8 | 1319.3 | 16.42 | 1311.7 | 10.97 | 0 | 35709 | 3089 | 211296 |
| M05B | 0.08369 | 0.00109 | 0.21839 | 0.00302 | 2.51875 | 0.03876 | 0.89861878 | 99.07 | 1285.3 | 25.24 | 1273.4 | 16 | 1277.5 | 11.18 | 31 | 31708 | 2727 | 194747 |
| M06 | 0.08343 | 0.00104 | 0.22635 | 0.00312 | 2.60257 | 0.03912 | 0.91701759 | 102.83 | 1279.2 | 24.28 | 1315.4 | 16.43 | 1301.4 | 11.03 | 11 | 27862 | 2388 | 165567 |
| M06B | 0.08332 | 0.00101 | 0.22896 | 0.00315 | 2.62886 | 0.03888 | 0.93023385 | 104.13 | 1276.4 | 23.66 | 1329.1 | 16.51 | 1308.7 | 10.88 | 20 | 27549 | 2354 | 161755 |
| M08 | 0.08248 | 0.00104 | 0.23277 | 0.0032 | 2.64559 | 0.03986 | 0.9124482 | 107.34 | 1256.8 | 24.28 | 1349 | 16.75 | 1313.4 | 11.1 | 9 | 37319 | 3162 | 214924 |
| M10† | 0.08513 | 0.00116 | 0.22338 | 0.0031 | 2.62046 | 0.04149 | 0.87649917 | 98.58 | 1318.4 | 26.35 | 1299.7 | 16.32 | 1306.4 | 11.64 | 0 | 25733 | 2241 | 153714 |
| M16 | 0.08476 | 0.00119 | 0.22455 | 0.00313 | 2.62276 | 0.04223 | 0.86570265 | 99.69 | 1309.9 | 27 | 1305.9 | 16.47 | 1307 | 11.84 | 0 | 18620 | 1613 | 110724 |
| M16B† | 0.08459 | 0.00127 | 0.22449 | 0.00315 | 2.61683 | 0.04421 | 0.83055529 | 99.96 | 1306.1 | 29.01 | 1305.6 | 16.6 | 1305.4 | 12.41 | 0 | 37325 | 3233 | 221656 |
| M17 | 0.08602 | 0.00112 | 0.2208 | 0.00305 | 2.61739 | 0.04017 | 0.90005154 | 96.08 | 1338.6 | 24.95 | 1286.1 | 16.11 | 1305.5 | 11.27 | 7 | 19241 | 1698 | 116763 |
| M18 | 0.08602 | 0.00102 | 0.22608 | 0.00309 | 2.67984 | 0.03903 | 0.9384403 | 98.15 | 1338.7 | 22.71 | 1313.9 | 16.27 | 1322.9 | 10.77 | 16 | 44510 | 3901 | 264636 |
| M19A | 0.08436 | 0.001 | 0.22896 | 0.00313 | 2.66156 | 0.03876 | 0.93872247 | 102.16 | 1300.9 | 22.77 | 1329 | 16.44 | 1317.9 | 10.75 | 7 | 34636 | 2975 | 203431 |
| M19B | 0.0828 | 0.00098 | 0.22549 | 0.0031 | 2.5727 | 0.03764 | 0.93966692 | 103.66 | 1264.5 | 22.83 | 1310.8 | 16.28 | 1292.9 | 10.7 | 47 | 39804 | 3355 | 238075 |
| M20 | 0.08563 | 0.00095 | 0.22632 | 0.00306 | 2.67057 | 0.0374 | 0.96545238 | 98.90 | 1329.8 | 21.4 | 1315.2 | 16.09 | 1320.3 | 10.35 | 0 | 163488 | 14317 | 967683 |
| M21 | 0.08445 | 0.00102 | 0.22845 | 0.00314 | 2.65847 | 0.03927 | 0.93048494 | 101.81 | 1302.8 | 23.26 | 1326.4 | 16.48 | 1317 | 10.9 | 0 | 30909 | 2655 | 182235 |
| M22 | 0.0851 | 0.00108 | 0.22838 | 0.00317 | 2.67809 | 0.04081 | 0.91087706 | 100.63 | 1317.7 | 24.38 | 1326 | 16.63 | 1322.4 | 11.27 | 2 | 20585 | 1782 | 121831 |
| M22B | 0.0851 | 0.0011 | 0.229 | 0.00319 | 2.68536 | 0.04144 | 0.90268862 | 100.87 | 1317.7 | 24.83 | 1329.2 | 16.75 | 1324.4 | 11.42 | 0 | 18487 | 1602 | 109343 |
| M24 | 0.08513 | 0.00107 | 0.22805 | 0.00316 | 2.67502 | 0.04062 | 0.91252363 | 100.45 | 1318.4 | 24.23 | 1324.3 | 16.59 | 1321.6 | 11.22 | 0 | 28125 | 2437 | 166697 |
| M25† | 0.08473 | 0.00136 | 0.22898 | 0.00328 | 2.6731 | 0.04781 | 0.80088979 | 101.52 | 1309.2 | 30.94 | 1329.1 | 17.2 | 1321 | 13.22 | 0 | 43989 | 3786 | 258830 |
| M26 | 0.08505 | 0.00104 | 0.23286 | 0.00323 | 2.72927 | 0.04094 | 0.92471157 | 102.50 | 1316.6 | 23.63 | 1349.5 | 16.9 | 1336.5 | 11.15 | 0 | 35654 | 3100 | 208015 |
| M28 | 0.08512 | 0.00116 | 0.23612 | 0.00333 | 2.76984 | 0.04458 | 0.87624606 | 103.66 | 1318.3 | 26.36 | 1366.5 | 17.39 | 1347.4 | 12.01 | 0 | 17576 | 1524 | 101322 |
| M29 | 0.08343 | 0.00106 | 0.23442 | 0.00324 | 2.69571 | 0.04113 | 0.90586777 | 106.14 | 1279.1 | 24.57 | 1357.6 | 16.9 | 1327.3 | 11.3 | 0 | 128372 | 10951 | 739181 |

Appendix 2. U-Pb isotopic age data for monazite analyses

Sample 115669

| Spot | $^{207}Pb/^{206}Pb$ | 1 σ | $^{206}Pb/^{238}U$ | 1 σ | $^{207}Pb/^{235}U$ | 1 σ | rho | Conc. (%) | $^{207}Pb/^{206}Pb$ age | 1 σ | $^{206}Pb/^{238}U$ age | 1 σ | $^{207}Pb/^{235}U$ age | 1 σ | $^{204}Pb$ | $^{206}Pb$ | $^{207}Pb$ | $^{238}Pb$ |
|---|---|---|---|---|---|---|---|---|---|---|---|---|---|---|---|---|---|---|
| M03 | 0.08331 | 0.00089 | 0.22727 | 0.0032 | 2.61064 | 0.03737 | 0.98362998 | 103.44 | 1276.3 | 20.74 | 1320.2 | 16.82 | 1303.6 | 10.51 | 20 | 454562 | 38546 | 2803357 |
| M06 | 0.08322 | 0.00092 | 0.2322 | 0.00326 | 2.66442 | 0.03865 | 0.96785115 | 105.63 | 1274.2 | 21.48 | 1346 | 17.04 | 1318.6 | 10.71 | 24 | 499619 | 42183 | 2996150 |
| M07A | 0.08404 | 0.00094 | 0.22485 | 0.00315 | 2.60544 | 0.03789 | 0.96332789 | 101.09 | 1293.4 | 21.52 | 1307.5 | 16.58 | 1302.2 | 10.67 | 19 | 410232 | 35053 | 2535399 |
| M07B | 0.08468 | 0.00093 | 0.2263 | 0.00317 | 2.64239 | 0.03828 | 0.96694038 | 100.53 | 1308.2 | 21.29 | 1315.1 | 16.69 | 1312.5 | 10.67 | 16 | 422306 | 36384 | 2598236 |
| M08 | 0.08379 | 0.00098 | 0.23387 | 0.00329 | 2.70224 | 0.04046 | 0.93954897 | 105.23 | 1287.5 | 22.68 | 1354.8 | 17.16 | 1329.1 | 11.1 | 14 | 483845 | 41004 | 2872836 |
| M09 | 0.08373 | 0.00095 | 0.23159 | 0.00327 | 2.67364 | 0.03954 | 0.95476 | 104.41 | 1286.1 | 22.02 | 1342.8 | 17.1 | 1321.2 | 10.93 | 25 | 329310 | 27961 | 1987176 |
| M11 | 0.08374 | 0.00102 | 0.22698 | 0.00319 | 2.62092 | 0.03995 | 0.92201943 | 102.52 | 1286.3 | 23.49 | 1318.7 | 16.76 | 1306.5 | 11.2 | 10 | 320244 | 27112 | 1954825 |
| M11B† | 0.08477 | 0.00112 | 0.22787 | 0.00323 | 2.66345 | 0.04268 | 0.88457672 | 101.01 | 1310.1 | 25.42 | 1323.3 | 16.94 | 1318.4 | 11.83 | 17 | 326375 | 27923 | 1984172 |
| M12 | 0.08548 | 0.00109 | 0.23278 | 0.00328 | 2.74386 | 0.04311 | 0.89683408 | 101.70 | 1326.4 | 24.59 | 1349 | 17.15 | 1340.4 | 11.69 | 25 | 464613 | 39980 | 2760494 |
| M13 | 0.08526 | 0.00105 | 0.22615 | 0.00319 | 2.65901 | 0.04082 | 0.91884247 | 99.46 | 1321.5 | 23.63 | 1314.3 | 16.75 | 1317.1 | 11.33 | 25 | 253459 | 21845 | 1554854 |
| M14 | 0.08519 | 0.00094 | 0.2271 | 0.00317 | 2.66722 | 0.03845 | 0.96828816 | 99.95 | 1319.9 | 21.29 | 1319.3 | 16.65 | 1319.4 | 10.64 | 16 | 247928 | 21495 | 1512111 |
| M15 | 0.08463 | 0.00093 | 0.23132 | 0.00324 | 2.69874 | 0.0389 | 0.97172477 | 102.64 | 1306.9 | 21.36 | 1341.4 | 16.94 | 1328.1 | 10.68 | 25 | 192968 | 16626 | 1157942 |
| M15B | 0.08423 | 0.00093 | 0.2246 | 0.00314 | 2.60815 | 0.03769 | 0.96744509 | 100.63 | 1297.9 | 21.33 | 1306.1 | 16.53 | 1302.9 | 10.61 | 15 | 323889 | 27762 | 2001143 |
| M16A | 0.08411 | 0.00093 | 0.23376 | 0.00327 | 2.71074 | 0.03912 | 0.96931866 | 104.56 | 1295.1 | 21.33 | 1354.2 | 17.1 | 1331.4 | 10.71 | 5 | 369428 | 31746 | 2195021 |
| M17B | 0.08458 | 0.00095 | 0.22184 | 0.00311 | 2.58663 | 0.03768 | 0.96237415 | 98.91 | 1305.8 | 21.68 | 1291.6 | 16.4 | 1296.9 | 10.67 | 9 | 363556 | 31382 | 2275791 |
| M18A | 0.08357 | 0.00097 | 0.22922 | 0.00321 | 2.64122 | 0.0391 | 0.94597649 | 103.73 | 1282.5 | 22.55 | 1330.4 | 16.83 | 1312.2 | 10.9 | 16 | 379872 | 32377 | 2293922 |
| M18B† | 0.09204 | 0.00127 | 0.23533 | 0.00335 | 2.98719 | 0.04912 | 0.86570914 | 92.79 | 1468.2 | 26.14 | 1362.4 | 17.46 | 1404.4 | 12.51 | 139 | 239273 | 22363 | 1404321 |
| M23 | 0.08292 | 0.001 | 0.22882 | 0.00322 | 2.61611 | 0.03965 | 0.92848459 | 104.81 | 1267.3 | 23.36 | 1328.3 | 16.87 | 1305.2 | 11.13 | 8 | 405937 | 34374 | 2456670 |
| M24 | 0.08283 | 0.00098 | 0.2358 | 0.00331 | 2.69259 | 0.04019 | 0.94045153 | 107.87 | 1265.2 | 22.69 | 1364.8 | 17.29 | 1326.4 | 11.05 | 0 | 361822 | 30652 | 2130196 |
| M26A | 0.08407 | 0.00099 | 0.23074 | 0.00326 | 2.67427 | 0.04002 | 0.94411061 | 103.42 | 1294.1 | 22.66 | 1338.4 | 17.07 | 1321.4 | 11.06 | 7 | 173144 | 14892 | 1046789 |
| M26B | 0.08278 | 0.00097 | 0.22766 | 0.00321 | 2.59806 | 0.03871 | 0.9463337 | 104.60 | 1264.1 | 22.49 | 1322.2 | 16.87 | 1300.1 | 10.92 | 9 | 280183 | 23779 | 1716076 |

Appendix 2. U-Pb isotopic age data for monazite analyses

Sample 115866

| Spot | $^{207}Pb/^{206}Pb$ | 1 σ | $^{206}Pb/^{238}U$ | 1 σ | $^{207}Pb/^{235}U$ | 1 σ | rho | Conc. (%) | $^{207}Pb/^{206}Pb$ age | 1 σ | $^{206}Pb/^{238}U$ age | 1 σ | $^{207}Pb/^{235}U$ age | 1 σ | $^{204}Pb$ | $^{206}Pb$ | $^{207}Pb$ | $^{238}Pb$ | Session |
|---|---|---|---|---|---|---|---|---|---|---|---|---|---|---|---|---|---|---|---|
| M01 | 0.08713 | 0.00099 | 0.22866 | 0.00336 | 2.74652 | 0.04154 | 0.97155044 | 97.37 | 1363.3 | 21.82 | 1327.4 | 17.61 | 1341.1 | 11.26 | 0 | 42129 | 3788 | 266778 | a |
| M01B | 0.08568 | 0.00099 | 0.22975 | 0.00337 | 2.71395 | 0.04118 | 0.96669591 | 100.17 | 1331 | 22.18 | 1333.2 | 17.66 | 1332.3 | 11.26 | 6 | 39336 | 3476 | 247380 | a |
| M01C | 0.08426 | 0.00098 | 0.23195 | 0.00338 | 2.69461 | 0.0409 | 0.96005239 | 103.56 | 1298.5 | 22.4 | 1344.7 | 17.71 | 1327 | 11.24 | 15 | 39950 | 3467 | 247593 | a |
| M01D | 0.08605 | 0.00101 | 0.22191 | 0.00326 | 2.63275 | 0.04047 | 0.95569022 | 96.45 | 1339.4 | 22.65 | 1291.9 | 17.21 | 1309.8 | 11.31 | 14 | 38254 | 3393 | 249304 | a |
| M01E | 0.08697 | 0.00105 | 0.22158 | 0.00324 | 2.65671 | 0.04102 | 0.94702828 | 94.89 | 1359.7 | 23.06 | 1290.2 | 17.08 | 1316.5 | 11.39 | 0 | 36311 | 3253 | 234845 | a |
| M01F | 0.08663 | 0.00106 | 0.23034 | 0.00337 | 2.75089 | 0.04279 | 0.94057077 | 98.82 | 1352.3 | 23.49 | 1336.3 | 17.68 | 1342.3 | 11.58 | 26 | 35941 | 3220 | 223541 | a |
| M01G | 0.0912 | 0.00111 | 0.22585 | 0.00328 | 2.8386 | 0.04381 | 0.94098932 | 90.49 | 1450.7 | 22.97 | 1312.7 | 17.23 | 1365.8 | 11.59 | 24 | 41503 | 3889 | 261448 | a |
| M01H | 0.08904 | 0.00108 | 0.2226 | 0.00322 | 2.73157 | 0.04212 | 0.93811198 | 92.21 | 1405 | 22.96 | 1295.6 | 17 | 1337.1 | 11.46 | 2 | 46064 | 4199 | 294408 | a |
| M02A | 0.08406 | 0.00093 | 0.22301 | 0.00328 | 2.58476 | 0.03863 | 0.98411312 | 100.29 | 1293.9 | 21.27 | 1297.7 | 17.28 | 1296.3 | 10.94 | 10 | 148108 | 12880 | 967942 | a |
| M02B† | 0.0945 | 0.00108 | 0.21909 | 0.00322 | 2.85484 | 0.04321 | 0.97102592 | 84.12 | 1518.2 | 21.34 | 1277.1 | 17.02 | 1370.1 | 11.38 | 79 | 99120 | 9684 | 656253 | a |
| M05A | 0.08699 | 0.00123 | 0.22964 | 0.00341 | 2.75399 | 0.04672 | 0.87531902 | 97.96 | 1360.3 | 27.05 | 1332.6 | 17.9 | 1343.2 | 12.64 | 18 | 40700 | 3625 | 253702 | a |
| M05B | 0.08537 | 0.00113 | 0.22279 | 0.00327 | 2.62223 | 0.04282 | 0.89882714 | 97.94 | 1323.9 | 25.56 | 1296.6 | 17.23 | 1306.9 | 12 | 23 | 58715 | 5105 | 376038 | a |
| M06 | 0.08814 | 0.00122 | 0.22858 | 0.00338 | 2.77623 | 0.04647 | 0.88340783 | 95.77 | 1385.6 | 26.32 | 1327 | 17.74 | 1349.2 | 12.49 | 32 | 34789 | 3125 | 217241 | a |
| M06B† | 0.14261 | 0.00217 | 0.26859 | 0.00415 | 5.27989 | 0.09366 | 0.87102171 | 67.89 | 2259.1 | 26.06 | 1533.6 | 21.07 | 1865.6 | 15.14 | 79 | 21730 | 3174 | 117153 | a |
| M07† | 0.08698 | 0.00097 | 0.22834 | 0.0033 | 2.73706 | 0.04076 | 0.97046994 | 97.48 | 1360.1 | 21.44 | 1325.8 | 17.3 | 1338.6 | 11.07 | 90 | 258227 | 23007 | 1617951 | a |
| M07A | 0.08598 | 0.00095 | 0.22414 | 0.00323 | 2.65598 | 0.03917 | 0.97713458 | 97.46 | 1337.7 | 21.14 | 1303.7 | 17.03 | 1316.3 | 10.88 | 19 | 148701 | 13108 | 949534 | a |
| M08† | 0.08416 | 0.00099 | 0.22514 | 0.00324 | 2.61089 | 0.03959 | 0.94906383 | 101.00 | 1296.1 | 22.63 | 1309 | 17.04 | 1303.7 | 11.13 | 18 | 237852 | 20475 | 1500752 | a |
| M08B | 0.08449 | 0.00093 | 0.22139 | 0.00318 | 2.57794 | 0.03791 | 0.97676062 | 98.88 | 1303.8 | 21.35 | 1289.2 | 16.78 | 1294.4 | 10.76 | 21 | 215216 | 18694 | 1384146 | a |
| M01A | 0.08583 | 0.00111 | 0.23159 | 0.00326 | 2.74053 | 0.04283 | 0.90070855 | 100.64 | 1334.2 | 24.93 | 1342.8 | 17.06 | 1339.5 | 11.63 | 0 | 24699 | 2154 | 146063 | b |
| M01B | 0.08946 | 0.00113 | 0.23373 | 0.00335 | 2.88279 | 0.04512 | 0.91574438 | 95.76 | 1413.9 | 23.84 | 1354 | 17.5 | 1377.4 | 11.8 | 3 | 20398 | 1841 | 122070 | b |
| M02A | 0.08549 | 0.0013 | 0.22602 | 0.00329 | 2.66408 | 0.04641 | 0.83557362 | 99.01 | 1326.7 | 29.16 | 1313.6 | 17.3 | 1318.6 | 12.86 | 14 | 23663 | 2059 | 144938 | b |
| M02B | 0.08474 | 0.00116 | 0.23111 | 0.0033 | 2.69997 | 0.04385 | 0.87919365 | 102.36 | 1309.4 | 26.38 | 1340.3 | 17.27 | 1328.4 | 12.03 | 15 | 25093 | 2164 | 149735 | b |
| M03A | 0.08706 | 0.00112 | 0.23001 | 0.0033 | 2.76171 | 0.04355 | 0.90982347 | 98.00 | 1361.9 | 24.58 | 1334.6 | 17.28 | 1345.3 | 11.76 | 0 | 17080 | 1510 | 103535 | b |
| M03B | 0.08707 | 0.00111 | 0.2277 | 0.00325 | 2.73423 | 0.04286 | 0.91054876 | 97.10 | 1362 | 24.38 | 1322.5 | 17.08 | 1337.8 | 11.65 | 9 | 18441 | 1630 | 112684 | b |
| M03C | 0.08594 | 0.00109 | 0.23001 | 0.00328 | 2.72622 | 0.04259 | 0.91280999 | 99.84 | 1336.8 | 24.47 | 1334.6 | 17.18 | 1335.6 | 11.61 | 0 | 15693 | 1370 | 94679 | b |
| M03D | 0.08596 | 0.00114 | 0.22669 | 0.00323 | 2.68704 | 0.04286 | 0.89328929 | 98.49 | 1337.3 | 25.49 | 1317.1 | 16.98 | 1324.9 | 11.8 | 0 | 16056 | 1402 | 97795 | b |
| M03E | 0.08671 | 0.00116 | 0.22372 | 0.00319 | 2.67543 | 0.04279 | 0.8915325 | 96.12 | 1354.1 | 25.54 | 1301.5 | 16.79 | 1321.7 | 11.82 | 22 | 15210 | 1339 | 93720 | b |
| M03F | 0.08347 | 0.00113 | 0.22417 | 0.0032 | 2.57992 | 0.04156 | 0.88614173 | 101.86 | 1280.1 | 26.2 | 1303.9 | 16.83 | 1295 | 11.79 | 5 | 20240 | 1721 | 124536 | b |
| M03G | 0.08699 | 0.00116 | 0.22692 | 0.00322 | 2.72196 | 0.0434 | 0.88996946 | 96.92 | 1360.2 | 25.49 | 1318.3 | 16.93 | 1334.5 | 11.84 | 0 | 15454 | 1365 | 93609 | b |
| M03H | 0.08851 | 0.00121 | 0.23251 | 0.00336 | 2.83737 | 0.04696 | 0.8731433 | 96.71 | 1393.5 | 26.01 | 1347.7 | 17.56 | 1365.5 | 12.42 | 14 | 20960 | 1854 | 126021 | b |
| M03I | 0.08712 | 0.00122 | 0.22906 | 0.00333 | 2.75149 | 0.04632 | 0.86356367 | 97.54 | 1363.2 | 26.81 | 1329.6 | 17.48 | 1342.5 | 12.54 | 18 | 16917 | 1476 | 103708 | b |
| M05A | 0.08593 | 0.00127 | 0.22559 | 0.00332 | 2.67259 | 0.04668 | 0.84259666 | 98.11 | 1336.6 | 28.35 | 1311.3 | 17.48 | 1320.9 | 12.91 | 0 | 26120 | 2248 | 163701 | b |
| M05B | 0.08676 | 0.00115 | 0.23858 | 0.00345 | 2.85391 | 0.0464 | 0.88942095 | 101.78 | 1355.2 | 25.35 | 1379.3 | 17.94 | 1369.8 | 12.22 | 0 | 22940 | 1997 | 135142 | b |
| M06A | 0.08606 | 0.0011 | 0.23101 | 0.0033 | 2.7409 | 0.04323 | 0.90571407 | 100.02 | 1339.5 | 24.62 | 1339.8 | 17.27 | 1339.6 | 11.73 | 12 | 22897 | 1987 | 137894 | b |
| M06B | 0.08669 | 0.00111 | 0.22756 | 0.00326 | 2.72002 | 0.04306 | 0.90493992 | 97.64 | 1353.7 | 24.6 | 1321.7 | 17.12 | 1333.9 | 11.75 | 0 | 19150 | 1676 | 117488 | b |
| M06C | 0.08681 | 0.00112 | 0.22452 | 0.00322 | 2.68731 | 0.04268 | 0.9030134 | 96.27 | 1356.3 | 24.62 | 1305.7 | 16.96 | 1325 | 11.75 | 15 | 20005 | 1748 | 124595 | b |
| M06D | 0.08601 | 0.00112 | 0.22476 | 0.00323 | 2.66534 | 0.04267 | 0.89766331 | 97.65 | 1338.4 | 25.06 | 1307 | 16.98 | 1318.9 | 11.82 | 6 | 20380 | 1764 | 126683 | b |
| M06E† | 0.10754 | 0.00146 | 0.24483 | 0.00357 | 3.62994 | 0.05971 | 0.8864535 | 80.30 | 1758.1 | 24.57 | 1411.8 | 18.47 | 1556.1 | 13.09 | 48 | 17444 | 1881 | 100139 | b |

Appendix 2. U-Pb isotopic age data for zircon analyses

Sample 113019

| Spot | $^{207}Pb/^{206}Pb$ | 1 σ | $^{206}Pb/^{238}U$ | 1 σ | $^{207}Pb/^{235}U$ | 1 σ | $^{208}Pb/^{232}Th$ | 1 σ | rho | Conc. (%) | $^{207}Pb/^{206}Pb$ age | 1 σ | $^{206}Pb/^{238}U$ age | 1 σ | $^{207}Pb/^{235}U$ age | 1 σ | $^{208}Pb/^{232}Th$ age | 1 σ | $^{204}Pb$ | $^{206}Pb$ | $^{207}Pb$ | $^{238}Pb$ | $^{232}Th$ | $^{238}U$ | Session |
|---|---|---|---|---|---|---|---|---|---|---|---|---|---|---|---|---|---|---|---|---|---|---|---|---|---|
| Z01† | 0.08529 | 0.00477 | 0.22431 | 0.00553 | 2.6373 | 0.1415 | 0.02919 | 0.00386 | 0.459493731 | 98.67 | 1322.2 | 105 | 1304.6 | 29 | 1311.1 | 40 | 581.5 | 76 | 0 | 468 | 40 | 23 | 885 | 2680 | 1 |
| Z04† | 0.08791 | 0.00365 | 0.24042 | 0.00481 | 2.91421 | 0.11655 | 0.06671 | 0.01213 | 0.500245338 | 100.60 | 1380.6 | 78 | 1388.9 | 25 | 1385.6 | 30 | 1305.3 | 230 | 4 | 579 | 51 | 14 | 224 | 2933 | 1 |
| Z05† | 0.08303 | 0.00457 | 0.24021 | 0.00566 | 2.74964 | 0.14622 | 0.09003 | 0.01333 | 0.443092507 | 109.28 | 1270.0 | 104 | 1387.8 | 29 | 1342.0 | 40 | 1742.5 | 247 | 33 | 450 | 37 | 17 | 211 | 2394 | 1 |
| Z06† | 0.09127 | 0.00538 | 0.23974 | 0.00639 | 3.01658 | 0.16943 | 0.15163 | 0.03824 | 0.474553186 | 95.39 | 1452.2 | 108 | 1385.3 | 33 | 1411.8 | 43 | 2853.5 | 671 | 13 | 391 | 36 | 10 | 77 | 2086 | 1 |
| Z07† | 0.09025 | 0.00395 | 0.23045 | 0.00481 | 2.86747 | 0.12061 | 0.01401 | 0.02386 | 0.496231043 | 93.45 | 1430.6 | 81 | 1336.9 | 25 | 1373.4 | 32 | 281.1 | 476 | 2 | 506 | 46 | 1 | 95 | 2689 | 1 |
| Z09† | 0.10164 | 0.00738 | 0.2398 | 0.00728 | 3.3602 | 0.23305 | 0.11669 | 0.01529 | 0.437721845 | 83.76 | 1654.3 | 129 | 1385.7 | 38 | 1495.2 | 54 | 2230.8 | 277 | 0 | 237 | 24 | 25 | 238 | 1242 | 1 |
| Z10† | 0.09464 | 0.0091 | 0.2284 | 0.00824 | 2.97999 | 0.27494 | 0.41485 | 0.12466 | 0.391028121 | 87.19 | 1520.9 | 171 | 1326.1 | 43 | 1402.5 | 70 | 7014.2 | 1781 | 0 | 134 | 12 | 6 | 16 | 734 | 1 |
| Z11† | 0.10796 | 0.00762 | 0.2494 | 0.00818 | 3.71202 | 0.24705 | 0.163 | 0.05999 | 0.492813168 | 81.32 | 1765.2 | 124 | 1435.4 | 42 | 1574.0 | 53 | 3052.1 | 1043 | 28 | 250 | 27 | 5 | 40 | 1270 | 1 |
| Z14 | 0.08606 | 0.00252 | 0.22107 | 0.0036 | 2.62311 | 0.07524 | 0.06541 | 0.00506 | 0.56772812 | 96.13 | 1339.4 | 56 | 1287.5 | 19 | 1307.1 | 21 | 1280.6 | 96 | 1 | 2401 | 211 | 413 | 6794 | 13144 | 1 |
| Z16† | 0.0926 | 0.00449 | 0.21825 | 0.00502 | 2.78628 | 0.12969 | 0.08138 | 0.00854 | 0.494160164 | 86.01 | 1479.6 | 89 | 1272.6 | 27 | 1351.9 | 35 | 1581.3 | 160 | 0 | 557 | 52 | 44 | 624 | 3346 | 1 |
| Z17 | 0.08532 | 0.00446 | 0.23262 | 0.00538 | 2.73636 | 0.13751 | 0.06902 | 0.01458 | 0.460229206 | 101.92 | 1322.8 | 98 | 1348.2 | 28 | 1338.4 | 37 | 1348.9 | 276 | 0 | 385 | 33 | 11 | 179 | 2071 | 1 |
| Z17B† | 0.09321 | 0.00215 | 0.23849 | 0.00364 | 3.06369 | 0.07161 | 0.03241 | 0.00216 | 0.652983722 | 92.41 | 1492.1 | 43 | 1378.9 | 19 | 1423.7 | 18 | 644.7 | 42 | 0 | 6676 | 617 | 377 | 14318 | 36080 | 1 |
| Z18† | 0.04574 | 0.01354 | 0.24233 | 0.01762 | 1.52814 | 0.44337 | 1.78147 | 1.79698 | 0.250608364 | - | 0.1 | 577 | 1398.8 | 91 | 941.8 | 178 | ****** | ******* | 0 | 115 | 5 | 2 | 2 | 589 | 1 |
| Z19† | 0.09209 | 0.00474 | 0.22059 | 0.00516 | 2.80065 | 0.13798 | 0.15403 | 0.04363 | 0.474795483 | 87.47 | 1469.0 | 95 | 1285.0 | 27 | 1355.7 | 37 | 2895.6 | 764 | 0 | 353 | 32 | 5 | 44 | 1978 | 1 |
| Z20 | 0.09942 | 0.00376 | 0.22134 | 0.00446 | 3.03321 | 0.11056 | 0.14124 | 0.0153 | 0.55281447 | 79.90 | 1613.2 | 69 | 1289.0 | 24 | 1416.0 | 28 | 2670.3 | 271 | 14 | 1426 | 140 | 63 | 544 | 8389 | 1 |
| Z21† | 0.09247 | 0.00354 | 0.23946 | 0.00479 | 3.05301 | 0.11308 | 0.08051 | 0.00666 | 0.540063669 | 93.70 | 1477.0 | 71 | 1383.9 | 25 | 1421.0 | 28 | 1565.1 | 125 | 22 | 908 | 83 | 77 | 1212 | 4891 | 1 |
| Z23† | 0.10196 | 0.00688 | 0.2315 | 0.00718 | 3.25401 | 0.20736 | 0.14116 | 0.23663 | 0.486706726 | 80.86 | 1660.0 | 120 | 1342.3 | 38 | 1470.1 | 50 | 2669.0 | 4191 | 0 | 302 | 30 | 0 | 7 | 1678 | 1 |
| Z24† | 0.08358 | 0.00568 | 0.22508 | 0.00621 | 2.59358 | 0.16899 | 0.16542 | 0.08058 | 0.423441419 | 102.02 | 1282.7 | 127 | 1308.6 | 33 | 1298.8 | 48 | 3094.2 | 1397 | 0 | 229 | 18 | 2 | 19 | 1277 | 1 |
| Z24B† | 0.10098 | 0.00891 | 0.23866 | 0.00908 | 3.32199 | 0.27708 | -0.44006 | 2.35907 | 0.456141256 | 84.02 | 1642.2 | 155 | 1379.7 | 47 | 1486.2 | 65 | ****** | ******* | 3 | 221 | 21 | 0 | 0 | 1181 | 1 |
| Z24C† | 0.09991 | 0.00581 | 0.24197 | 0.00652 | 3.33307 | 0.18437 | 0.1539 | 0.03149 | 0.487124811 | 86.10 | 1622.5 | 104 | 1396.9 | 34 | 1488.8 | 43 | 2893.3 | 552 | 8 | 306 | 30 | 10 | 79 | 1646 | 1 |
| Z25A | 0.0793 | 0.0063 | 0.22809 | 0.00413 | 2.75802 | 0.08799 | 0.07308 | 0.02116 | 0.567554929 | 96.21 | 1376.7 | 61 | 1324.5 | 22 | 1344.3 | 24 | 1425.7 | 399 | 1 | 1701 | 149 | 171 | 2599 | 9682 | 1 |
| Z25A† | 0.08774 | 0.00286 | 0.2419 | 0.0073 | 2.6445 | 0.20231 | 0.07295 | 0.00437 | 0.394469303 | 118.40 | 1179.6 | 149 | 1396.6 | 38 | 1313.1 | 56 | 1423.3 | 82 | 4 | 239 | 18 | 7 | 125 | 1275 | 1 |
| Z26A† | 0.11202 | 0.01289 | 0.22115 | 0.01124 | 3.41491 | 0.3673 | 0.70505 | 0.40879 | 0.472539047 | 70.29 | 1832.4 | 195 | 1288.0 | 59 | 1507.8 | 84 | ****** | 4846 | 0 | 138 | 15 | 4 | 7 | 825 | 1 |
| Z26B† | 0.09341 | 0.00416 | 0.22688 | 0.0049 | 2.92126 | 0.12435 | 0.07899 | 0.00529 | 0.507369421 | 88.10 | 1496.2 | 82 | 1318.1 | 26 | 1387.4 | 32 | 1536.7 | 99 | 0 | 475 | 44 | 59 | 797 | 2575 | 1 |
| Z27 | 0.08637 | 0.00214 | 0.22053 | 0.00335 | 2.62489 | 0.06424 | 0.07 | 0.00769 | 0.620701372 | 95.40 | 1346.6 | 47 | 1284.7 | 18 | 1307.6 | 18 | 1367.6 | 145 | 20 | 3131 | 272 | 33 | 496 | 17193 | 1 |
| Z28A | 0.09035 | 0.00245 | 0.22971 | 0.00378 | 2.86028 | 0.07695 | 0.08583 | 0.00555 | 0.611662455 | 93.04 | 1432.7 | 51 | 1333.0 | 20 | 1371.5 | 20 | 1664.3 | 103 | 8 | 2235 | 200 | 111 | 1416 | 12516 | 1 |
| Z28B† | 0.09201 | 0.00329 | 0.22688 | 0.00431 | 2.87752 | 0.09914 | 0.04635 | 0.0097 | 0.551379345 | 89.81 | 1467.6 | 67 | 1318.1 | 23 | 1376.0 | 26 | 915.7 | 187 | 16 | 690 | 63 | 11 | 268 | 3776 | 1 |
| Z29† | 0.11242 | 0.00583 | 0.23187 | 0.00603 | 3.59259 | 0.17609 | 0.16361 | 0.01451 | 0.530573694 | 73.10 | 1838.9 | 91 | 1344.3 | 32 | 1547.9 | 39 | 3062.7 | 252 | 25 | 486 | 54 | 59 | 393 | 2702 | 1 |
| Z30A† | 0.09099 | 0.00356 | 0.21297 | 0.00419 | 2.67149 | 0.10035 | 0.09681 | 0.01462 | 0.523759325 | 86.05 | 1446.4 | 73 | 1244.6 | 22 | 1320.6 | 28 | 1867.7 | 269 | 0 | 700 | 63 | 16 | 171 | 4032 | 1 |
| Z30B† | 0.09392 | 0.00549 | 0.23253 | 0.00607 | 3.01028 | 0.1678 | 0.15974 | 0.07783 | 0.468300516 | 89.46 | 1506.5 | 107 | 1347.7 | 32 | 1410.2 | 42 | 2995.5 | 1356 | 0 | 301 | 28 | 3 | 25 | 1628 | 1 |
| Z31† | 0.09207 | 0.00323 | 0.22626 | 0.00416 | 2.87161 | 0.09752 | 0.10836 | 0.00953 | 0.541398829 | 89.52 | 1468.8 | 65 | 1314.9 | 22 | 1374.5 | 26 | 2079.5 | 174 | 14 | 769 | 70 | 34 | 328 | 4220 | 1 |
| Z32A | 0.0924 | 0.00423 | 0.23228 | 0.00522 | 2.95862 | 0.12973 | 0.25207 | 0.03292 | 0.512516033 | 94.88 | 1419.0 | 79 | 1346.4 | 27 | 1397.1 | 33 | 4543.7 | 531 | 0 | 976 | 89 | 33 | 139 | 5403 | 1 |
| Z32B | 0.08962 | 0.00473 | 0.23429 | 0.0057 | 2.89473 | 0.14502 | 0.0877 | 0.01048 | 0.485625255 | 95.72 | 1417.5 | 98 | 1356.9 | 30 | 1380.5 | 38 | 1699.1 | 195 | 0 | 922 | 83 | 61 | 691 | 4520 | 1 |
| Z33A | 0.0897 | 0.00383 | 0.22 | 0.00461 | 2.72025 | 0.1112 | 0.06268 | 0.00594 | 0.512604337 | 90.34 | 1419.0 | 79 | 1281.9 | 24 | 1334.0 | 30 | 1228.8 | 113 | 0 | 997 | 90 | 66 | 1082 | 5590 | 1 |
| Z33B† | 0.11361 | 0.00615 | 0.22698 | 0.00605 | 3.555 | 0.18164 | 0.13166 | 0.01478 | 0.521670039 | 70.97 | 1858.0 | 95 | 1318.6 | 32 | 1539.6 | 40 | 2499.9 | 264 | 27 | 354 | 40 | 30 | 231 | 2009 | 1 |
| Z01 | 0.0883 | 0.00283 | 0.20875 | 0.00368 | 2.54084 | 0.07911 | 0.08116 | 0.0064 | 0.566196614 | 87.99 | 1389.0 | 60 | 1222.2 | 20 | 1283.8 | 23 | 1577.2 | 120 | 0 | 1949 | 175 | 85 | 998 | 11688 | 2 |
| Z02 | 0.08894 | 0.00192 | 0.21939 | 0.0032 | 2.68948 | 0.05851 | 0.06813 | 0.00232 | 0.670457682 | 91.15 | 1402.8 | 41 | 1278.6 | 17 | 1325.6 | 16 | 1332.1 | 44 | 0 | 3779 | 341 | 734 | 10197 | 21267 | 2 |
| Z03 | 0.08706 | 0.00241 | 0.2195 | 0.00344 | 2.63434 | 0.07178 | 0.06902 | 0.01288 | 0.575164788 | 93.93 | 1361.8 | 52 | 1279.2 | 18 | 1310.3 | 20 | 1349.1 | 243 | 10 | 1355 | 119 | 17 | 238 | 7524 | 2 |
| Z05 | 0.08613 | 0.00168 | 0.21643 | 0.003 | 2.5695 | 0.05103 | 0.0675 | 0.00267 | 0.697954078 | 94.18 | 1341.1 | 37 | 1263.0 | 16 | 1292.0 | 15 | 1320.3 | 51 | 7 | 5501 | 479 | 567 | 7868 | 30807 | 2 |
| Z06 | 0.0905 | 0.00274 | 0.20935 | 0.00358 | 2.61117 | 0.07713 | 0.07406 | 0.00695 | 0.578924431 | 85.32 | 1436.1 | 57 | 1225.3 | 19 | 1303.8 | 22 | 1444.0 | 131 | 29 | 1964 | 180 | 62 | 805 | 11649 | 2 |
| Z07 | 0.08871 | 0.00278 | 0.23816 | 0.00404 | 2.91198 | 0.08889 | 0.07174 | 0.00482 | 0.555709761 | 98.52 | 1397.8 | 59 | 1377.1 | 21 | 1385.0 | 23 | 1400.3 | 91 | 2 | 1389 | 124 | 84 | 1113 | 7088 | 2 |
| Z09† | 0.09504 | 0.00344 | 0.22766 | 0.00431 | 2.98265 | 0.1044 | 0.07652 | 0.00591 | 0.540869303 | 86.48 | 1528.9 | 67 | 1322.2 | 23 | 1403.2 | 27 | 1490.4 | 111 | 0 | 781 | 75 | 66 | 826 | 4297 | 2 |
| Z10 | 0.09078 | 0.00278 | 0.22093 | 0.00384 | 2.7647 | 0.08274 | 0.056 | 0.00866 | 0.58077649 | 89.24 | 1441.9 | 57 | 1286.8 | 20 | 1346.1 | 22 | 1101.4 | 166 | 0 | 1600 | 148 | 26 | 466 | 9224 | 2 |
| Z11 | 0.09194 | 0.00254 | 0.21246 | 0.00342 | 2.69233 | 0.07294 | 0.08246 | 0.01027 | 0.594171013 | 84.71 | 1466.0 | 52 | 1241.9 | 18 | 1326.4 | 20 | 1601.5 | 192 | 4 | 1486 | 138 | 31 | 369 | 8488 | 2 |
| Z13 | 0.08651 | 0.0029 | 0.23748 | 0.00429 | 2.83188 | 0.09252 | 0.16822 | 0.01769 | 0.552929135 | 101.79 | 1349.5 | 63 | 1373.6 | 22 | 1364.0 | 25 | 3142.6 | 306 | 0 | 1353 | 119 | 44 | 255 | 7243 | 2 |
| Z14† | 0.08594 | 0.00347 | 0.22046 | 0.00426 | 2.61151 | 0.10225 | 0.05178 | 0.03729 | 0.493523881 | 96.07 | 1336.8 | 76 | 1284.3 | 23 | 1303.9 | 29 | 1020.5 | 717 | 4 | 683 | 59 | 3 | 58 | 3875 | 2 |

Sample 113019 continued

| Spot | $^{207}Pb/^{206}Pb$ | 1 σ | $^{206}Pb/^{238}U$ | 1 σ | $^{207}Pb/^{235}U$ | 1 σ | $^{208}Pb/^{232}Th$ | 1 σ | rho | Conc. (%) | $^{207}Pb/^{206}Pb$ age | 1 σ | $^{206}Pb/^{238}U$ age | 1 σ | $^{207}Pb/^{235}U$ age | 1 σ | $^{208}Pb/^{232}Th$ age | 1 σ | $^{204}Pb$ | $^{206}Pb$ | $^{207}Pb$ | $^{238}Pb$ | $^{232}Th$ | $^{238}U$ | Session |
|---|---|---|---|---|---|---|---|---|---|---|---|---|---|---|---|---|---|---|---|---|---|---|---|---|---|
| Z15 | 0.09188 | 0.00313 | 0.22186 | 0.00393 | 2.80971 | 0.093 | 0.1023 | 0.01049 | 0.535170407 | 88.18 | 1464.9 | 63 | 1291.7 | 21 | 1358.1 | 25 | 1968.7 | 192 | 1 | 768 | 71 | 28 | 268 | 4257 | 2 |
| Z16 | 0.08863 | 0.00352 | 0.21485 | 0.00426 | 2.62484 | 0.10046 | 0.08725 | 0.0113 | 0.518064583 | 89.86 | 1396.1 | 74 | 1254.6 | 23 | 1307.6 | 28 | 1690.7 | 210 | 21 | 1120 | 100 | 33 | 381 | 6572 | 2 |
| Z17† | 0.08814 | 0.00337 | 0.23582 | 0.00455 | 2.86518 | 0.1065 | 0.11047 | 0.01026 | 0.519078529 | 98.51 | 1385.6 | 72 | 1364.9 | 24 | 1372.8 | 28 | 2118.0 | 187 | 0 | 900 | 80 | 42 | 378 | 4885 | 2 |
| Z18† | 0.09315 | 0.00279 | 0.21915 | 0.00372 | 2.81356 | 0.08244 | 0.05909 | 0.00735 | 0.579321522 | 85.68 | 1490.9 | 56 | 1277.4 | 20 | 1359.2 | 22 | 1160.4 | 140 | 19 | 1033 | 97 | 24 | 404 | 5853 | 2 |
| Z19 | 0.08931 | 0.00335 | 0.22111 | 0.00422 | 2.72186 | 0.09871 | 0.07943 | 0.00662 | 0.526270102 | 91.28 | 1410.7 | 70 | 1287.7 | 22 | 1334.4 | 27 | 1544.9 | 124 | 24 | 877 | 79 | 56 | 692 | 4915 | 2 |
| Z20 | 0.0858 | 0.00437 | 0.2391 | 0.00543 | 2.82667 | 0.13827 | 0.07393 | 0.01351 | 0.464266556 | 103.63 | 1333.6 | 96 | 1382.0 | 28 | 1362.6 | 37 | 1441.6 | 254 | 25 | 786 | 68 | 20 | 265 | 3943 | 2 |
| Z22 | 0.08916 | 0.00241 | 0.22258 | 0.00374 | 2.73509 | 0.07398 | 0.06552 | 0.00629 | 0.62121618 | 92.04 | 1407.6 | 51 | 1295.5 | 20 | 1338.0 | 20 | 1282.7 | 119 | 14 | 4055 | 362 | 73 | 1124 | 24386 | 2 |
| Z23† | 0.08893 | 0.00507 | 0.23736 | 0.00589 | 2.90952 | 0.15931 | 0.09317 | 0.02126 | 0.453196003 | 97.89 | 1402.5 | 105 | 1372.9 | 31 | 1384.4 | 41 | 1800.5 | 393 | 0 | 412 | 37 | 12 | 129 | 2225 | 2 |
| Z24† | 0.10145 | 0.0059 | 0.21759 | 0.00594 | 3.04208 | 0.16706 | 0.07949 | 0.02419 | 0.497102179 | 76.88 | 1650.8 | 104 | 1269.1 | 31 | 1418.2 | 42 | 1546.0 | 453 | 15 | 591 | 61 | 12 | 152 | 3337 | 2 |
| Z27† | 0.08369 | 0.00407 | 0.2333 | 0.00499 | 2.69132 | 0.12595 | 0.00429 | 0.01653 | 0.457038698 | 105.17 | 1285.3 | 92 | 1351.7 | 26 | 1326.1 | 35 | 86.5 | 333 | 0 | 609 | 51 | 0 | 138 | 3135 | 2 |
| Z28 | 0.09152 | 0.00324 | 0.22213 | 0.00419 | 2.8029 | 0.09633 | 0.06809 | 0.00356 | 0.548848965 | 88.73 | 1457.4 | 66 | 1293.1 | 22 | 1356.3 | 26 | 1331.5 | 67 | 19 | 1070 | 98 | 143 | 2098 | 6170 | 2 |
| Z29 | 0.09615 | 0.00431 | 0.22232 | 0.00502 | 2.94712 | 0.1262 | 0.08795 | 0.01388 | 0.527307135 | 83.45 | 1550.7 | 82 | 1294.1 | 26 | 1394.1 | 32 | 1703.8 | 258 | 12 | 879 | 84 | 25 | 291 | 5148 | 2 |
| Z31 | 0.08794 | 0.00267 | 0.21726 | 0.0037 | 2.63401 | 0.07824 | 0.09198 | 0.00847 | 0.573337735 | 91.76 | 1381.2 | 57 | 1267.4 | 20 | 1310.2 | 22 | 1778.6 | 157 | 2 | 1247 | 110 | 41 | 432 | 7161 | 2 |
| Z32† | 0.10205 | 0.00568 | 0.21772 | 0.00586 | 3.06311 | 0.16128 | 0.22679 | 0.04466 | 0.511188846 | 76.41 | 1661.8 | 100 | 1269.8 | 31 | 1423.5 | 40 | 4131.4 | 736 | 28 | 710 | 72 | 23 | 106 | 4299 | 2 |
| Z33 | 0.12913 | 0.00502 | 0.23026 | 0.00495 | 4.09871 | 0.15064 | 0.27961 | 0.01968 | 0.58491611 | 64.04 | 2086.1 | 67 | 1335.9 | 26 | 1654.0 | 30 | 4983.5 | 311 | 16 | 767 | 99 | 105 | 363 | 4130 | 2 |
| Z34 | 0.08515 | 0.00361 | 0.22068 | 0.00458 | 2.59039 | 0.10599 | 0.13854 | 0.02493 | 0.50722747 | 97.47 | 1318.8 | 80 | 1285.5 | 24 | 1297.9 | 30 | 2622.4 | 443 | 24 | 1056 | 90 | 20 | 148 | 6160 | 2 |
| Z35 | 0.09175 | 0.00347 | 0.21065 | 0.00405 | 2.66414 | 0.09642 | 0.06895 | 0.00503 | 0.53123108 | 84.28 | 1462.1 | 70 | 1232.3 | 22 | 1318.6 | 27 | 1347.6 | 95 | 0 | 1248 | 114 | 106 | 1464 | 7079 | 2 |
| Z36 | 0.09006 | 0.00291 | 0.21137 | 0.00361 | 2.62466 | 0.08168 | 0.0592 | 0.00299 | 0.548808941 | 86.64 | 1426.7 | 61 | 1236.1 | 19 | 1307.6 | 23 | 1162.5 | 57 | 0 | 1854 | 166 | 488 | 7521 | 10168 | 2 |
| Z37† | 0.08487 | 0.00345 | 0.24344 | 0.0047 | 2.84797 | 0.1117 | 0.0862 | 0.0127 | 0.492252755 | 107.02 | 1312.4 | 77 | 1404.5 | 24 | 1368.3 | 29 | 1671.3 | 236 | 17 | 704 | 59 | 18 | 206 | 3471 | 2 |
| Z38† | 0.08217 | 0.00358 | 0.22209 | 0.00448 | 2.51579 | 0.10588 | 0.06198 | 0.00974 | 0.479302246 | 103.47 | 1249.5 | 83 | 1292.9 | 24 | 1276.6 | 31 | 1215.5 | 185 | 3 | 634 | 52 | 17 | 271 | 3505 | 2 |

† indicates analysis was discarded due to noisy isotopic signal and/or low counts

Appendix 2. Sample 113019- trace element abundance of zircon and garnet

Garnet trace element concentrations with minimum detection limit filtered.

| Element | GT01 | 1 σ | GT02 | 1 σ | GT03 | 1 σ | GT05 | 1 σ | GT06 | 1 σ | GT07 | 1 σ | GT08 | 1 σ | GT09 | 1 σ | GT10 | 1 σ | GT11 | 1 σ |
|---|---|---|---|---|---|---|---|---|---|---|---|---|---|---|---|---|---|---|---|---|
| Mg24 | 23524.49 | 925.26 | 25367.03 | 1005.21 | 26040.54 | 1042.53 | 18964.5 | 774.85 | 23324.15 | 972.65 | 20267.72 | 879.07 | 20415.6 | 897.48 | 21885.56 | 979.12 | 22137.41 | 1005 | 18879.62 | 870.33 |
| Al27 | 133745.3 | 4873.31 | 130215.48 | 4751.49 | 129860.82 | 4755.42 | 114943.05 | 4224.92 | 126617.7 | 4653.5 | 112979.8 | 4170.3 | 110254.15 | 4071.52 | 116175.74 | 4314.51 | 115222.98 | 4283.51 | 105665.34 | 3934.03 |
| Si29 | 241081.88 | 13061.28 | 238734.11 | 13009.85 | 230739.73 | 12688.05 | 208341.39 | 11662.33 | 242935.91 | 13826.89 | 215395.22 | 12667.68 | 197242.69 | 11746.18 | 220908.67 | 13354.46 | 205754.48 | 12604.02 | 185647.22 | 11528.54 |
| Ca43 | 87429.37 | 2941.32 | 87059.15 | 2933.09 | 89005.28 | 3016.42 | 83475.64 | 2836.05 | 89005.28 | 2998.22 | 78431.28 | 2626.7 | 76687.41 | 2554.62 | 82690.9 | 2773.83 | 80117.97 | 2674.56 | 76330.05 | 2537.42 |
| Ti47 | 328.58 | 14.91 | 373.63 | 16.8 | 648.64 | 28.03 | 233.47 | 11.63 | 678.87 | 30.55 | 479.12 | 22.68 | 482 | 23.03 | 460.03 | 22.71 | 515.97 | 25.57 | 511.38 | 25.68 |
| Ti49 | 323.97 | 36.78 | 387.17 | 43.47 | 637.03 | 70.2 | 251.14 | 34.12 | 706.69 | 88.95 | 475.49 | 67.47 | 496.34 | 72.94 | 473.64 | 72.87 | 512.96 | 81.55 | 540.99 | 88.94 |
| Cr53 | 58.89 | 4.16 | 47.09 | 3.69 | 88.24 | 5.25 | 65.84 | 4.5 | 78.89 | 5.08 | 14.47 | 2.52 | 35.35 | 2.86 | 54.67 | 3.91 | 66.02 | 4.13 | 104.3 | 5.72 |
| Mn55 | 7483.21 | 265.07 | 6756.49 | 240.54 | 6305.19 | 226.24 | 6228.89 | 226.53 | 6190.31 | 227.72 | 6743.33 | 254.3 | 6502.56 | 247.19 | 6052.62 | 233.17 | 5992.49 | 232.98 | 5858.35 | 230.01 |
| Fe56 | 229732.94 | 13476.69 | 218084.48 | 13026.45 | 215064.59 | 13123.62 | 189327.25 | 12114.89 | 205845.84 | 13872.76 | 189517.58 | 13897.52 | 188644.98 | 14231.89 | 193415.88 | 15029.7 | 190886.91 | 15259.19 | 171238.89 | 14079.65 |
| Fe57 | 86511.43 | 4243.22 | 83392.45 | 4166.9 | 82078.67 | 4192.57 | 72433.5 | 3881.68 | 79432.83 | 4484 | 75525.02 | 4649.08 | 73768.14 | 4676.49 | 76410.97 | 4998.33 | 75102.16 | 5061.37 | 69387.36 | 4818.28 |
| Y89 | 57.19 | 2.2 | 61.49 | 2.39 | 73.28 | 2.87 | 67.04 | 2.7 | 67.25 | 2.77 | 54.86 | 2.37 | 44 | 1.93 | 65.27 | 2.92 | 72.08 | 3.28 | 40.39 | 1.88 |
| Zr90 | 0.49 | 0.15 | 1.56 | 0.18 | 0.93 | 0.17 | 0.66 | 0.16 | 113.68 | 5.69 | 2.65 | 0.2 | 2.16 | 0.17 | 3.71 | 0.28 | 2.51 | 0.2 | 0.448 | 0.093 |
| La139 | <0.118 | 0.042 | <0.108 | 0.04 | <0.114 | 0.041 | <0.119 | 0.042 | <0.109 | 0.04 | 0.096 | 0.031 | <0.077 | 0.03 | <0.078 | 0.03 | <0.074 | 0.028 | <0.067 | 0.025 |
| Ce140 | <0.090 | 0.032 | 0.275 | 0.04 | <0.103 | 0.038 | <0.106 | 0.038 | <0.091 | 0.034 | <0.073 | 0.029 | 0.18 | 0.026 | 0.121 | 0.029 | 0.213 | 0.032 | <0.057 | 0.022 |
| Pr141 | <0.080 | 0.03 | <0.077 | 0.029 | <0.077 | 0.028 | <0.079 | 0.029 | <0.082 | 0.03 | <0.056 | 0.021 | <0.053 | 0.02 | <0.058 | 0.023 | <0.059 | 0.021 | <0.046 | 0.018 |
| Nd146 | <0.48 | 0.18 | <0.46 | 0.17 | <0.51 | 0.19 | <0.49 | 0.18 | <0.52 | 0.19 | <0.35 | 0.14 | <0.31 | 0.12 | <0.37 | 0.14 | 0.47 | 0.12 | <0.31 | 0.11 |
| Sm147 | <0.63 | 0.24 | <0.55 | 0.2 | 0.56 | 0.2 | 0.86 | 0.25 | <0.65 | 0.23 | <0.45 | 0.17 | 0.51 | 0.14 | <0.48 | 0.18 | <0.44 | 0.17 | <0.36 | 0.14 |
| Eu153 | 0.351 | 0.064 | 0.285 | 0.057 | 0.319 | 0.061 | 0.275 | 0.057 | 0.275 | 0.055 | 0.217 | 0.044 | 0.266 | 0.045 | 0.288 | 0.049 | 0.217 | 0.045 | 0.243 | 0.037 |
| Gd157 | 2.7 | 0.26 | 2.01 | 0.26 | 1.56 | 0.23 | 2.05 | 0.21 | 1.36 | 0.24 | 1.86 | 0.18 | 1.57 | 0.18 | 1.46 | 0.21 | 1.47 | 0.18 | 2.28 | 0.19 |
| Tb159 | 1.116 | 0.065 | 1.087 | 0.066 | 0.536 | 0.046 | 0.629 | 0.05 | 0.545 | 0.047 | 0.631 | 0.044 | 0.527 | 0.04 | 0.537 | 0.044 | 0.568 | 0.044 | 0.903 | 0.058 |
| Dy163 | 9.28 | 0.39 | 10.05 | 0.42 | 6.49 | 0.31 | 8.01 | 0.37 | 6.27 | 0.3 | 7.49 | 0.32 | 5.44 | 0.25 | 6.75 | 0.31 | 7.78 | 0.33 | 8.41 | 0.35 |
| Ho165 | 2.18 | 0.1 | 2.51 | 0.12 | 2.67 | 0.13 | 2.76 | 0.13 | 2.45 | 0.12 | 2.16 | 0.11 | 1.631 | 0.086 | 2.38 | 0.12 | 2.75 | 0.14 | 1.667 | 0.091 |
| Er166 | 5.99 | 0.28 | 6.58 | 0.3 | 14 | 0.59 | 9.08 | 0.41 | 12.28 | 0.53 | 6.33 | 0.3 | 5.47 | 0.27 | 9.36 | 0.44 | 9.8 | 0.46 | 3.87 | 0.2 |
| Tm169 | 0.815 | 0.052 | 0.985 | 0.057 | 4.03 | 0.17 | 1.353 | 0.072 | 3.04 | 0.14 | 0.892 | 0.051 | 0.969 | 0.054 | 1.761 | 0.088 | 1.542 | 0.079 | 0.517 | 0.037 |
| Yb172 | 5.72 | 0.31 | 7.19 | 0.36 | 54.77 | 2.17 | 9.82 | 0.48 | 37.26 | 1.56 | 6.63 | 0.34 | 8.31 | 0.41 | 14.88 | 0.71 | 11.43 | 0.56 | 3.67 | 0.22 |
| Lu175 | 0.728 | 0.051 | 0.951 | 0.058 | 14.2 | 0.55 | 1.292 | 0.073 | 10.29 | 0.41 | 0.778 | 0.048 | 1.434 | 0.072 | 2.3 | 0.11 | 1.544 | 0.079 | 0.485 | 0.036 |
| Hf178 | <0.37 | 0.13 | <0.37 | 0.13 | <0.37 | 0.13 | <0.35 | 0.13 | 2.82 | 0.27 | <0.27 | 0.11 | <0.253 | 0.091 | <0.28 | 0.11 | <0.251 | 0.092 | <0.213 | 0.079 |
| Pb206 | <0.42 | 0.15 | 0.44 | 0.16 | <0.45 | 0.17 | <0.39 | 0.15 | <0.48 | 0.18 | 0.41 | 0.12 | <0.27 | 0.11 | 0.46 | 0.14 | <0.36 | 0.14 | <0.235 | 0.091 |
| Pb208 | <0.233 | 0.084 | 0.38 | 0.09 | <0.248 | 0.091 | <0.211 | 0.078 | 0.248 | 0.09 | 0.44 | 0.07 | <0.171 | 0.066 | 0.481 | 0.076 | 0.379 | 0.067 | <0.136 | 0.051 |
| Th232 | <0.091 | 0.033 | <0.139 | 0.046 | <0.103 | 0.038 | <0.107 | 0.038 | <0.104 | 0.039 | <0.065 | 0.026 | <0.067 | 0.024 | <0.084 | 0.031 | <0.074 | 0.027 | <0.061 | 0.024 |
| U238 | <0.078 | 0.029 | <0.081 | 0.029 | <0.066 | 0.026 | <0.072 | 0.026 | <0.079 | 0.031 | <0.048 | 0.019 | <0.051 | 0.019 | 0.074 | 0.019 | <0.049 | 0.019 | <0.047 | 0.018 |

Garnet grain 1

Garnet grain 2

Garnet trace element concentrations normalised to chondrite.

| Element | GT01 | GT02 | GT03 | GT05 | GT06 | GT07 | GT08 | GT09 | GT10 | GT11 |
|---|---|---|---|---|---|---|---|---|---|---|
| Location | rim | int | core | rim | core | rim | int | core | int | rim |
| Mg24 | 0.1645 | 0.1774 | 0.1821 | 0.1326 | 0.1631 | 0.1417 | 0.1428 | 0.153 | 0.1548 | 0.132 |
| Al27 | 10.37 | 10.09 | 10.07 | 8.91 | 9.82 | 8.76 | 8.55 | 9.01 | 8.93 | 8.19 |
| Si29 | 1.507 | 1.492 | 1.442 | 1.302 | 1.518 | 1.346 | 1.233 | 1.381 | 1.286 | 1.16 |
| Ca43 | 6.48 | 6.45 | 6.59 | 6.18 | 6.59 | 5.81 | 5.68 | 6.13 | 5.93 | 5.65 |
| Ti47 | 0.502 | 0.571 | 0.992 | 0.357 | 1.038 | 0.733 | 0.737 | 0.703 | 0.789 | 0.782 |
| Ti49 | 0.495 | 0.592 | 0.97 | 0.384 | 1.08 | 0.73 | 0.76 | 0.72 | 0.78 | 0.83 |
| Cr53 | 0.0148 | 0.01185 | 0.0222 | 0.0166 | 0.0198 | 0.00364 | 0.00889 | 0.01375 | 0.0166 | 0.0262 |
| Mn55 | 2.545 | 2.298 | 2.145 | 2.119 | 2.106 | 2.294 | 2.212 | 2.059 | 2.038 | 1.993 |
| Fe56 | 0.826 | 0.784 | 0.774 | 0.681 | 0.74 | 0.682 | 0.679 | 0.696 | 0.687 | 0.616 |
| Fe57 | 0.311 | 0.3 | 0.295 | 0.261 | 0.286 | 0.272 | 0.265 | 0.275 | 0.27 | 0.25 |
| Y89 | 25.42 | 27.33 | 32.57 | 29.8 | 29.89 | 24.38 | 19.56 | 29.01 | 32.03 | 17.95 |
| Zr90 | 0.088 | 0.282 | 0.169 | 0.12 | 20.52 | 0.478 | 0.389 | 0.669 | 0.453 | 0.081 |
| La139 | 0 | 0 | 0 | 0 | 0 | 0.262 | 0 | 0 | 0 | 0 |
| Ce140 | 0 | 0.288 | 0 | 0 | 0 | 0 | 0.188 | 0.126 | 0.223 | 0 |
| Pr141 | 0 | 0 | 0 | 0 | 0 | 0 | 0 | 0 | 0 | 0 |
| Nd146 | 0 | 0 | 0 | 0 | 0 | 0 | 0 | 0 | 0.66 | 0 |
| Sm147 | 0 | 0 | 2.44 | 3.74 | 0 | 0 | 2.23 | 0 | 0 | 0 |
| Eu153 | 4.04 | 3.28 | 3.67 | 3.17 | 3.16 | 2.49 | 3.06 | 3.31 | 2.5 | 2.79 |
| Gd157 | 8.83 | 6.57 | 5.11 | 6.69 | 4.45 | 6.08 | 5.13 | 4.78 | 4.81 | 7.45 |
| Tb159 | 19.24 | 18.73 | 9.24 | 10.84 | 9.39 | 10.87 | 9.09 | 9.26 | 9.8 | 15.57 |
| Dy163 | 24.37 | 26.37 | 17.02 | 21.01 | 16.46 | 19.66 | 14.28 | 17.71 | 20.41 | 22.07 |
| Ho165 | 25.58 | 29.44 | 31.35 | 32.44 | 28.75 | 25.38 | 19.17 | 27.96 | 32.28 | 19.59 |
| Er166 | 24.07 | 26.44 | 56.23 | 36.45 | 49.32 | 25.42 | 21.96 | 37.58 | 39.37 | 15.54 |
| Tm169 | 22.89 | 27.68 | 113.18 | 37.99 | 85.41 | 25.05 | 27.23 | 49.48 | 43.31 | 14.52 |
| Yb172 | 23.08 | 29.01 | 220.84 | 39.59 | 150.23 | 26.73 | 33.52 | 60 | 46.08 | 14.8 |
| Lu175 | 19.1 | 24.96 | 372.81 | 33.91 | 270.06 | 20.43 | 37.64 | 60.4 | 40.54 | 12.74 |
| Hf178 | 0 | 0 | 0 | 0 | 15.73 | 0 | 0 | 0 | 0 | 0 |
| Pb206 | 0 | 0.121 | 0 | 0 | 0 | 0.112 | 0 | 0.125 | 0 | 0 |
| Pb208 | 0 | 0.104 | 0 | 0 | 0.068 | 0.121 | 0 | 0.132 | 0.104 | 0 |
| Th232 | 0 | 0 | 0 | 0 | 0 | 0 | 0 | 0 | 0 | 0 |
| U238 | 0 | 0 | 0 | 0 | 0 | 0 | 0 | 6.09 | 0 | 0 |
| LREE (Sm/La) | - | - | - | - | - | - | - | - | - | - |
| HREE (Lu/Gd) | 2.16 | 3.80 | 72.96 | 5.07 | 60.69 | 3.36 | 7.34 | 12.64 | 8.43 | 1.71 |
| MHREE (Lu/Sm) | - | - | 152.79 | 9.07 | - | - | 16.88 | - | - | - |
| Eu/Eu* | - | - | 1.04 | 0.63 | - | - | 0.90 | - | - | - |

Gt06 not plotted due to potential zircon contamination

Garnet grain 1
Garnet grain 2

Appendix 2. Sample 113019- trace element abundance of zircon and garnet

Zircon trace element concentrations with minimum detection limit filtered.

| Element | Z06-1 | 1 σ | Z07-1 | 1 σ | Z10-1 | 1 σ | Z17-1 | 1 σ | Z25A-1 | 1 σ | Z32A-1 | 1 σ | Z32B-1 | 1 σ | Z01-1 | 1 σ | Z02-2 | 1 σ | Z03-2 | 1 σ | Z07-2 | 1 σ |
|---|---|---|---|---|---|---|---|---|---|---|---|---|---|---|---|---|---|---|---|---|---|---|
| **Al27** | 1565.48 | 99.7 | 27.79 | 1.87 | 10.64 | 0.9 | 2.39 | 0.45 | 35.76 | 2.67 | <1.71 | 0.71 | 40.92 | 3.57 | 261.5 | 19.81 | 6846.63 | 434.59 | 1994.12 | 129.84 | 3910.71 | 251.66 |
| **Si29** | 210042.94 | 23069.73 | 200352.61 | 22027.12 | 201494.11 | 22183.52 | 183774.33 | 20289.28 | 191206.98 | 21204.96 | 184856.34 | 20644.99 | 193481.2 | 21732.33 | 228765.72 | 27551.98 | 210995.72 | 23983.98 | 291500.19 | 34641.85 | 229666.61 | 26978.92 |
| **Ti49** | 122.71 | 11.98 | 16.99 | 6.63 | <19.22 | 7.98 | 21.7 | 6.68 | <26.87 | 10.95 | <27.15 | 11.33 | <53.22 | 22.48 | <236.21 | 113.58 | <107.39 | 54.48 | <250.62 | 124.65 | <212.65 | 89.52 |
| **V51** | 37.01 | 2.14 | 0.28 | 0.1 | <0.31 | 0.13 | <0.26 | 0.11 | <0.38 | 0.16 | <0.42 | 0.18 | <0.84 | 0.37 | <4.04 | 1.91 | 19.63 | 1.82 | <4.09 | 2.11 | <3.12 | 1.32 |
| **Fe57** | 2750.08 | 125.21 | <13.10 | 5.36 | 18.19 | 6.72 | <12.73 | 5.13 | <21.66 | 8.9 | <21.87 | 9.19 | <42.77 | 18.21 | <192.98 | 90.48 | <84.44 | 44.28 | <210.82 | 105.29 | 281.45 | 73.3 |
| **Y89** | 34.38 | 1.44 | 39.71 | 1.68 | 51.95 | 2.23 | 48.74 | 2.17 | 55.2 | 2.6 | 58.65 | 2.96 | 32.57 | 1.79 | 38.37 | 2.74 | 114.69 | 5.67 | 105.96 | 6.02 | 48.23 | 2.72 |
| **Zr90** | 536731.88 | 21174.89 | 592522 | 23604.46 | 551329.75 | 22202.2 | 555290.13 | 22915.08 | 566582.31 | 24048.93 | 543533.81 | 24190.78 | 522171.75 | 23644.51 | 516854.91 | 19828.34 | 556370.56 | 21314.21 | 567058.38 | 21854.93 | 560932.5 | 21582.43 |
| **Nb93** | 2.74 | 0.14 | 2.87 | 0.15 | 2.67 | 0.15 | 2.66 | 0.14 | 2.59 | 0.18 | 2.33 | 0.18 | 2.38 | 0.24 | 2.36 | 0.79 | 2.51 | 0.5 | 2.35 | 0.7 | 2.95 | 0.65 |
| **La139** | <0.024 | 0.01 | <0.0222 | 0.0092 | 0.027 | 0.012 | <0.0212 | 0.0086 | <0.036 | 0.015 | <0.036 | 0.016 | <0.075 | 0.034 | <0.33 | 0.16 | 5.75 | 0.31 | <0.32 | 0.17 | 1.18 | 0.15 |
| **Ce140** | 0.296 | 0.019 | 0.191 | 0.015 | 0.047 | 0.01 | 0.189 | 0.016 | 0.206 | 0.024 | 0.215 | 0.026 | 0.503 | 0.056 | 1.3 | 0.2 | 4.78 | 0.28 | 0.83 | 0.17 | 0.75 | 0.12 |
| **Pr141** | 0.0467 | 0.0077 | <0.0166 | 0.0068 | <0.0191 | 0.008 | <0.0156 | 0.0062 | <0.027 | 0.011 | <0.026 | 0.011 | <0.051 | 0.023 | <0.23 | 0.11 | 1.93 | 0.14 | <0.24 | 0.12 | <0.211 | 0.087 |
| **Nd146** | 0.11 | 0.036 | <0.094 | 0.038 | 0.152 | 0.045 | 0.138 | 0.04 | <0.152 | 0.066 | <0.153 | 0.068 | <0.31 | 0.14 | <1.45 | 0.67 | 17.7 | 1.09 | <1.57 | 0.7 | <1.30 | 0.53 |
| **Sm147** | <0.094 | 0.038 | <0.130 | 0.052 | 0.204 | 0.058 | 0.13 | 0.048 | <0.196 | 0.083 | <0.187 | 0.084 | <0.37 | 0.16 | <1.60 | 0.79 | 2.69 | 0.49 | <1.75 | 0.84 | <1.58 | 0.66 |
| **Eu153** | 0.097 | 0.014 | 0.085 | 0.014 | <0.037 | 0.016 | 0.206 | 0.017 | 0.143 | 0.024 | 0.159 | 0.027 | 0.116 | 0.045 | <0.44 | 0.21 | 1.45 | 0.16 | <0.50 | 0.24 | <0.41 | 0.17 |
| **Gd157** | 0.848 | 0.056 | 0.955 | 0.066 | 0.818 | 0.072 | 1.282 | 0.081 | 1.3 | 0.12 | 1.41 | 0.13 | 0.62 | 0.17 | <1.59 | 0.79 | 5.26 | 0.61 | 3.07 | 0.96 | <1.41 | 0.6 |
| **Tb159** | 0.255 | 0.014 | 0.337 | 0.017 | 0.393 | 0.021 | 0.403 | 0.02 | 0.493 | 0.03 | 0.513 | 0.033 | 0.272 | 0.034 | 0.39 | 0.14 | 1 | 0.1 | 1 | 0.18 | 0.51 | 0.1 |
| **Dy163** | 3.35 | 0.14 | 3.61 | 0.15 | 4.48 | 0.19 | 4.59 | 0.2 | 5.4 | 0.27 | 5.52 | 0.3 | 3.05 | 0.23 | 3.88 | 0.65 | 6.47 | 0.53 | 9.52 | 0.96 | 5.38 | 0.53 |
| **Ho165** | 1.098 | 0.049 | 1.168 | 0.053 | 1.511 | 0.07 | 1.567 | 0.076 | 1.738 | 0.095 | 1.83 | 0.11 | 0.947 | 0.071 | 0.87 | 0.17 | 2.42 | 0.17 | 3.28 | 0.28 | 1.34 | 0.14 |
| **Er166** | 3.64 | 0.16 | 4.24 | 0.19 | 4.77 | 0.22 | 5.27 | 0.25 | 5.81 | 0.31 | 7.12 | 0.42 | 3.89 | 0.27 | 4.56 | 0.53 | 6.58 | 0.46 | 11.86 | 0.9 | 4.7 | 0.42 |
| **Tm169** | 0.679 | 0.029 | 0.814 | 0.035 | 0.916 | 0.04 | 0.959 | 0.043 | 1.124 | 0.057 | 1.383 | 0.074 | 0.77 | 0.056 | 1.01 | 0.14 | 0.974 | 0.096 | 1.81 | 0.2 | 0.93 | 0.11 |
| **Yb172** | 6.58 | 0.25 | 8.67 | 0.33 | 8.63 | 0.34 | 9.68 | 0.39 | 10.19 | 0.45 | 13.06 | 0.61 | 7.29 | 0.41 | 6.61 | 0.8 | 6.67 | 0.54 | 16.47 | 1.26 | 8.17 | 0.64 |
| **Lu175** | 1.018 | 0.041 | 1.244 | 0.05 | 1.154 | 0.048 | 1.371 | 0.058 | 1.349 | 0.066 | 1.897 | 0.096 | 1.231 | 0.076 | 1.23 | 0.17 | 1.09 | 0.11 | 3.05 | 0.26 | 1.29 | 0.13 |
| **Hf178** | 11012.95 | 348.41 | 11540.14 | 365.07 | 11638.08 | 368.2 | 11262.09 | 356.27 | 11180.01 | 353.94 | 10579.98 | 335.02 | 11485.36 | 364.08 | 10903.65 | 351.3 | 12246.17 | 390.86 | 11749.17 | 379.02 | 11743.15 | 374.4 |
| **Ta181** | 0.051 | 0.017 | <0.039 | 0.017 | 0.074 | 0.019 | 0.062 | 0.017 | <0.064 | 0.029 | <0.051 | 0.025 | <0.149 | 0.057 | <0.58 | 0.25 | 0.22 | 0.12 | <0.53 | 0.31 | <0.47 | 0.21 |
| **Th232** | 0.566 | 0.038 | 0.295 | 0.029 | 0.126 | 0.026 | 0.929 | 0.055 | 0.86 | 0.075 | 0.387 | 0.053 | 0.613 | 0.098 | 0.73 | 0.3 | 2.18 | 0.31 | 0.82 | 0.38 | 0.85 | 0.23 |
| **U238** | 12.94 | 0.66 | 12.12 | 0.64 | 3.38 | 0.19 | 11.82 | 0.7 | 9.06 | 0.6 | 12.21 | 0.89 | 4.88 | 0.4 | 5.84 | 0.65 | 11.42 | 0.85 | 10.02 | 0.97 | 6.58 | 0.56 |

| Element | Z22-2 | 1 σ | Z29-2 | 1 σ | Z31-2 | 1 σ | Z05-2 | 1 σ |
|---|---|---|---|---|---|---|---|---|
| **Al27** | 6845.83 | 448.25 | 79.14 | 5.37 | 119.42 | 8.76 | 2506.92 | 176.44 |
| **Si29** | 266527.59 | 31725.02 | 144684.39 | 16446.46 | 191460.05 | 21950.31 | 299409.81 | 44303.85 |
| **Ti49** | <206.07 | 106.05 | <30.80 | 12.51 | 48.67 | 26.85 | <623.47 | 309.03 |
| **V51** | 4.99 | 1.98 | <0.53 | 0.2 | 0.86 | 0.46 | <9.28 | 4.75 |
| **Fe57** | 280.57 | 92.12 | <24.78 | 10.1 | 35.2 | 21.62 | <501.63 | 244.21 |
| **Y89** | 72.67 | 4.52 | 39.66 | 1.9 | 38.78 | 2.21 | 125.32 | 8.97 |
| **Zr90** | 531580.38 | 20658.82 | 504081.28 | 19525.5 | 534719 | 20823.31 | 496765.59 | 19768.62 |
| **Nb93** | 1.97 | 0.68 | 2.01 | 0.17 | 2.76 | 0.38 | <2.69 | 1.55 |
| **La139** | 4.04 | 0.34 | <0.042 | 0.016 | <0.059 | 0.039 | <0.85 | 0.46 |
| **Ce140** | 15.25 | 0.83 | 0.283 | 0.025 | 0.402 | 0.055 | 0.96 | 0.4 |
| **Pr141** | 1.69 | 0.19 | <0.029 | 0.012 | 0.05 | 0.025 | 0.94 | 0.31 |
| **Nd146** | 9.07 | 1.09 | <0.190 | 0.077 | <0.23 | 0.13 | <3.54 | 1.8 |
| **Sm147** | 3.4 | 0.87 | <0.233 | 0.094 | 0.39 | 0.2 | <4.14 | 2.16 |
| **Eu153** | 0.74 | 0.22 | 0.114 | 0.025 | <0.080 | 0.055 | <1.10 | 0.54 |
| **Gd157** | 6.59 | 1.06 | 0.81 | 0.11 | 1.15 | 0.23 | <4.27 | 2.05 |
| **Tb159** | 0.65 | 0.14 | 0.33 | 0.025 | 0.343 | 0.048 | <0.65 | 0.35 |
| **Dy163** | 6.61 | 0.77 | 3.69 | 0.2 | 3.42 | 0.31 | 9.47 | 1.6 |
| **Ho165** | 2.1 | 0.22 | 1.196 | 0.059 | 1.11 | 0.088 | 3.95 | 0.49 |
| **Er166** | 6.8 | 0.64 | 4.05 | 0.19 | 4.06 | 0.29 | 22.71 | 2.02 |
| **Tm169** | 1.05 | 0.16 | 0.66 | 0.032 | 0.732 | 0.062 | 6.76 | 0.59 |
| **Yb172** | 7.53 | 0.84 | 5.74 | 0.24 | 6.84 | 0.44 | 85.75 | 4.79 |
| **Lu175** | 1.63 | 0.19 | 0.911 | 0.04 | 1.05 | 0.078 | 21.23 | 1.1 |
| **Hf178** | 10800.79 | 348.53 | 10406.74 | 329.51 | 11267.77 | 358.65 | 11764.35 | 389.64 |
| **Ta181** | <0.51 | 0.24 | 0.087 | 0.031 | <0.094 | 0.059 | <1.55 | 0.72 |
| **Th232** | 0.59 | 0.32 | 0.619 | 0.065 | 0.78 | 0.14 | 28.01 | 2.58 |
| **U238** | 3.19 | 0.49 | 5.95 | 0.4 | 5.37 | 0.47 | 51.33 | 4.43 |

Zircon trace element concentrations normalised to chondrite.

| Element | Z06-1 | Z07-1 | Z10-1 | Z17-1 | Z25A-1 | Z32A-1 | Z32B-1 | Z01-1 | Z02-2 | Z03-2 | Z07-2 | Z22-2 | Z29-2 | Z31-2 | Z05-2 |
|---|---|---|---|---|---|---|---|---|---|---|---|---|---|---|---|
| Al27 | 0.1214 | 0.00215 | 0.00082 | 0.00019 | 0.00277 | 0 | 0.00317 | 0.0203 | 0.531 | 0.155 | 0.303 | 0.531 | 0.00613 | 0.00926 | 0.194 |
| Si29 | 1.31 | 1.25 | 1.26 | 1.15 | 1.2 | 1.16 | 1.21 | 1.43 | 1.32 | 1.82 | 1.44 | 1.67 | 0.9 | 1.2 | 1.87 |
| Ti49 | 0.188 | 0.026 | 0 | 0.033 | 0 | 0 | 0 | 0 | 0 | 0 | 0 | 0 | 0 | 0.074 | 0 |
| V51 | 0.435 | 0.0033 | 0 | 0 | 0 | 0 | 0 | 0 | 0.231 | 0 | 0 | 0.059 | 0 | 0.0101 | 0 |
| Fe57 | 0.00989 | 0 | 0.00007 | 0 | 0 | 0 | 0 | 0 | 0 | 0 | 0.00101 | 0.00101 | 0 | 0.00013 | 0 |
| Y89 | 15.28 | 17.65 | 23.09 | 21.66 | 24.53 | 26.07 | 14.48 | 17.05 | 50.97 | 47.09 | 21.44 | 32.3 | 17.62 | 17.24 | 55.7 |
| Zr90 | 96883.01 | 106953.43 | 99518.01 | 100232.88 | 102271.18 | 98110.8 | 94254.83 | 93295.11 | 100427.9 | 102357.11 | 101251.35 | 95953.14 | 90989.4 | 96519.67 | 89668.88 |
| Nb93 | 7.31 | 7.65 | 7.13 | 7.09 | 6.92 | 6.22 | 6.35 | 6.29 | 6.69 | 6.27 | 7.87 | 5.26 | 5.35 | 7.37 | 0 |
| La139 | 0 | 0 | 0.074 | 0 | 0 | 0 | 0 | 0 | 15.66 | 0 | 3.21 | 11.01 | 0 | 0 | 0 |
| Ce140 | 0.309 | 0.2 | 0.049 | 0.197 | 0.215 | 0.225 | 0.526 | 1.36 | 5 | 0.87 | 0.78 | 15.93 | 0.296 | 0.42 | 1 |
| Pr141 | 0.341 | 0 | 0 | 0 | 0 | 0 | 0 | 0 | 14.08 | 0 | 0 | 12.37 | 0 | 0.37 | 6.83 |
| Nd146 | 0.155 | 0 | 0.213 | 0.194 | 0 | 0 | 0 | 0 | 24.9 | 0 | 0 | 12.76 | 0 | 0 | 0 |
| Sm147 | 0 | 0 | 0.88 | 0.56 | 0 | 0 | 0 | 0 | 11.64 | 0 | 0 | 14.7 | 0 | 1.68 | 0 |
| Eu153 | 1.12 | 0.98 | 0 | 2.37 | 1.65 | 1.83 | 1.33 | 0 | 16.63 | 0 | 0 | 8.47 | 1.31 | 0 | 0 |
| Gd157 | 2.77 | 3.12 | 2.67 | 4.19 | 4.26 | 4.6 | 2.02 | 0 | 17.18 | 10.04 | 0 | 21.54 | 2.65 | 3.76 | 0 |
| Tb159 | 4.4 | 5.82 | 6.77 | 6.95 | 8.5 | 8.84 | 4.69 | 6.72 | 17.3 | 17.22 | 8.74 | 11.15 | 5.69 | 5.91 | 0 |
| Dy163 | 8.8 | 9.49 | 11.75 | 12.05 | 14.16 | 14.49 | 8.01 | 10.2 | 16.99 | 24.99 | 14.13 | 17.35 | 9.69 | 8.98 | 24.85 |
| Ho165 | 12.9 | 13.72 | 17.76 | 18.41 | 20.42 | 21.56 | 11.13 | 10.18 | 28.48 | 38.54 | 15.79 | 24.68 | 14.06 | 13.04 | 46.39 |
| Er166 | 14.63 | 17.03 | 19.14 | 21.15 | 23.35 | 28.58 | 15.61 | 18.33 | 26.43 | 47.62 | 18.89 | 27.3 | 16.25 | 16.31 | 91.2 |
| Tm169 | 19.08 | 22.85 | 25.74 | 26.95 | 31.56 | 38.84 | 21.64 | 28.23 | 27.36 | 50.74 | 26.13 | 29.37 | 18.53 | 20.57 | 189.77 |
| Yb172 | 26.52 | 34.97 | 34.81 | 39.02 | 41.1 | 52.66 | 29.39 | 26.65 | 26.9 | 66.43 | 32.96 | 30.37 | 23.13 | 27.56 | 345.78 |
| Lu175 | 26.73 | 32.65 | 30.29 | 35.98 | 35.41 | 49.79 | 32.3 | 32.31 | 28.59 | 80.15 | 33.75 | 42.76 | 23.92 | 27.56 | 557.28 |
| Hf178 | 61524.88 | 64470.07 | 65017.23 | 62916.7 | 62458.13 | 59106.01 | 64164.04 | 60914.25 | 68414.37 | 65637.83 | 65604.19 | 60339.62 | 58138.18 | 62948.45 | 65722.61 |
| Ta181 | 1.97 | 0 | 2.85 | 2.37 | 0 | 0 | 0 | 0 | 8.59 | 0 | 0 | 0 | 3.36 | 0 | 0 |
| Th232 | 13.31 | 6.94 | 2.97 | 21.86 | 20.23 | 9.09 | 14.42 | 17.18 | 51.26 | 19.39 | 20.03 | 13.89 | 14.57 | 18.24 | 658.95 |
| U238 | 1060.73 | 993.56 | 277.02 | 969.01 | 742.45 | 1000.93 | 400.27 | 479.07 | 936.25 | 821.65 | 539.16 | 261.71 | 487.84 | 440.57 | 4207.61 |
| LREE (Sm/La) | - | - | 11.89 | - | - | - | - | - | 0.74 | - | 0.00 | 1.34 | - | - | - |
| HREE (Lu/Gd) | 9.65 | 10.46 | 11.34 | 8.59 | 8.31 | 10.82 | 15.99 | - | 1.66 | 7.98 | - | 1.99 | 9.03 | 7.33 | - |
| MHREE (Lu/Sm) | - | - | 34.42 | 64.25 | - | - | - | - | 2.46 | - | - | 2.91 | - | 16.40 | - |
| Eu/Eu* | - | - | - | 1.55 | - | - | - | - | 1.18 | - | - | 1.37 | - | - | - |

RECORD 2019/8

# METAMORPHIC AND ISOTOPIC CHARACTERISATION OF PROTEROZOIC BELTS AT THE MARGINS OF THE NORTH AND WEST AUSTRALIAN CRATONS

Anderson

This Record is published in digital format (PDF) and is available as a free download from the DMIRS website at <www.dmp.wa.gov.au/GSWApublications>.

Further details of geoscience products can be obtained by contacting:

Information Centre
Department of Mines, Industry Regulation and Safety
100 Plain Street
EAST PERTH WESTERN AUSTRALIA 6004
Phone: +61 8 9222 3459 Fax: +61 8 9222 3444
www.dmp.wa.gov.au/GSWApublications